GENERAL MOTORS

ENGINEERING JOURNAL

Volume 7 - - - - Number
July-August-September, 19

for educators
in the fields of engineerin
and allied sciences

On Research in General Motors

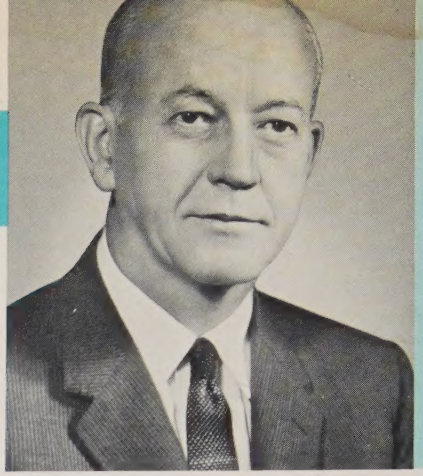

IT HAS been said many times that in our business we either move forward or we move backward. There is no such thing as standing still. This is true not only of our business but of all business and indeed of all forms of constructive activity. A tree that stops growing is dead. The alternative to progress is not just lack of progress but decay.

Fortunately, the growth expectations of the automobile industry appear to be very promising for the ten-year period ahead. The nation's population is increasing. By 1970 the projected increase will amount to 33 million people or about one-fifth of today's population. The number of families also will increase by 20 per cent, and family incomes should show a rise of 15 per cent or more. With higher family incomes and a continuing trend toward suburban living, more families will be encouraged and enabled to own two or more cars. This factor, combined with a further increase in car-owning households from three out of four to more than four out of five, can be expected to bring the normal domestic market for new passenger cars to about 8 million units a year by 1970. Total sales of cars and trucks would then average between 9 and 9½ million units a year compared with last year's total of just over 7 million.

However, all of this does not mean that the market will be there just for the taking. An increasing number of other products and services will be competing for the prospective buyer's attention. Thus, if we are to grow in our industry, we shall have to continue to offer each year products that are better than those of the year before, and we shall have to promote them vigorously and sell them energetically.

In General Motors, our efforts to develop and introduce better products depend heavily upon our research programs. We continually seek new scientific and engineering knowledge. Primarily we are concerned with areas of interest that relate to our civilian business or to our national defense contracts. We have engaged in research activities in these areas throughout most of our history, and much of General Motors' growth can be attributed to the developments resulting from such work.

Our research is conducted essentially in two ways:

(a) by personnel of the GM Research Laboratories located at the Technical Center in Warren, Michigan, where the bulk of our long-range studies are made, and

(b) by personnel in those GM Divisions which maintain their own laboratories for work on projects directly concerning their business.

Some basic subject areas recently explored by GM scientists and engineers are: crystallography, friction, electronics, thermodynamics, and radioactive isotopes. Experiments also are being conducted with methods of directly converting chemical and nuclear energy to electrical and mechanical applications. Other projects involve materials and control systems relating to the nation's programs for missile and space vehicle development. Several recent research projects undertaken in General Motors are described in the selection of papers published in this issue of the JOURNAL.

It is through such research activities that we strive to broaden our scientific knowledge in order to apply it to the development of new products and the improvement of existing ones. Only if we are effective in these efforts can we hope to meet our expanding market opportunities and make progress in our operations with accompanying benefits to our employes, shareholders, dealers, suppliers, and customers.

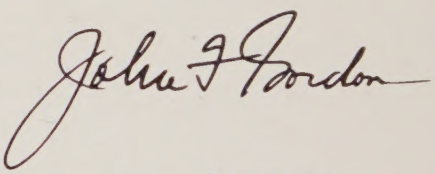

John F. Gordon,
President

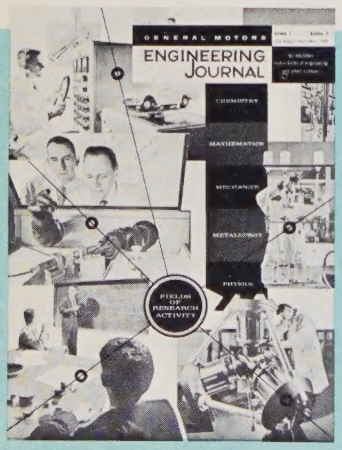

THE COVER

This issue's cover design by artist Ernest W. Scanes depicts activities in five principal fields of research in which GM scientists and research engineers are engaged. At the upper right is shown a typical phase of a chemist's work—precision analysis using anion exchange columns. At the lower right is shown a tetrahedral anvil press used in metallurgical research to study the effects of extreme pressures and temperatures on the physical properties of solids. A recent contribution to bearing research was the analytical solution by GM mathematicians (lower left) of Reynold's equation for the finite hydrodynamic bearing which gives a more accurate picture of pressure distribution between a journal and bearing. Fundamental knowledge of nuclear physics has been applied to many unique industrial uses of radioisotopes such as using a liquid isotope to measure the wall thicknesses of experimental hollow turbine blades and vanes (left, center). In the field of mechanics, research engineers have developed a handling simulator (top left) which permits visual observation of how varying such parameters as wheelbase, steering gear ratio, weight distribution, tire properties, and suspension geometry affect response to steering wheel movement.

CONTENTS

RESEARCH PAPERS IN THIS ISSUE

CLASSROOM PROBLEMS

OTHER FEATURES

GENERAL MOTORS
ENGINEERING
JOURNAL

Vol. 7 July-Aug.-Sept. 1960 No. 3

Published with the help of General Motors engineers and scientists everywhere

The GENERAL MOTORS ENGINEERING JOURNAL is published quarterly by the Educational Relations Section of the Public Relations Staff, General Motors Corporation. It is intended primarily as a medium for presenting to educators in the fields of engineering and allied sciences the results of General Motors research and engineering developments in both the product and production fields.

Address: EDUCATIONAL RELATIONS SECTION, Public Relations Staff, General Motors Corporation, General Motors Technical Center, Warren, Michigan.

Research and Growth

By DR. LAWRENCE R. HAFSTAD
Vice President in Charge of
General Motors
Research Laboratories

IF WE were to apply the psychological technique called word association to the concept of research, what are the associations, the words, that this concept calls up? Most of us, of course, would begin with these synonyms of Webster's: "studious inquiry," the "search for new facts," the "revision of accepted conclusions." But we would not stop there. Our experience would lead us to continue with words like "ideas," "analysis," "experimentation," or "development." We might even blurt out "inspiration" and, in the next breath, "disillusion." Then, after a moment's reflection, we would likely sum it all up with "growth."

Research, of course, means many things to many people. At the General Motors Research Laboratories, it means all of the above and more to us, but particularly "growth." Without growth an industrial organization stagnates. Its technology withers and its production lags, starved by a lack of product improvement and advance. The mechanism behind improvement and advance is research, research organized on a broad scale and including both basic and applied functions. Research can be depended upon to improve products or to create new ones from new ideas only when it operates on a backlog of fundamental knowledge provided by a program of primary studies. New points of view and new information are required. These are the trademarks of growth. They result from constant examination and re-examination, from cross-fertilization and communication, and from the frequent review of basic principles.

The areas of the Research Laboratories activities, identified in the accompanying chart, appropriately branch out into product concerns of General Motors and, in turn, are rooted in the fundamental sciences for optimum growth both in concepts and applications. The functional importance of those areas rooted in basic theory has been demonstrated again and again in our product history. The knowledge derived from studies in fields like heat energy, metallurgy, polymers, and electronics has brought such developments as the high compression engine, the gas turbine, aluminum alloy blocks

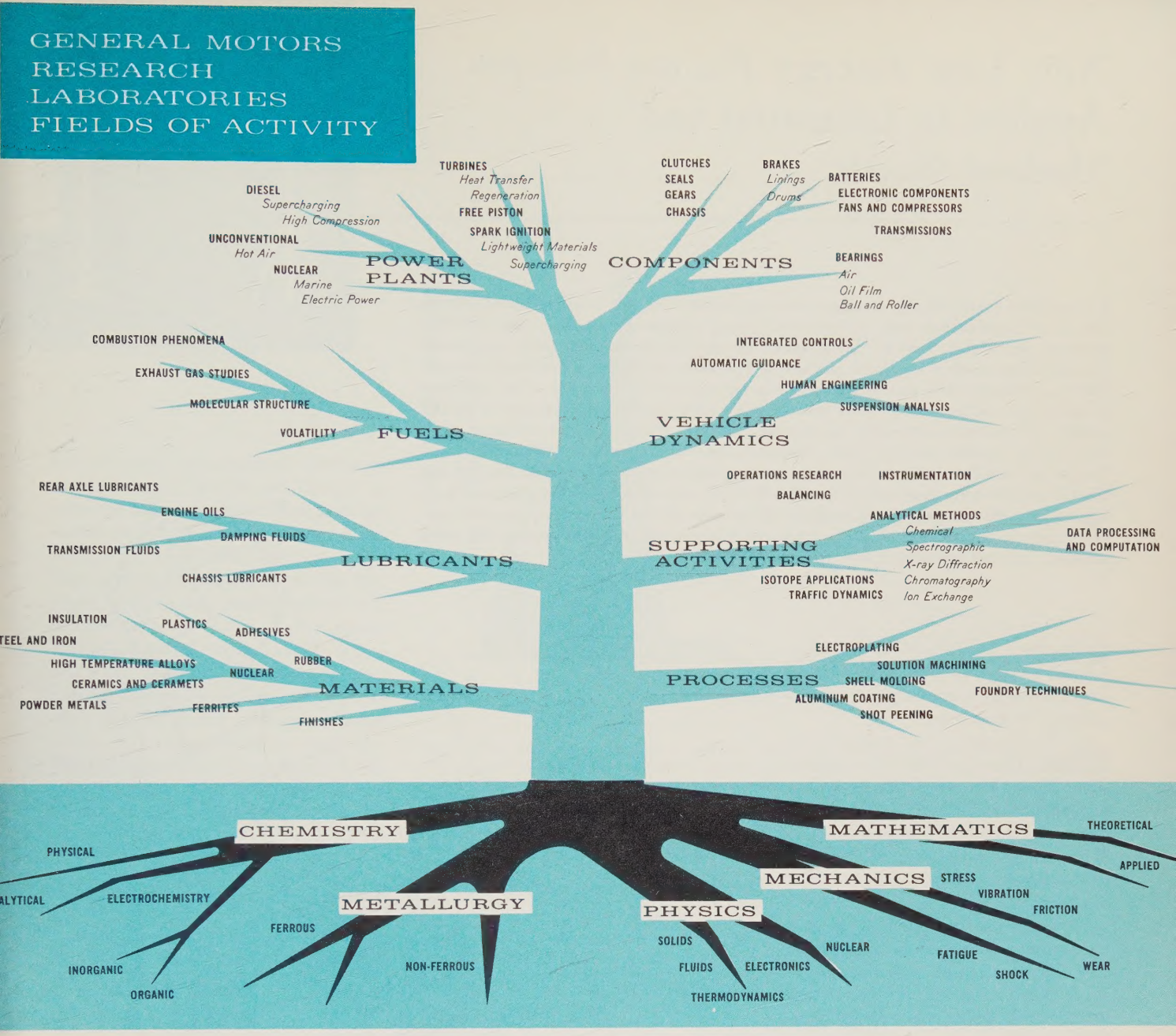

and pistons, durable gloss-retaining finishes, and automatic instrumentation.

The need for growth, for refinement and improvement, is a constant challenge. The greater the need, the more diversified must be the attack in solving and marshalling the forces of nature. Growth lies in change, in probing natural phenomena to advance the frontiers of knowledge. Growth cannot come from a confined effort. It can only come from the exploitation of all our resources, mental and physical, and from a truly fundamental assault on the still numerous facets of the unknown.

Some of our recent research has concerned studies in friction, including rolling friction in its relation to ball steel structure and sliding friction as affected by lubricant composition, problems in the internal stresses and fatigue of metals, and the development of low-energy radiographic sources. These topics, discussed in this issue of the JOURNAL, are typical of the longer range and more fundamental side of our work even though potentially imminent applications exist for the results.

In view of its potential applications, for example, it is not surprising that we at the Research Laboratories are studying intensively the phenomenon of rolling friction since it relates to the problem of energy loss from internal molecular movement in various materials under stress. Nor are we behind in other areas of our work in advancing the frontiers of knowledge and in converting the unknown to the useful known. By helping to keep our corporate technology dynamic and active, I believe we are contributing to the general welfare of industry, and to human progress. The English philosopher Spencer has observed, "Progress is not an accident, but a necessity . . . It is a part of nature." As it is the essence of research, growth is also the key to progress.

New Low Energy Photon Sources Applied to Industrial and Medical Needs

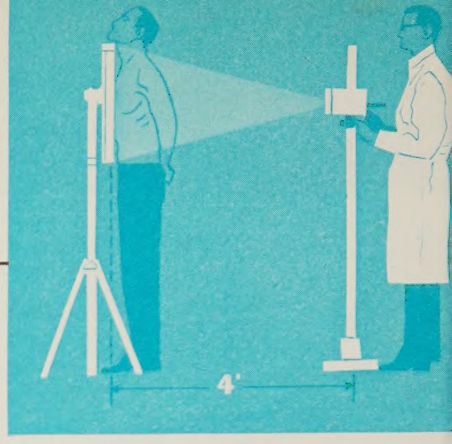

A long time industrial and medical need has existed for low energy, sealed photon sources for applications such as thickness gaging, radiography at short source-to-film distance, and special medical radiography. To find photon sources with the desired characteristics, nuclear physicists at the GM Research Laboratories evaluated two new sources, samarium-145 and gadolinium-153, along with thulium-170. The radiation characteristics of the sources were studied while each source was contained in special holders. As an aid in comparing the sources, two new terms, "photon emission rate" and "photon specific activity," were defined to describe the emitted radiation rate and the specific activity of the sources. The resulting experiments showed that Sm-145 and Gd-153 sources were more useful than Tm-170 for certain radiography, thickness gaging, and liquid-level gaging applications. As a result of the experiments, another low energy photon source, Sm-153, was developed which is capable of producing, for some purposes, medical radiograms with equipment that is easily portable.

SINCE THE END of World War II, scientists have accelerated their quest for more knowledge about the possible applications of radioisotopes.

In the industrial and medical fields especially, there is a need for low energy, sealed photon sources of radioisotopes for such applications as radiography at short source-to-film distances, thickness gaging of low density materials or thin sections of high density materials, and for special medical radiography.

To qualify for these applications, photon sources are needed which are low in cost, emit pure gamma or X-radiation in the 5- to 150-kev range, have half-lives of six months or longer, and have high specific activity. Shorter half-life sources may sometimes qualify if they are particularly outstanding in other respects.

Several years ago nuclear physicists at the Isotope Laboratory, GM Research Laboratories, began evaluating new low energy photon sources to determine their adaptability to these industrial and medical applications.

Experimental sealed sources of samarium-145 and gadolinium-153 were produced by neutron irradiation of the appropriate enriched (separated) stable isotopes. A sealed source of thulium-170 also was purchased and compared during the experiments.

The Oak Ridge National Laboratory, at the request of the GM Research

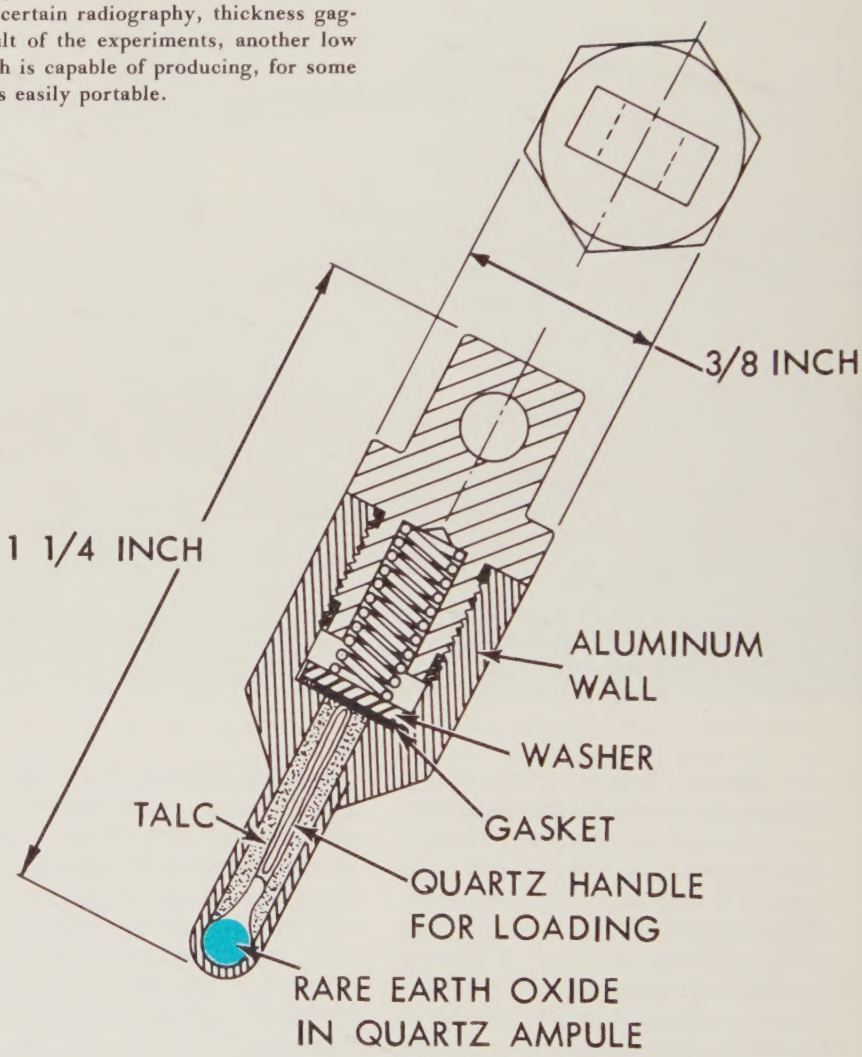

Fig. 1—A cut-away diagram of an experimental radiation source assembly used during the experiments with Sm-145 and Gd-153 is shown here. The inside diameters of the quartz ampules were approximately 0.079 in. The wall thickness of the quartz ampules was approximately 0.008 in. The ampules were irradiated in a flux position of 4.3×10^{13} n per cm^2-sec and received a total nvt of 7.7×10^{19}. For experiments using Sm-153 in the form of a Sm_2O_3-Al cermet pellet, the source assembly was modified to include a screw seal with a soft metal gasket in place of the spring shown in this diagram.

By FARNO L. GREEN
and WILLARD D. CHEEK
General Motors
Research Laboratories

How two new definitions aid source comparison

Laboratories, encapsulated the stable parent isotopes Sm-144 and Gd-152 in spherical quartz ampules. These ampules contained 8.5 mg of Sm_2O_3, enriched to 81.5 per cent Sm-144, and 8.4 mg of Gd_2O_3, enriched to 15.0 per cent Gd-152. These ampules then were irradiated with thermal neutrons in the nuclear reactor at Chalk River, Ontario, Canada, to produce the radioisotopes Sm-145 and Gd-153. When the radioactive capsules were received at the Research Laboratories, they were placed in aluminum holders with walls approximately 0.015 in. thick (Fig. 1). The holders were shaped so that radiation was emitted

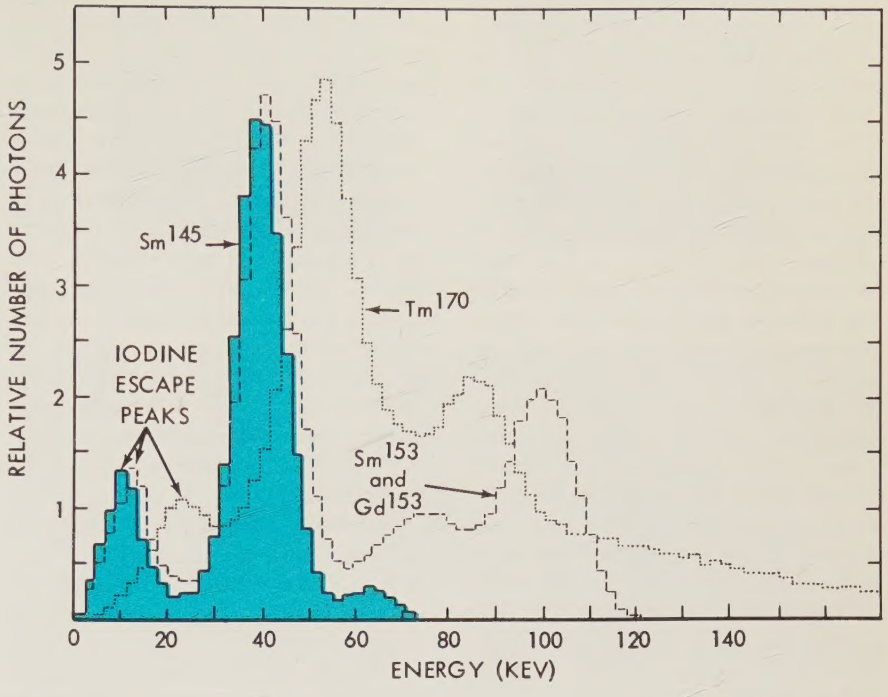

Fig. 2—This chart shows the photon spectra of the Sm-145, Sm-153, Gd-153, and Tm-170 radiation sources observed during the experiments with a 1.75-in. by 2-in. NaI (Tl) crystal and a 100-channel pulse height analyzer. The iodine escape peaks are characteristic of the NaI crystal and not of the radioisotope emission. The number of photons under the escape peaks are added during analyses of spectra to the number shown for the most abundant low energy photon in each case.

LOW ENERGY PHOTON SOURCES

RADIO-ISOTOPE	METHOD OF PRODUCTION	CROSS SECTION FOR PRODUCTION (BARNS)	HALF-LIFE (DAYS)	MODE OF DECAY	PHOTON EMISSIONS[a] (KEV)	SOURCE COMPOSITION AND IRRADIATION	SOURCE SIZE
Sm^{145}	(n, γ) from enriched Sm^{144}	$> 2^b$	$\sim 240^c$	Electron capture	39 (K X ray), 61	8.5 mg Sm_2O_3 encapsulated in quartz; irradiated 7×10^{19} nvt Chalk River NRX Reactor	0.085 in. (2.1 mm) diameter sphere
Gd^{153}	(n, γ) from enriched Gd^{152}	$> 15^b$	$\sim 240^c$	Electron capture	42 (K X ray), 72, 100	8.4 mg Gd_2O_3 encapsulated in quartz; irradiated as above	0.079 in. (2.0 mm) diameter sphere
Tm^{170}	(n, γ) from natural Tm^{169}	130^d	129^d	β^-	52 (K X ray following internal conversions), 84, bremsstrahlung	50 mg Tm_2O_3 in welded Al, prepared by Technical Operations, Inc.	0.079 in. (2.0 mm) diameter x 0.079 in. (2.0 mm) long cylinder

[a] PHOTON SPECTRA SHOWN IN FIG. 2
[b] TENTATIVE VALUE BASED ON GM RESEARCH LABORATORIES MEASUREMENTS; ADDITIONAL MEASUREMENTS REQUIRED
[c] BEST ESTIMATE BASED ON LITERATURE VALUES AND GM RESEARCH LABORATORIES MEASUREMENTS TO DATE
[d] LITERATURE VALUE; ADDITIONAL MEASUREMENTS DESIRABLE

Table I—The above table lists some of the characteristics of the low energy photon sources studied.

uniformly in approximately 3π steradians.

The purchased Tm-170 source was fabricated by Technical Operations, Inc. The source material, approximately 50 mg of Tm_2O_3, was encapsulated in aluminum and sealed inside a stainless steel jacket. Radiation was emitted somewhat uniformly in approximately 2.5π steradians.

The radiation characteristics of the sources were studied (Fig. 2) while each source was contained in its metal assembly. Samarium-145 and Gd-153 decay by electron capture and, therefore, no bremsstrahlung from beta decay and no annihilation gammas were observed (Table I). The principal photons emitted were a 38.6-kev (Pm Kα) X-ray and a 61-kev gamma ray from Sm-145[1] and a 51.5-kev (Eu Kα) X-ray, and 72- and 100-kev gamma rays from Gd-153[2]. The Tm-170 is reported to decay by beta emission followed by an 84-kev gamma ray[3]. As in previous studies, the beta rays were observed to yield bremsstrahlung, some of which had higher energy and lower intensity than the 52.4-kev (Yb Kα) internal conversion X-rays and 84-kev photons which are characteristic of thulium nucleii.

New Terms Help Describe Source Characteristics

When comparing radiation sources used for radiography or for certain thickness gaging applications, it is important for the engineers and nuclear physicists to know the rate at which each source emits useful radiation. Partial information is conventionally stated using the term "specific activity" (disintegration rate per unit mass) which can be stated for a source only if the decay scheme is accurately known. Because of conflicting information concerning the decay schemes and cross sections of the Sm-145, Gd-153, and Tm-170 radioisotopes, it was impossible to state their specific activities accurately. In addition, for accurate statement of the useful emitted radiation rate, other factors must be known, such as, the radiation absorbed in the radioactive material and in the source holder.

As a result, two new terms, *photon emission rate* and *photon specific activity*, were used to describe the emitted radiation rate and the radiation rate per unit radioactive material volume of the radiation sources. Both terms refer to quantities which are of maximum importance to the user and which can be measured with relative ease. They allow theoretical discussions of decay schemes without affecting the numerical quantities used to describe the actual industrial and medical utility of these sources.

Photo Emission Rate

The photon emission rate is defined as the number of photons emitted from the source per unit time. The term *source* is understood to mean the assembly of the radioactive material in whatever containment capsule is necessary for handling and for radiological safety when in use. The photon emission rate is measured in *source units* where:

one source unit (su) = 3.7×10^{10}* emissions per second

and

one millisource unit (msu) = 3.7×10^{7} emissions per second.

The relationship between photon source units and millicuries is shown by the following example. Assume that a radioisotope of 10 millicuries weighs five

*This is the number of disintegrations per second in one curie of activity, and was chosen for simplicity in relating the new term to the old units of curies when desirable.

PHOTON SOURCE INTENSITIES

SOURCE	PHOTONS (KEV)	MEASURED (MARCH 11, 1958)		ESTIMATED MAXIMUM[c]	
		PHOTON EMISSION RATE (msu)[a]	PHOTON SPECIFIC ACTIVITY (su/g)[b]	PHOTON EMISSION RATE (msu)[a]	PHOTON SPECIFIC ACTIVITY (su/g)[b]
Sm^{145} (8.5 mg Sm_2O_3)	39	0.85	0.100	22.1	2.60
	61	0.05	0.006	1.3	.16
	all > 61	0.02	0.002	.5	.05
	Total	0.92	0.108	23.9	2.81
Gd^{153} (8.4 mg Gd_2O_3)	42	8.3	0.99	216	25.8
	72	2.2	0.26	57	6.8
	100	4.0	0.48	104	12.5
	Total	14.5	1.73	377	45.1
Tm^{170} (50 mg Tm_2O_3)	52	41.[d]	0.82[d]	410[e]	8.2[e]
	84	18.[d]	0.36[d]	180[e]	3.6[e]
	additional bremsstrahlung	16.[d]	0.32[d]	160[e]	3.2[e]
	Total	75.[d]	1.50[d]	750[e]	15.0[e]

[a] 1 msu = 3.7×10^{7} EMISSIONS PER SECOND (SEE TEXT)
[b] 1 su/g = 3.7×10^{10} EMISSIONS PER SECOND/GRAM (SEE TEXT)
[c] BASED ON IRRADIATION AT 10^{14} n/cm^2-sec FOR ONE HALF-LIFE SHOWN IN TABLE I
[d] FOR A NOMINAL SOURCE INTENSITY OF 2.2 CURIES
[e] BASED ON MAXIMUM SOURCE INTENSITY QUOTED BY SOME U.S.A. SUPPLIERS OF TM^{170}. SOURCES OF THE SIZE INDICATED

Table II—The photon emission rates and the photon specific activities of the sources used for the study are given in this table. The estimated maximum photon emission rates and photon specific activities which should be obtained from present reactors with high neutron fluxes also are indicated.

mg and is solid in form with negligible self-absorption of its own radiation. It is contained in a capsule of negligible absorption properties. This hypothetical radioisotope decays 100 per cent of the time by K orbital electron capture and also has an unconverted 90-kev gamma ray for every disintegration. There are no other gammas. In describing this source by the new terms:

K X-ray emission rate = 10 msu or
3.7×10^8 emissions per second

90-kev emission rate = 10 msu or
3.7×10^8 emissions per second

Total photon emission rate = 20 msu or
7.4×10^8 emissions per second.

If the containment capsule does not have negligible absorption for the K X-ray but, for example, attenuates the photon by 10 per cent (transmits 90 per cent of the X-rays) then the appropriate description is:

K X-ray emission rate = 0.9×10 msu
= 9 msu.

Photon Specific Activity

By the new definition, photon specific activity is the photon emission rate per unit mass of source material and is measured in source units per unit mass of radioactive material inside the containment capsule. In the example above, the description is:

X-ray specific activity

$$= \frac{10 \text{ msu}}{5 \text{ mg}} = 2 \text{ su per g}$$

90-kev gamma specific activity
= 2 su per g

Total photon specific activity
= 4 su per g.

These new terms and units simplify quantitative utilization and comparison of radiation sources because they state quantities which are actually used in radiography and in gaging (Table II). These quantities also can be easily measured in the laboratory with a gamma ray spectrometer and a balance. They do not require theoretical manipulation as do quantities such as the curie which implies precise knowledge of a theoretical decay scheme in addition to laboratory measurements.

Experiments Provided Data For Industrial Applications

To investigate possible industrial applications of the photon sources, various castings made of aluminum and magnesium, such as automobile pistons, whose thicknesses varied from 0.087 in. to 1.0 in. were radiographed with Sm-145, Gd-153, and Tm-170 (Fig. 3). Generally, the source with the lowest energy photons, like Sm-145, gave the greatest subject contrast as was anticipated.

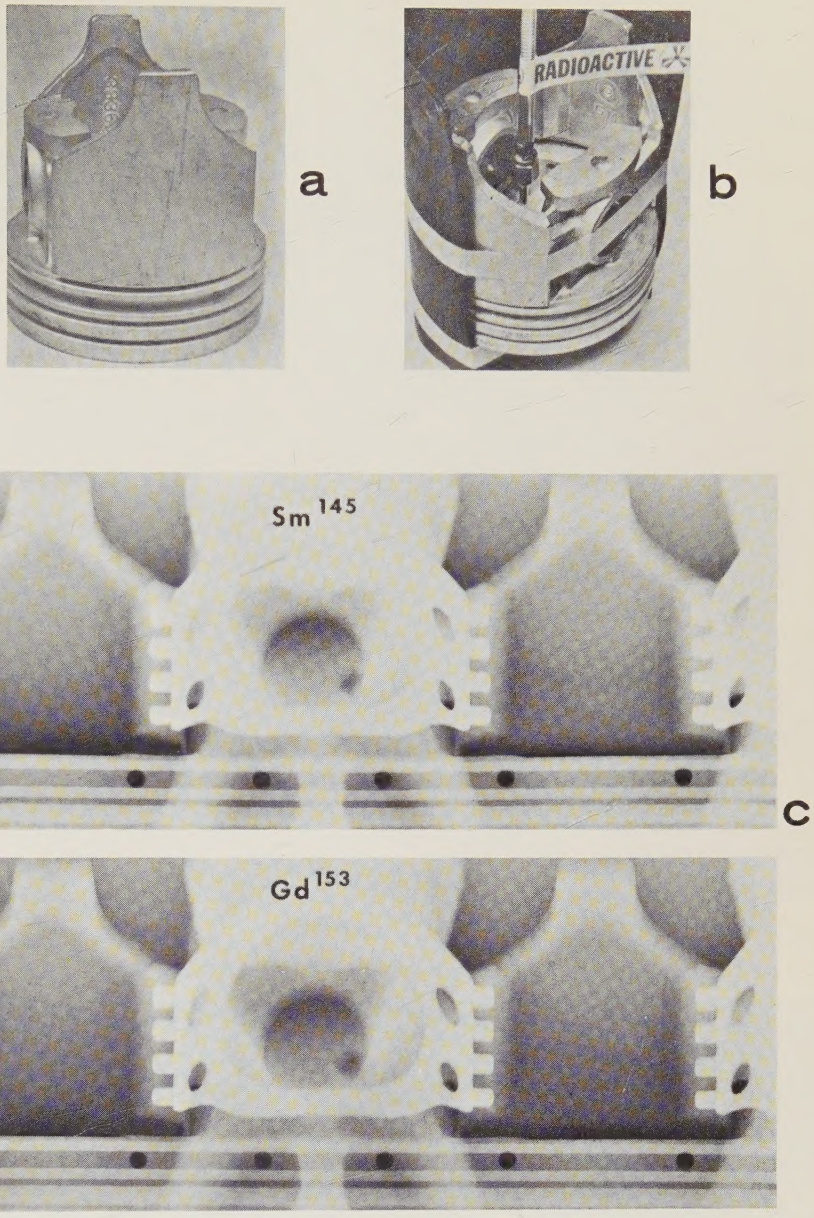

Fig. 3—Inside-out radiographs were made of standard aluminum pistons (a) by placing the radioactive source assembly inside the piston and taping the film to the outside (b). A comparison of radiographs made with Sm-145 and Gd-153 sources (c) indicates that Sm-145 provides the best subject contrast in the ring area.

Thin steel objects of less than 0.8-in. thickness also were radiographed with Tm-170 and Gd-153. In the 0.8-in. range, Gd-153 gave the best results from the standpoint of shortest exposure based on the assumption that all the sources were of equal principal (most abundant) photon intensity. Gd-153 also gave improved sensitivity in the 0.15-in. to 0.8-in. range. Other experiments showed that copper or brass objects of less than 0.15-in. thickness were best radiographed with Sm-145, when minimum exposure times were not required.

In short source-to-film experiments, radiographs of aluminum circular wedges of various diameters were made with all three sources (Fig. 4). The Sm-145 source gave the greatest sensitivity on thin sections.

Radiation patterns for each of the sources also were studied to determine whether the sources had panoramic

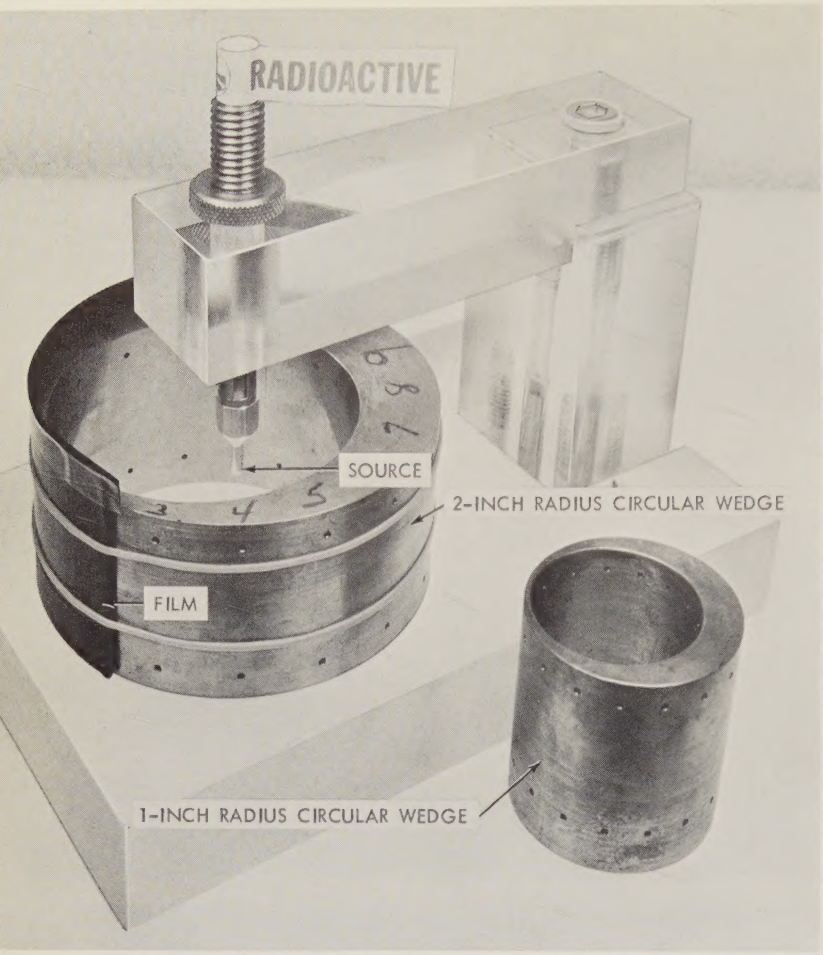

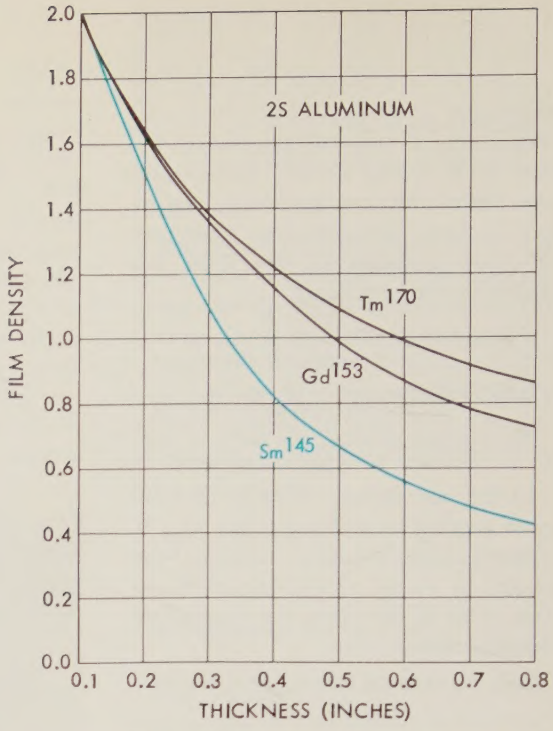

Fig. 4—To investigate the sources for possible inside-out radiography uses at short source-to-film distances, film was wrapped around the outside surface of an aluminum cylindrical wedge (left). The source was then placed on the axis of the surface, giving a 2-in. source-to-film distance. A graph showing the resulting film densities indicates the greatest sensitivity was obtained from Sm-145, particularly at the smaller thicknesses.

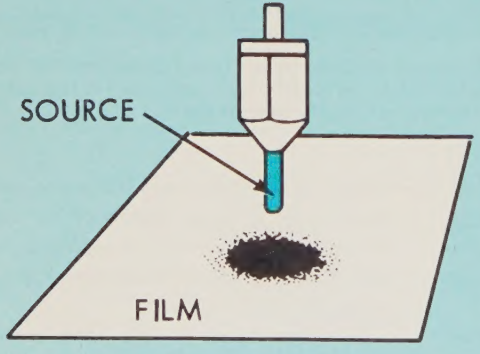

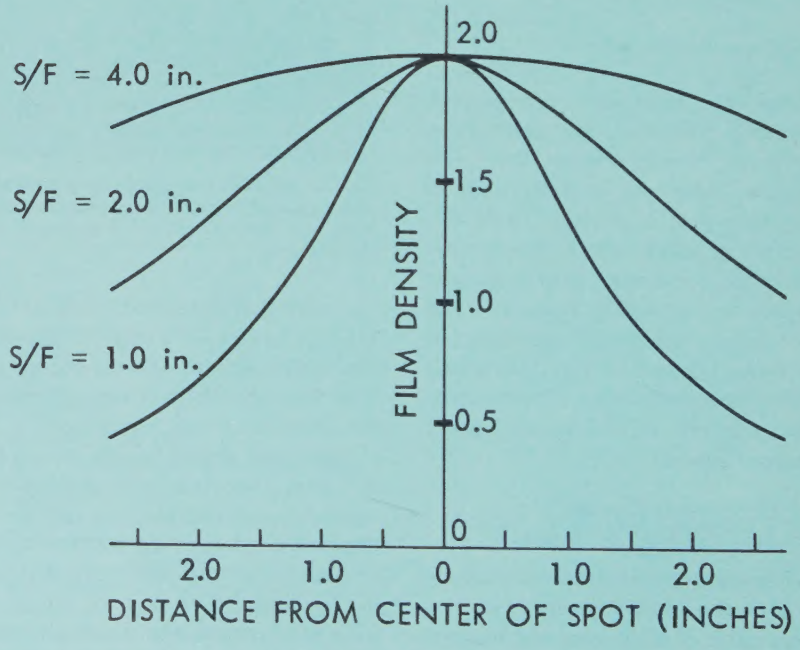

Fig. 5—Radiation patterns for a typical source were obtained by placing a 0.25-in. aluminum sheet between the source assembly and the film (left). The radiographic film density pattern for the test conducted with Gd-153 is shown at the right.

radiography uses, particularly at short source-to-film distances where it is important that the intensity of the radiation emitted from the source be as geometrically uniform as possible. A typical result was the one obtained with Gd-153 in which the area of approximate uniform exposure was small at the one-inch source-to-film distance but became greater as the distance was increased (Fig. 5).

Another area in which the Sm-145 and Gd-153 sources were effective was in thickness gaging of thin aluminum and steel sections. By studying the regions of greatest slope on absorption curves obtained from the experiments, it was possible to predict what ranges could be used most effectively for thickness gaging (Fig. 6). These curves also are useful in calculating wall thicknesses of pipe which can be used with liquids of various specific gravities for effective determination of liquid levels.

New Photon Source Used in Lightweight X-ray Unit

Although the primary purpose of these studies of low energy photon sources was to find industrial applications, the possibilities of medical uses also were examined. As a result of this work, a short-lived radioisotope, Sm-153, was developed and is now experimentally producing medical radiograms of diagnostic quality comparable to conventional X-rays.

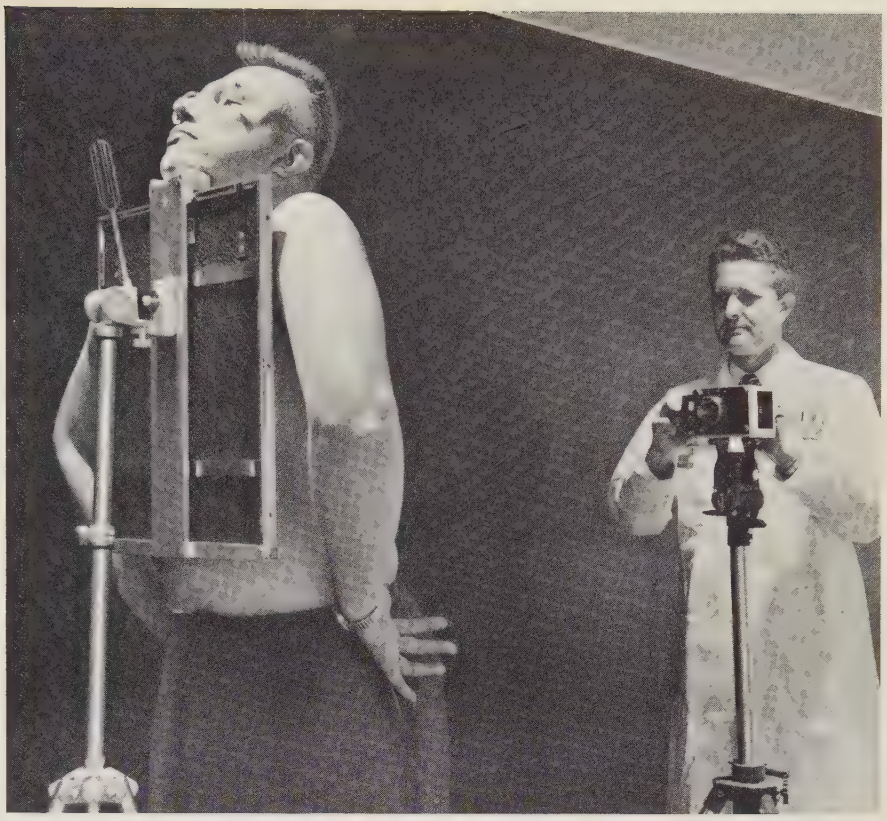

Fig. 7—Chest radiographs using a Sm-153 source can be made with this lightweight portable equipment consisting of a film holder (left foreground) mounted on a tripod and a portable shielded source on an adjustable stand (rear).

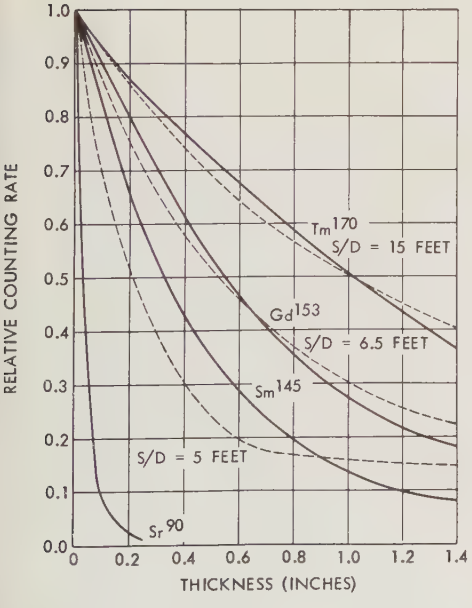

Fig. 6—The solid line absorption curves for aluminum shown here were obtained with a Geiger-Mueller detector while the dotted curves were obtained with a NaI (Tl) crystal detector. The slight variation between the curves is principally due to the difference in detector sensitivities as a function of photon energy. For comparison, a strontium-90 beta absorption curve is plotted with the photon data.

Recently a Sm-153 source was used to make a radiograph of a patient's chest, believed to be the first diagnostic radiograph of its kind made with a radioisotope (Fig. 7). The radioactive Sm-153 source and its shield, weighing only 18 lb, also is believed to be the first complete X-ray energy source which can be held in one hand and yet is capable of making a chest radiograph. The portability of this new technique will eventually make it possible to perform medical radiography in places and situations that are unpractical for conventional X-ray equipment such as remote geographical areas, field use, emergencies, and disasters.

The main disadvantage of Sm-153 is its two-day half-life which requires the source to be reactivated after it is used for a week or so.

Conclusion

The experiments proved that Sm-145, Sm-153, and Gd-153 have numerous applications, especially in inside-out investigations of objects inaccessible to 360-degree panoramic X-ray tubes, and in radiography of thin steel sections and low density materials such as aluminum and animal tissue and bone.

Factors that should be considered, however, before the sources are applied to individual problems are the available photon specific activities, required sensitivities, shielding requirements, half-life of the sources, and cost.

Bibliography

1. Callendine, G. W., Jr., Carey, W. E., and Pool, M. L., "X-rays Associated with Samarium 145," *Bulletin American Physics Society*, 2:24G8, verbal report, (January 30, 1957).
2. Bhattacherjee, S. K. and Raman, S., "Decay of Gd-153," *Nuclear Physics*, Vol. 1 (June 1956), pp. 486-98.
3. Day, P. P., "K-Capture Branch in Tm-170," *Physical Review*, 102, 1572 (1956).

A Thermal Energy Storage System for Solar Powered Earth Satellite Power Plants

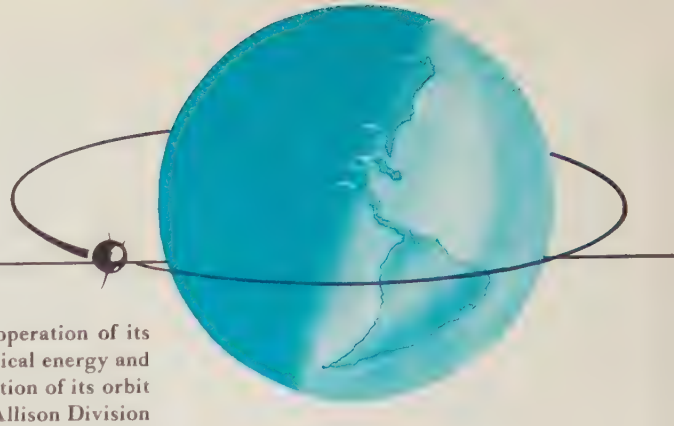

An earth satellite which depends upon solar energy for the continuous operation of its power plant requires some type of system to convert solar energy to electrical energy and also to store this energy for use when the satellite passes through that portion of its orbit shaded from the sun. As part of an energy conversion research program, Allison Division research engineers have developed a proposed thermal energy storage system for an earth satellite which can be used with either a thermomechanical or thermoelectric energy conversion system. The proposed system uses the latent heat of fusion of lithium hydride as the means for storing energy and has the potential of storing enough energy to supply up to 45 watt-hr per lb of storage system weight. This output is somewhat greater than that currently being predicted for rechargeable storage batteries and regenerative fuel cells.

An orbiting earth satellite spends a considerable portion of time in the shadow of the earth. At altitudes less than 1,000 miles a satellite may spend a maximum of 35 to 40 minutes shaded from the sun. If the operation of the satellite's power plant is dependent upon the conversion of solar energy to electrical energy by such methods as solar cells, thermomechanical engines, or thermoelectric devices, and if equipment within the satellite is to operate continuously, some means must be provided to store the converted solar energy needed to operate the power plant when the satellite passes through the shaded portion of its orbit.

The methods available for storing energy may be divided into three categories: (a) electrochemical, which includes batteries and fuel cells, (b) mechanical, which could be springs or flywheels, and (c) thermal. The thermal method may use either the sensible heat associated with a temperature change, the latent heat in a phase change, or other thermodynamic processes involving heat, such as the heat of formation or dissociation.

As part of a broad energy conversion research program at Allison Division, work has been conducted on a study of thermomechanical and thermoelectric energy conversion systems and thermal energy storage systems for solar powered earth satellites. One phase of this study concerned a review of the present state of the art regarding the electrical output provided by electrochemical and mechanical energy conversion and storage systems. The remainder of the study was devoted to developing a proposed thermal energy storage system for use with either a thermomechanical or thermoelectric energy conversion system. The system proposed by Allison researchers provides more electrical output per lb of storage system weight than is provided by currently available or feasible electrochemical systems for earth satellite application.

Weight Problems Limit Electrochemical Storage Systems

Batteries and fuel cells are prime examples of one way to store and generate energy by electrochemical means. Batteries, which can be fully discharged at low drain rates, have very high energy storage capacities.

For application as an earth satellite energy storage system, nickel-cadmium batteries can be expected to deliver as much as 20 watt-hr per lb of storage system weight. The familiar lead-acid batteries will deliver 12 watt-hr per lb[1]. Rechargeable silver-zinc batteries, with a capacity of from 30 to 40 watt-hr per lb, are now available[2,3]. Capacities of from 60 to 80 watt-hr per lb for these batteries have been mentioned (references 2 through 7) but are not presently possible. Such capacities would be for one-discharge use at low drain rates. However, batteries applied to an earth satellite energy storage application would require as many as 6,000 charge-discharge cycles per year. Complete discharge during each cycle would greatly exceed the endurance capabilities of batteries. One solution would be to discharge the batteries only 10 per cent of their one-discharge capability, but this would impose a weight penalty.

A fuel cell, usually considered to be a primary energy source, has the inherent disadvantage of other fuel expending power sources. A fuel-cell system, however, can be designed which is regenerative. That is, with the proper choice of reactants, the electrical output of the primary conversion system can restore the products of the reaction to its original constituents by electrolysis. Fuel cells have been designed with a capacity as high as 300 watt-hr per lb[2,4]. This output, however, can be realized only over longer discharge periods than are encountered in an earth satellite application. Available regenerative fuel cells have capacities of approximately 10 watt-hr per lb for the length of energy storage time involved in low-altitude earth satellite applications[1].

Stress Problems Limit Mechanical Energy Storage Systems

Flywheels and springs have been used as dynamic energy storage systems for many applications of short duration, thus indicating their consideration for earth satellite use.

For use as an energy storage system in a satellite, a flywheel would drive an electric generator during the shaded portion of the orbit and would restart the conversion device when the satellite passed into the lighted portion of the orbit. (This assumes that a rotating conversion device is used.) The ideal energy content of a flywheel, which can be easily determined, has a limiting value because of stress considerations. A fly-

By CURTIS L. WALKER
and
JAMES D. MATCHETT
Allison Division

Energy stored by the latent heat of fusion

wheel with its weight concentrated at the rim is limited to an energy storage capacity of approximately 10 watt-hr per lb.

The rotating speeds required to store 10 watt-hr per lb in a moderately sized flywheel would be very high. In addition to bearing problems, the gearbox needed for these speeds could easily weigh as much as the flywheel. Another problem would be inertial effects, which would cause a satellite to spin when energy was taken from a single flywheel. This problem could be alleviated by using two counterrotating flywheels.

The problems inherent in an energy storage system using a flywheel suggest that a reliable flywheel capable of storing as much as 10 watt-hr per lb of usable energy per lb of flywheel system weight seems optimistic.

The use of springs as a dynamic energy storage system for an earth satellite is unreasonable because they have a capacity on the order of only 0.10 watt-hr per lb.

Thermal Energy Storage System Based on Latent Heat of Fusion

The storage of energy as heat is not a new idea. Yet, despite many favorable factors, thermal energy storage systems for space satellites have apparently received only a small fraction of the attention that other energy storage devices, such as batteries, have received. Nevertheless, the problems associated with thermal energy storage appear no more formidable than the problems which still confront the other energy storage methods suitable for satellite application.

Exploring the possibilities of using thermal energy for an earth satellite application, Allison researchers developed a proposed solar-to-electrical energy conversion system using a thermal energy reservoir (Fig. 1).

One problem involved in the development of the proposed system was to find the proper thermal storage material which would have such desirable properties as:

- High heat capacity
- High heat of transformation during a change of state
- Ability to operate near the peak temperature of the thermodynamic cycle being considered.

Since the conversion system would require a constant temperature output, a sensible heat storage could not be used because of the wide temperature excursions required. The use of the latent heat of vaporization would lead to undue bulk and problems of boiling in a gravity-free environment. The most promising means for storing energy, therefore, appeared to be the use of latent heat of fusion, where a material changes from a solid state to a liquid state at a constant melting temperature.

Studies were made of several elements and compounds having high heat of fusion and melting points in a usable range for common thermodynamic cycles. One compound which satisfied the requirements for a thermal storage material was lithium hydride[8]. This material has an estimated heat of fusion of 4,700 ± 600 cal per mole[9] (900 to 1,200 Btu per lb), which is considerably higher than any other material. Lithium hydride also has a useful melting point temperature of 1,256° F. The material, therefore, has a thermal storage capacity of approximately 260 watt-hr per lb. Additional properties of lithium hydride (LiH) are:

Specific heat = 1.0 Btu per lb °F

Thermal conductivity = 4.2 Btu per hr-ft- °F

Density at 20° C = 48.5 lb per cu ft

Density of melt = 36.1 lb per cu ft.

Once a suitable thermal storage material was decided upon, a proposed design was then developed for a solar absorber, heat reservoir, and heat transfer loop (Fig. 2). The reservoir heat exchanger is designed as a group of individually encased, conically shaped slugs of LiH. When the satellite is in the rays of the sun, the solar energy melts the LiH and energy is stored. When the satellite passes in the shadow of the earth, the LiH freezes and thermal energy is delivered to the system.

The slugs of LiH take heat from a heat transfer fluid (one of the alkali metals or their alloys) as it comes from the solar collector and rejects the fluid at a nearly constant temperature. During the shaded portion of the satellite's orbit, the heat exchanger continues to reject the fluid at a constant temperature which is near the phase change temperature.

In the proposed design of the heat reservoir, the lithium hydride accounts for approximately 60 per cent of the total weight of the energy storage system, although some of the weight should not be charged entirely to the heat reservoir. This reduces the storage capacity to approximately 150 watt-hr per lb.

The engine used to drive the satellite's power generator could be a typical mercury vapor turbine engine, with a possible efficiency of approximately 10 per cent, or a recently developed reciprocating engine operating on the Stirling cycle, which has developed efficiencies as high as 40 per cent.

An energy conversion system efficiency range of 10 to 30 per cent results in an

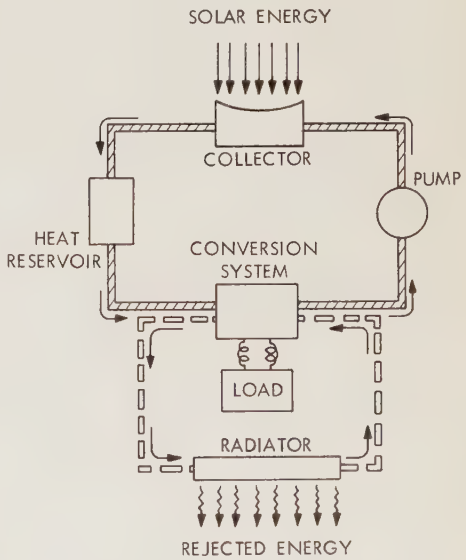

Fig. 1—This diagram illustrates a solar-to-electrical energy conversion system proposed by Allison Division which uses a thermal energy, or heat, reservoir. This system, which would store energy for use when an earth satellite passed through the shaded portion of its orbit, could operate continuously without the problems inherent in a restarting system.

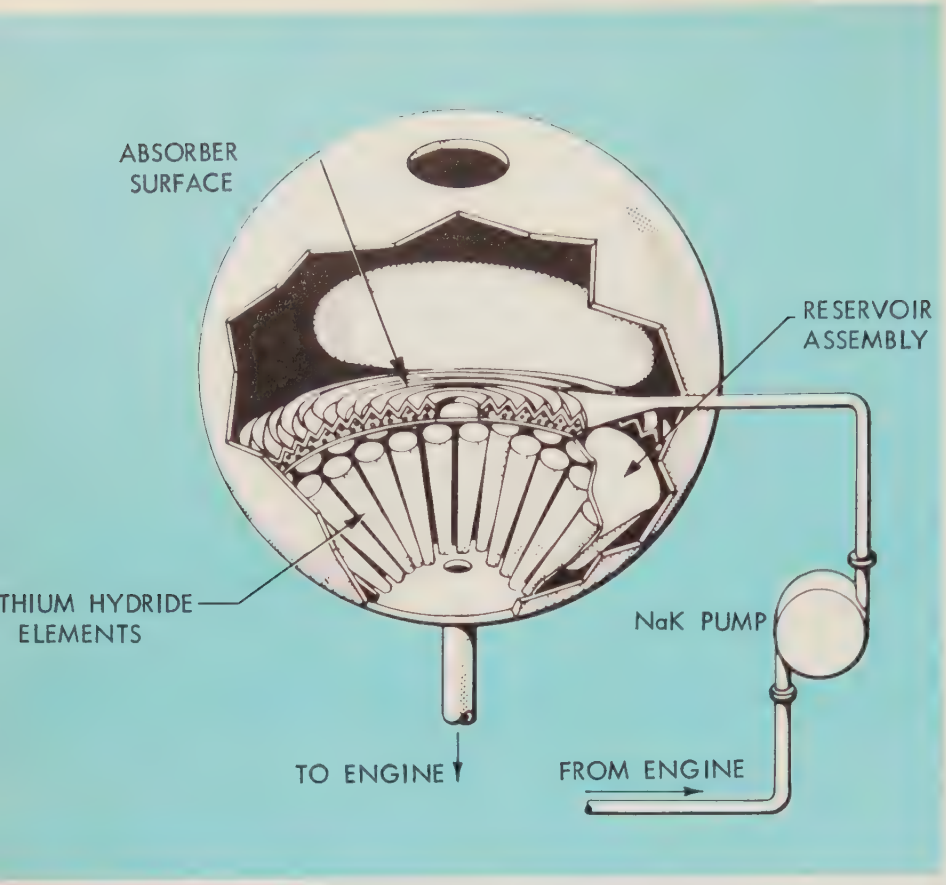

Fig. 2—This is a proposed design of a solar absorber, heat reservoir, and heat transfer loop for converting solar energy to electrical energy in an earth satellite during the period when it passes through the shaded portion of its orbit.

Solar energy, concentrated by a collector, passes through the aperature and hits the absorber surface, where the solar energy is converted to thermal energy. A liquid metal circulating system transfers the heat to the heat reservoir assembly, which consists of a group of conically shaped stainless steel cones containing lithium hydride. The slugs of lithium hydride take heat from the circulating liquid metal, such as sodium-potassium alloy (NaK), and rejects the fluid at a nearly constant temperature. The heat of fusion of lithium hydride is used for the thermal energy storage process. When the satellite is exposed to the sun, the excess solar energy melts the lithium hydride and energy is stored. When the satellite is in the shadow of the earth, the lithium hydride freezes and thermal energy is delivered to the system.

The slugs of lithium hydride are placed with the thickest portion at the heat transfer fluid inlet where the heat absorption and heat rejection will be greatest. This causes the fusion front to become parallel to the centerline of the slug so that isolated pockets of the material are not formed, thereby improving the efficiency of the process. In this design, the lithium hydride accounts for approximately 60 per cent of the total storage system weight and can potentially store enough energy to supply up to 45 watt-hr of electrical output per lb of storage system weight.

electrical output-to-storage system weight of from 15 to 45 watt-hr per lb. With further developmental work on both the heat exchanger and purity of the lithium hydride, it is expected that values as high as 60 watt-hr per lb can be attained.

Conclusions

In regard to the electrochemical and mechanical energy storage systems studied, the following conclusions can be drawn:

- Despite the potential ability of batteries with high storage capacities, a penalty in weight must be paid for the rapid charge and discharge rates required for earth satellite application
- Fuel cells of the regenerative type, although quite durable and reliable, also have too much weight
- A flywheel with weight concentrated at the rim is limited in energy storage capacity by stress considerations.

The thermal energy storage system proposed by Allison researchers, on the other hand, offers a distinct energy output-to-weight advantage over the other energy storage systems (Table I). Because it operates continuously, the proposed system eliminates the problem of starting and stopping the energy conversion device each time the satellite passes from the shaded to the unshaded portion of its orbit. The system also is unaffected by cyclic operation, high temperatures, and the absence of gravity—problems which seriously affect other systems.

COMPARISON OF ENERGY STORAGE SYSTEMS

ENERGY STORAGE SYSTEM	USABLE STORAGE CAPACITY (WATT-HR PER LB)
BATTERIES	3 to 4
FUEL CELLS	10
FLYWHEELS	10
LITHIUM HYDRIDE	15 to 45

Table I—This listing indicates the advantage in energy storage capacity provided by the proposed thermal energy storage system using lithium hydride.

Bibliography

1. von Doenhoff, A. E. and Hallissy, J. M. Jr., "Systems Using Solar Energy for Auxiliary Space Vehicle Power," *I.A.S. Report No. 59-40.*
2. Huth, J. H., "Power for Satellites," *A.S.M.E. Paper No. 59-AV-3.*
3. Yardney Silvercel, Technical Bulletin published by the Yardney Electric Corporation, New York, 1953.
4. Eisenberg, M., "Electrochemical Energy Sources for Space Flight Applications," *American Rocket Society Paper No. 866-59.*
5. Rosenblum, L., "Small Power Plants for Use in Space," *Aero/Space Engineering*, Vol. 17, No. 7 (July 1958), p. 30.
6. Vinal, G. W., *Primary Batteries* (New York: John Wiley and Sons, Inc., 1950).
7. Stem, J. M., "Solar-Mechanical Power Plant Design Problems," *A.I.E.E. Paper CP 59-903.*
8. A Compendium of Data on Lithium and Selected Compounds of Lithium, Published by the Lithium Corporation of America, February 1958.
9. Messer, C. E., Lithium Corporation of America. Personal communication between the authors and Mr. Messer, December 11, 1959.

A Study of Residual Stresses in Hardened Steel Induced by Phase Transformations

By DONALD P. KOISTINEN
and RICHARD E. MARBURGER
General Motors
Research Laboratories

Recent advancements in the application of X-ray diffraction techniques to the measurement of residual stresses in hardened steel have made it possible to make studies on the effects of mechanical and thermal treatments in steel which, heretofore, have been impractical. Such studies are being conducted at the General Motors Research Laboratories. One study has resulted in new knowledge on the origin and distribution of residual macrostresses beneath mechanically finished surfaces and those found in exceedingly shallow surface layers on carburized and through-hardened steels. X-ray diffraction methods also are being applied to gain more knowledge on the origin of microstresses in hardened steel and their effect on its mechanical behavior. Progress has been made on obtaining quantitative information on the distribution of microstresses and the changes which accompany tempering.

X-ray diffraction applied to gain more knowledge on stress formation and metal fatigue

THE RECENT DEVELOPMENT of accurate and practicable X-ray diffraction methods for measuring residual stresses in hardened steel has made possible the study of macro and microstresses induced by phase transformations, particularly in thin surface layers. Large residual stresses may be caused by several inherent properties of steel:

- A large volume expansion is associated with the transformation from austenite to the various body-centered cubic phases
- Small changes in chemistry of the steel may cause large changes in the temperature range in which transformations occur
- The hardened structure may exhibit dimensional instability under applied forces, during subsequent heat treatment, or under the combined action of both.

This paper deals primarily with macrostresses in hardened steels and discusses some of the stress distributions found after various processing treatments. The origin of these stresses as deduced from auxiliary X-ray diffraction and metallographic data is described. Also, some preliminary results of a study of microstresses in hardened steels are presented.

Carburizing Produces Residual Compressive Stresses in Case

Carburizing is a surface hardening process whereby carbon is introduced into the surface of an easily fabricated low-carbon steel to produce an extremely hard, long wearing case. It has become increasingly apparent that a valuable by-product of these case hardening treatments is the existence of residual compressive stresses generally found in the hardened surface layers. A widely held theory on the origin of these compressive stresses is that the surface layers have a greater tendency to expand during the hardening process owing to their higher carbon content. Since the core resists this expansion, the surface layers are in compression.

The distribution of residual compressive stresses through carburized cases on numerous steels was studied at the GM Research Laboratories and a consistent distribution pattern was found (Fig. 1). The results of the study tended to disprove the theory on the origin of compressive stresses in hardened surface layers. If the compressive stresses were the result of a greater tendency for the surface layers to expand during the hardening process owing to a higher carbon content, it could then be expected that the maximum compression would occur at or very near the surface. However, the maximum compression occurred at about three-fifths of the case depth for all samples studied. Hence, another explanation was needed for the origin of these stresses.

This was brought about by a further study made on the residual compressive stress distribution in a carburized case on S.A.E. 8620 steel (Fig. 2). This study also showed the distribution of retained austenite through the case, as determined by an X-ray diffraction technique using integrated intensities[1]. In this study the maximum compression again occurred at about three-fifths of the case depth. One important fact which also became apparent was that some relationship existed between the amount of austenite retained and the residual compressive stress.

This relationship was then derived from studies of the austenite-martensite transformation. For low alloy steels the amount of austenite retained is a function of the difference between the ultimate quenching temperature T_q and the M_s temperature[2]. By utilizing X-ray diffraction, it was found that this relationship can be expressed by the following simple exponential equation[3]:

$$V_\gamma = \exp\left[(-6.11)(10^{-3})(M_s - T_q)\right]$$

where

V_γ = the volume fraction of retained austenite

M_s and T_q are in °F.

If the quenching temperature is the room temperature, the M_s temperature at each depth can be calculated from the retained austenite content at that depth. For the sample of S.A.E. 8620 steel studied, the M_s temperature of the core was approximately 700°F. The surface did not start to transform until it had cooled to about 320°F.

Since no large temperature gradients existed in the steel when it had cooled to these low temperatures, it was immediately apparent that transformation in a carburized piece of steel begins in the core and proceeds outward through the case. When the core transforms, the three to four per cent volume expansion accompanying the austenite-martensite

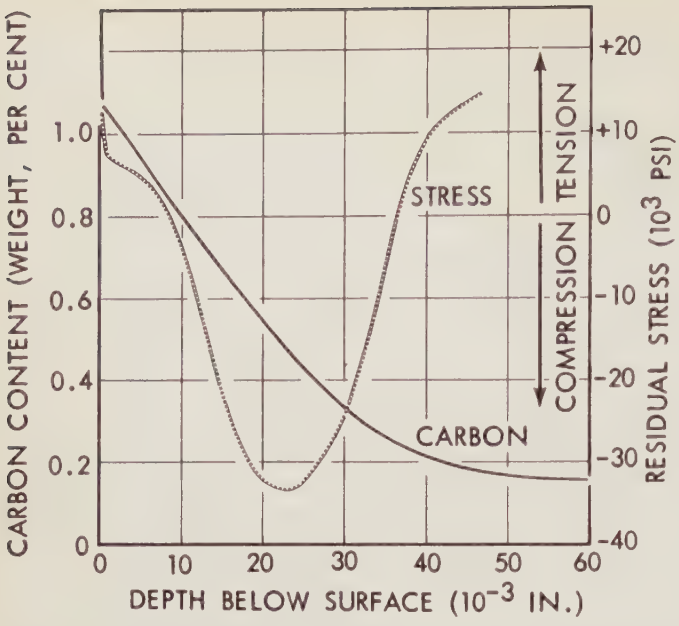

Fig. 1—This graph summarizes the residual stress and carbon distributions through a carburized case on S.A.E. 1018 steel. Data for the carbon distributions were determined at the GM Research Laboratories from chemical analyses of layers removed from a piece heat treated simultaneously with the specimen used for the X-ray measurements of stress. If the case depth is defined as the point where the carbon content becomes the constant value of the base steel, then the maximum compression occurs at about 60 per cent of the case depth. This was true of all samples studied. If the reason why the compressive stresses were formed followed the widely held theory that they are the result of a greater tendency for the surface layers to expand during hardening owing to a higher carbon content, it would be expected that the maximum compression would occur at or very near the surface. However, compression was found to occur at about three-fifths of the case depth.

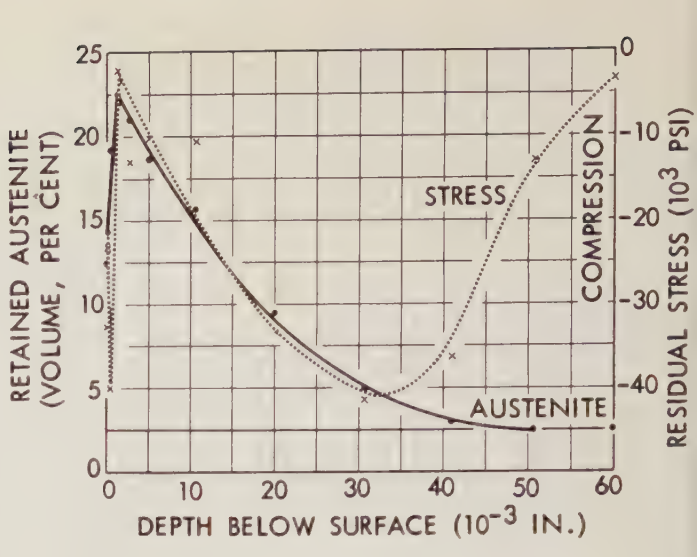

Fig. 2—To arrive at a better understanding of how compressive stresses are induced by carburizing, studies were made on residual stress distribution in carburized steel. This graph shows the residual stress and retained austenite distributions through a carburized case on S.A.E. 8620 steel. The retained austenite varied in the same manner as the carbon content. Increasing the carbon content increased the amount of austenite retained. The case depth, therefore, may be defined as the point where the austenite content becomes the constant value of the core. For this S.A.E. 8620 steel, the maximum compression occurred at about three-fifths of the case depth. This was the same result obtained from the study made on a carburized case on S.A.E. 1018 steel (Fig. 1). Of equal or greater interest was the fact that the slope of the residual stress curve followed the shape of the austenite curve in the region between the point of maximum compression and the surface. It was apparent, therefore, that there was some relationship between the amount of austenite retained and the residual compressive stress.

transformation is easily accommodated by plastic deformation of the soft and ductile austenitic case. But when the case transforms later, the accompanying growth is opposed by the previously transformed core. Hence, the case is in compression. Near the surface, where a large amount of austenite remains untransformed, there is less growth and, therefore, the amount of compression decreases correspondingly (Fig. 2).

Tensile Stresses Induced in Decarburized Surface Layers

Lowering the carbon content in the surface of high carbon steel induces an effect opposite to that of carburizing with respect to the type of stresses generated. Decarburized surface layers have residual tensile stresses.

This was brought out in an electron metallographic study made to determine the origin of a residual tensile stress of 70,000 psi which was measured in the surface layer of a piece of hardened S.A.E. 52100 steel. An electron micrograph of the cross section of the surface layers (Fig. 3) showed a layer of fine pearlite at the surface, indicating a surface decarburization. This pearlite transformation during the quench occurred at high temperature before the interior was transformed to a hardened structure of martensite containing retained austenite and undissolved carbides. As the interior grew during the transformation, it forced the surface layer of pearlite into the tensile stress of 70,000 psi. This stress value is very near the yield strength for pearlite and provided a plausible explanation of why some parts heat treated with this specimen exhibited quench cracking.

Surface Grinding Can Produce Both Tensile and Compressive Stresses

Investigations also have been made on the types of stresses found in mechanically finished parts. One such study was that made of a ground surface on a sample of S.A.E. 52100 steel. This sample was loaned to the GM Research Laboratories by a group engaged in a broad study[4,5] on the residual stresses induced by grinding and their effect on fatigue endurance.

The sample was found to have had an extremely steep stress gradient (Fig. 4) which necessitated application of a previously developed X-ray penetration correction[6]. The corrected stress for the sample varied from 80,000 psi compression at the surface to 40,000 psi tension at a depth of 0.0007 in. Tensile stress existed to a depth of more than 0.003 in. It was apparent that a stress distribution of this type—very large compressive values at the surface and very high tensile stress values immediately beneath the surface—was the result of two separate causes.

If the cause of the compressive stress at the surface were the only one operating, the compressive stress would be balanced by a subsurface tensile stress of relatively low magnitude spread over a rather large volume. Such a distribution was not observed.

The cause of the surface compression was easily attributed to mechanical deformation of the surface layers, but the cause of the high subsurface tensile stresses was not as easy to pinpoint and had to be deduced from auxiliary data. Previous work on the X-ray measurement of residual stresses[6] resulted in a simple

measurement of the width of martensite diffraction lines in terms of $I/(a + b)$, where I is the intensity maximum and a and b are values used in the measurement of macrostresses. The previous work also showed that the width of the diffraction line increased with increasing hardness. When data for the width of the diffraction line, as defined by $I/(a + b)$, were plotted on the same graph showing the distribution of residual stresses with depth (Fig. 4), the diffraction lines increased in width to the same depth as the stress was tensile. A narrow diffraction line at the surface was evidence that the steel was softer in that region—that is, tempering had occurred owing to the heat generated by the grinding process. Previous investigators[7] have shown that there is a significant volume contraction associated with the tempering process in a steel having the composition of S.A.E. 52100. It was concluded, therefore, that the cause of the high subsurface tensile stress was due to a shrinkage of the surface layers as they were tempered while the base material remained unaffected.

Fig. 3—This is an electron micrograph of the cross section of the surface layers of a piece of hardened S.A.E. 52100 steel. This electron metallographic study was made to determine the origin of a residual tensile stress of 70,000 psi which was measured in this surface layer. The hardened structure shown is martensitic containing austenite and undissolved carbides. As can be seen, however, a layer of fine pearlite, approximately 0.0001 in. thick, is found at the surface. Since fine pearlite forms at a high temperature, it obviously formed during the quench before the interior transformed to martensite. As the interior grew during transformation it forced the surface layer of pearlite into the tensile stress of 70,000 psi. This value of stress is very near the yield strength for pearlite and provides a plausible explanation of why some parts heat treated with this specimen exhibited quench cracking.

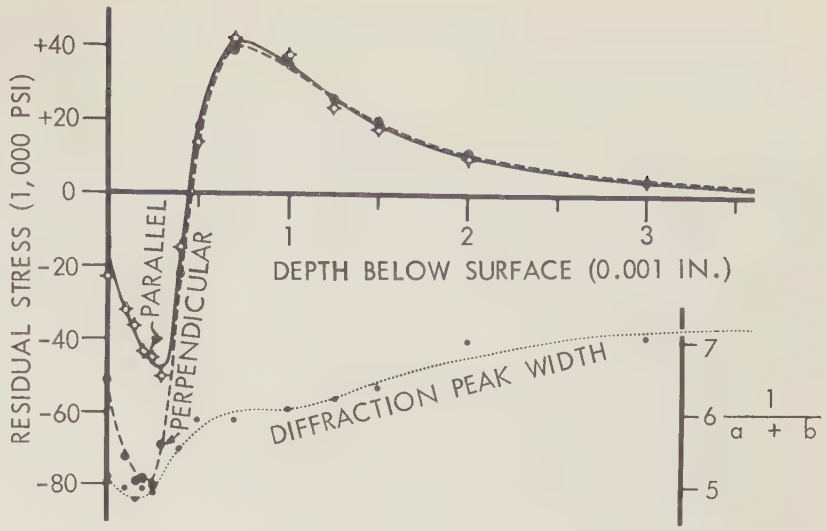

Fig. 4—An example of the type of stresses found in mechanically finished parts is illustrated in this graph which shows the stress distribution beneath a ground surface on S.A.E. 52100 steel. The graph shows the residual stress distributions parallel and perpendicular to the direction of grinding and the variation of X-ray diffraction peak width over the same depth. To handle the steep stress gradients found in this sample, it was necessary to develop an X-ray penetration correction. The corrected stress varied from 80,000 psi compression at the surface to 40,000 psi tension at a depth of 0.0007 in. The tensile stresses existed to a depth of more than 0.003 in. A stress distribution of this type—very large compressive values at the surface and very high tensile stress values immediately beneath the surface—is the result of two separate causes. The surface compression is ascribed to mechanical deformation of the surface layers. The source of the high subsurface tensile stress, however, requires more of an explanation.

Previous to this study of stresses induced by grinding, a simple method was developed for measuring the width of martensite diffraction lines in terms of $I/(a + b)$, where I is the intensity maximum and a and b are values used in the measurement of macrostresses. It also was found that the width of the diffraction line increased with increasing hardness.

When data for the width of the diffraction line, as defined by $I/(a + b)$, were plotted along with the distribution of residual stresses with depth, the diffraction lines increased in width to the same depth as the stress was tensile. The narrower diffraction line at the surface was evidence that the steel was softer in this region—that is, tempering had occurred because of the heat generated by the grinding operation. In steel of this composition, it has been found that there is a significant volume contraction associated with the tempering process. It may be concluded, therefore, that the tensile stress is due to a shrinkage of the surface layers as they are tempered while the base material remains unaffected.

Under some grinding conditions, only the surface compressive stresses have been observed (no subsurface tensile peak). This implies that little if any heating of subsurface layers occurred during the grinding and only the mechanical deformation at the surface generated residual stresses. Under other grinding conditions the stresses were tensile from the surface to the interior, indicating that the shrinkage due to the heating is of greater consequence than the mechanical deformation of the surface layers.

Preliminary Studies Made on Microstress Distribution in Steel

All of the studies discussed so far were possible, in theory at least, because some mechanical method could be used to measure macrostresses. The study of microstresses, however, appears to be the exclusive domain of X-ray diffraction methods.

The GM Research Laboratories is now conducting a study of microstresses in hardened steels with the aim of defining their origin and effect on the mechanical behavior of steel. It is apparent that the extremely broad X-ray diffraction lines of hardened steel reflect a wide distribution of microstresses generated by the austenite-martensite transformation. To reach any conclusions regarding the association of these stresses with the crystallography of the transformation, it is necessary to obtain quantitative information on the distribution of the microstresses. Preliminary results in this area have been obtained.

Studies were made on a series of S.A.E. 52100 steel samples which were austeni-

tized at 1,550°F, oil quenched, and tempered at various temperatures up to 1,000°F. Plots were then made of the martensite (211) diffraction line of each specimen. A typical result was that obtained from the specimen tempered at 600°F (Fig. 5). The plot showed an extremely broad peak, being more than 20° wide from background to background. Under conditions of the experiment, instrument broadening was less than 1/20 of the width of this peak and did not have a significant effect on its shape.

Experience gained in developing a method for measuring macrostresses indicated that it was first necessary to correct the raw data for significant Θ-dependent intensity factors and for the background[6]. The next step was to plot the intensity as a function of the interplanar spacing d rather than the diffraction angle 2Θ. It was believed that if the broad peak represented a symmetrical distribution of microstrains in the steel, it would be symmetrical as a function of the interplanar spacing d but not necessarily as a function of the diffraction angle 2Θ. The results obtained are shown as the solid black line in Fig. 6. The corrected peak is symmetrical within the experimental error.

Having achieved symmetry, an attempt was then made to determine a mathematical expression for the data. If lattice distortion were the predominant cause of the wide diffraction peak, then a normal probability density function (Gaussian distribution) would be expected[8]. An attempt was made to fit a Gaussian distribution to the data.

A Gaussian whose parameters were determined from the maximum point and width at 60.7 per cent of the maximum was found to be too narrow at the base. A large fraction of the intensity in the tails of the experimental curve (Fig. 6) was left unexplained. A similar difficulty was encountered if other distributions, such as the Lorentzian $A/(1 + k^2x^2)$, were fitted to the peak. However, one method used in the attempt to fit a Gaussian distribution to the data gave a clue to the true distribution. In this method, the cumulative per cent of the total intensity was plotted at equal increments of the interplanar spacings d on probability scale graph paper. This paper is designed so that if the distribution is Gaussian, the cumulative per cent of the total population at equal intervals of the other variable will plot as a straight line. The experimental data gave a zig zag line. This was interpreted as the superposition of two Gaussians symmetrical about the same line.

An exact analytical expression for the intensity distribution through the diffraction peak was achieved as follows. The parameters for a Gaussian were determined from the tails of the experimental curve where the intensity dropped below 20 counts per sec (Fig. 6). It was found that an exact fit could be made to the tails by a Gaussian of standard deviation $\sigma = 0.0083$Å. The intensity of this Gaussian was then calculated at 0.001Å intervals (the larger solid points in Fig. 6) and subtracted from the corrected experimental intensity. The remaining intensity was found to be a symmetrical curve (dashed line Fig. 6). This curve proved to be a Gaussian of $\sigma = 0.0043$Å.

Within a very small error, therefore, the experimentally determined intensity distribution through the (211) diffraction line can be expressed mathematically as a sum of two Gaussian distributions of significantly different parameters:

$$I(d) = I_1 \exp\left[-\frac{(d - d_0)^2}{2\sigma_1^2}\right] + I_2 \exp\left[-\frac{(d - d_0)^2}{2\sigma_2^2}\right]$$

where

d = interplanar spacing
d_0 = mean interplanar spacing
σ_1 and σ_2 = standard deviations.

The martensite (200) line for this specimen also can be expressed as a sum of two Gaussians. In fact, these two different diffraction peaks can be fitted with the sum of two Gaussians for the entire tempered series. As the diffraction peak gets sharper upon tempering, the two standard deviations σ_1 and σ_2 for a given line decrease in a related manner.

If it is assumed that these two Gaussians reflect some physical reality in the steel—that is, that there are actually two distinct

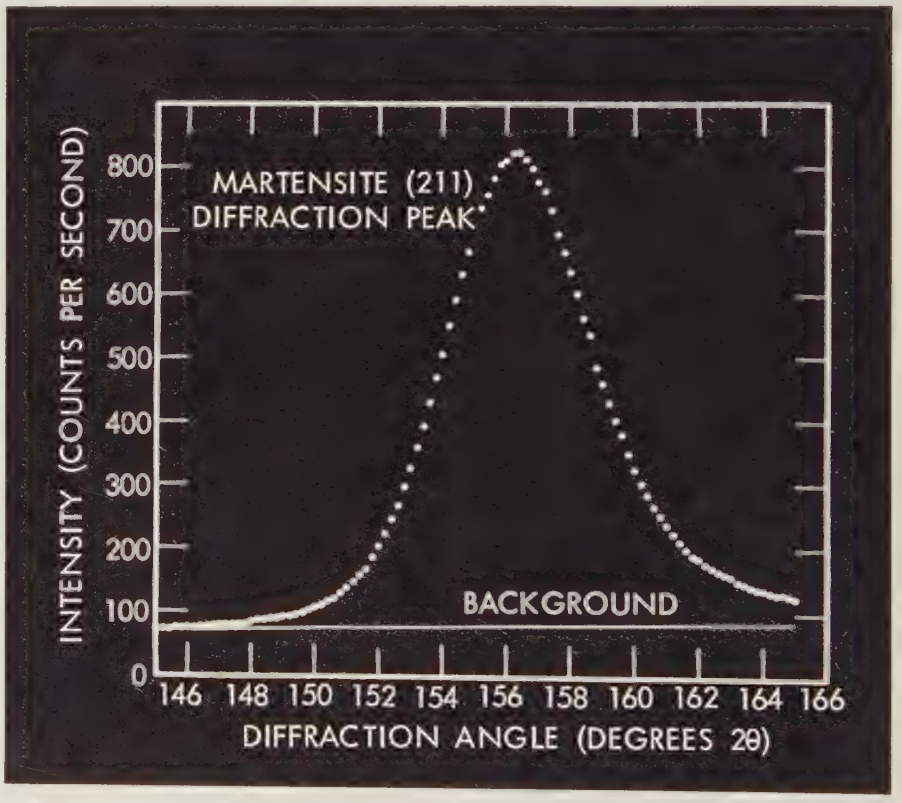

Fig. 5—The martensite (211) diffraction line of a specimen of S.A.E. 52100 steel tempered at 600° F shows the asymmetrical intensity distribution above a background, represented by the solid line at the bottom of the graph. The background was determined from studies using an austenitic manganese steel which had no diffraction line in this angular range. As can be seen, the peak is extremely broad, being more than 20° wide from background to background. It was believed that if the broad peak represented a symmetrical distribution of microstrains in the steel, it would be symmetrical as a function of the interplanar spacing d but not necessarily as a function of the diffraction angle 2Θ. As a result, the experimental intensity was corrected and plotted as a function of the interplanar spacing rather than the diffraction angle. The corrected diffracted intensity is shown as the solid line in Fig. 6.

distributions of microstresses in the steel —the following questions might then be asked concerning the nature of the austenite-martensite transformation:

- Are there two distinct modes of transformation or two separate habit planes?
- Does the plate-like shape of martensite crystals restrict the degree of microstrain in one dimension to a smaller value than in the other direction?

Questions such as these indicate the direction research is heading as regards the origin and distribution of microstresses in steel.

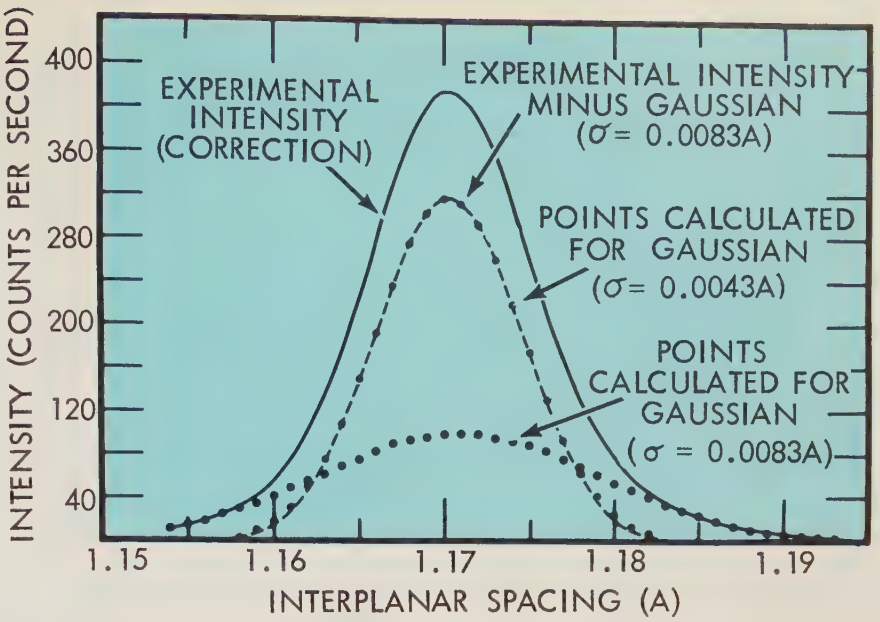

Fig. 6—This plot shows the symmetrical distribution of the corrected diffracted intensity (Fig. 5) as a function of the interplanar spacing. Also shown is the fit of this distribution to the sum of two normal probability density (Gaussian) functions. The parameters for a Gaussian were determined from the tails of the experimental curve, where the intensity dropped below 20 counts per second (cps). An exact fit was made to the tails by a Gaussian of standard deviation of $\sigma = 0.0083$A. The intensity in this Gaussian was then calculated at 0.001A intervals (plotted as the larger solid points) and subtracted from the corrected experimental intensity. The remaining intensity was a symmetric curve, as shown by the dashed line. This curve was a Gaussian of $\sigma = 0.0043$A, as indicated by the excellent fit to the smaller solid points which were calculated, at 0.001A intervals, from a Gaussian of this parameter. Thus, within a very small error, the experimentally determined intensity distribution through the (211) diffraction line was expressed as the sum of two Gaussian distributions of significantly different parameters.

Summary

The X-ray diffraction measurement techniques used by the GM Research Laboratories have helped to provide valuable information on residual stresses in hardened steel and how such stresses are introduced by various processing means.

Investigations on carburized steels indicate a close relationship between phase composition and residual stress distributions through the carburized case. Results have shown that residual compressive stresses are caused by the expansion which accompanies the austenite-martensite transformation in the case after the core has transformed.

Studies made on residual stresses in ground surfaces on steel show that compressive stresses are developed at the surface and tensile stresses immediately beneath the surface. The cause of the surface compression has been ascribed to the mechanical deformation of the surface layers during the grinding process. The tensile stresses are due to a shrinkage of the layers immediately beneath the surface as they are tempered while the base material remains unaffected.

Basic studies are presently being made on the origin and distribution of microstresses in hardened steel. The broad X-ray diffraction lines of hardened steel reflect a wide distribution of microstresses generated during the austenite-martensite transformation. The use of X-ray diffraction has shown that the distribution of microstrains in martensite can be expressed mathematically. The form of the mathematical expression suggests that there may be two distinct modes, or mechanisms, operating during the austenite-martensite transformation. The exact nature and relationship of these two mechanisms are the object of further research.

Bibliography

1. Averbach, B. L., and Cohen, M., "X-Ray Determination of Retained Austenite by Integrated Intensities," *Transactions of the American Institute of Mining and Metallurgical Engineers*, Vol. 176 (1940), p. 40.
2. Harris, W. J., and Cohen, M., "Stabilization of the Austenite-Martensite Transformation," *Transactions of the American Institute of Mining and Metallurgical Engineers*, Vol. 180 (1949), p. 447.
3. Koistinen, D. P., and Marburger, R. E., "A General Equation Prescribing the Extent of the Austenite-Martensite Transformation in Pure Iron-Carbon Alloys and Plain Carbon Steels," *Acta Metallurgica*, Vol. 7 (1959), p. 59.
4. Letner, H. R., "Influence of Grinding Fluids Upon Residual Stresses in Hardened Steel," *Transactions of the American Society of Mechanical Engineers*, Vol. 79 (1957), p. 149.
5. Tarasov, L. P., Hyler, W. S., and Letner, H. R., "Effect of Grinding Conditions and Resultant Residual Stresses on the Fatigue Strength of Hardened Steel," *Proceedings of the American Society for Testing Materials*, Vol. 57 (1957), p. 601.
6. Marburger, R. E., and Koistinen, D. P., *X-Ray Measurement of Residual Stresses in Hardened Steel*, presented at the Second Symposium on Internal Stresses and Fatigue in Metals, sponsored by the General Motors Research Laboratories, (New York: Elsevier Publishing Company, (1959), pp. 98-109.
7. Balluffi, R. W., Cohen, M., and Averbach, B. L., "The Tempering of Chromium Steels," *Transactions of the American Society for Metals*, Vol. 43 (1951), p. 497.
8. Warren, B. E., and Averbach, B. L., "The Effect of Cold-Work Distortion on X-Ray Patterns," *Journal of Applied Physics*, Vol. 21 (1950), p. 595.

Diffusion—A Means of Semiconductor Device Fabrication

From the theory on the use of semiconductor materials, it is known that the proper functioning of a semiconductor device, such as a transistor, depends upon the presence of a small amount of a certain impurity in the material. In the fabrication of such devices, therefore, the placement and the concentration of impurities are important requirements—placement being the more stringent of the two. Impurity placement is done by two basic techniques: *alloying* and *diffusion*. Alloying, although well adapted to device fabrication, has some limitations such as uneven penetration over large areas and difficulty in controlling the precise depth of penetration in certain applications. The diffusion technique is an improvement over alloying; however, it is somewhat complicated and not completely understood. Thus, researchers are seeking more knowledge of diffusion and its application to fabrication of semiconductor devices. At Delco Radio Division, studies of germanium and silicon diffusion technology have shown that impurities can be precisely placed over large areas and that nonhomogeneous impurity distribution can be used to advantage in devices. These studies also resulted in a relatively easy bench method of measuring impurity distribution. Such measurement is one of the problems hampering diffusion research.

THE ACCURATE CONTROL of impurity placement and concentration in semiconductor materials is a necessity for the fabrication of semiconductor devices. Exceedingly small amounts of impurities are required[1,2]. As an indication of the amounts, it is sufficient to say that traces of impurities which defy detection by chemical analysis methods can alter the resistivity of a monocrystal semiconductor by several orders of magnitude.

The placement of the impurities is the more stringent requirement because of the extreme precision with which they must be located. Often, the physical dimensions determining location must be held to 0.0001 in. ±0.00003 in., a realm beyond that of machining operations. Two basic techniques used for such placement are *alloying* and *diffusion*.

A brief analysis of the alloying technique and some of its limitations will aid in understanding why diffusion is being studied in a search for improved devices.

Alloying Process Has Limitations in Device Fabrication

In the alloying process a selected impurity, such as gallium, is diluted in a solvent metal preform which then is placed in contact with the semiconductor and heated in suitable graphite restraining fixtures (Fig. 1). When equilibrium is reached at a certain temperature, a definite volume of semiconductor, which is proportional to the volume of solvent, is dissolved. When the system cools, the semiconductor recrystallizes onto the undissolved material as a single crystal. A fixed proportion (which is only a tiny fraction of the total amount present) of the impurity and solvent freeze in the semiconductor lattice. In power transistors fabricated by Delco Radio Division, gallium is the impurity, indium is the solvent metal, and germanium is the semiconductor material. Group III elements, such as gallium, have one electron less than the germanium atom they displace and act to dope* germanium *P-type* (positive charge carriers). Conversely, group V elements, such as antimony, are used to dope germanium *N-type*.

The alloying process is well adapted to device fabrication but has certain limitations which can best be illustrated by a discussion of the diffused silicon power rectifier and the diffused base high frequency germanium transistor.

The silicon power rectifier requires a large junction area to achieve its current handling capabilities. The junctions on each side of the wafer also need to be planar and parallel if the diode is to have the maximum reverse voltage inherent in its design. A single region of local penetration of 0.001 in. can reduce the diode voltage rating from 250 volts to 50 volts.

On large areas even penetrations are difficult to obtain by the alloying process. If a fixed volume of semiconductor is to be dissolved, variations in the area wetted by the solvent must necessarily be reflected in depth variations. Simultane-

*The action of introducing impurities into semiconductor materials is called *doping*.

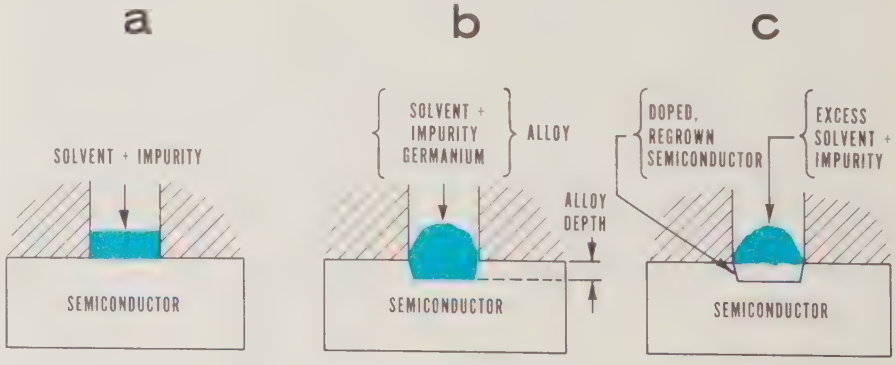

Fig. 1—The three required stages of the formation of an alloy junction are shown here. The solvent and the impurity are placed in contact with the semiconductor and heated (a). When equilibrium of the solvent-semiconductor system reaches a certain temperature, a definite volume of semiconductor, which is proportional to the volume of solvent, is dissolved (b). When the system is cooled, the semiconductor recrystallizes onto the undissolved material as a doped single crystal (c). The solvent takes on a rounded shape after melting due to surface tension forces.

By Dr. ROBERT F. MILLER
Delco Radio
Division

Advantages: more accurate impurity placement, improved electrical properties

ous wetting by the solvent metal does not always occur because of localized time delays caused by microscopic irregularities on the surface of the semiconductor. A delay in wetting results in an uneven alloy front at equilibrium (Fig. 2). Alloying in silicon also introduces strains on the material increasing the probability of electrical and mechanical rejects. Diffusion overcomes these disadvantages and, in addition, permits the introduction of higher impurity concentrations resulting in a smaller reverse leakage current than would be the case using the alloying process (Fig. 2).

High frequency germanium transistors, capable of amplification in the 0.5 to 200-megacycle range, must satisfy two basic conditions. First, the transit time for the electrical carriers within the device must be appreciably less than the time variation of the input signal to minimize attenuation and phase shift of the output. Practically all of this time is required by the injected carriers to traverse the base region between the emitter (injecting) and collector (collecting) junctions. Unlike the vacuum tube, in which the electrons can be accelerated to high velocities by the application of large potentials, the carriers injected into a base region of homogeneous resistivity move only by thermal diffusion—that is, they move from regions of high concentration to regions of low concentration by means of their thermal agitation. This condition necessitates the use of very narrow base widths.

A 200-megacycle transistor would require a P-type germanium base width less than 0.0003 in. In the case of P-type silicon this would be about 0.00018 in. because the carriers move slower than in germanium. The use of N-type germanium or silicon would necessitate a further reduction in the width by a factor of $1/\sqrt{2}$ for each of the respective cases. Such alloying can be accomplished when the penetration is very shallow[3]. However, if the starting wafer must be thick enough for conventional processing (0.003 in.), deep alloying is required for a narrow base width. In this case, the 0.0003 in. dimension of the base is smaller than errors in alloy depth. The problem is analogous to accurately obtaining the difference between two large, nearly identical numbers. If the difference is smaller than the error of either number, the operation cannot be carried out to yield a useful result.

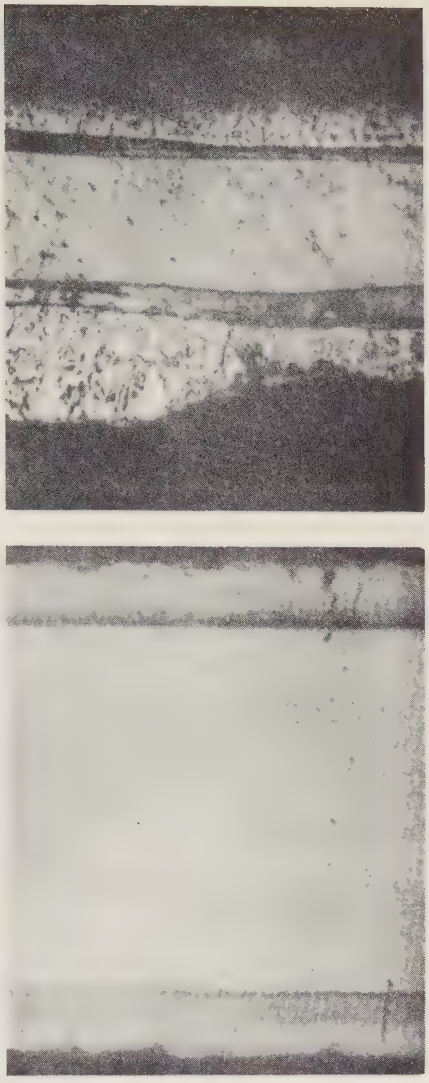

Fig. 2—This comparison illustrates some of the limitations of the alloying process—uneven penetration of the impurity over large junction areas and the difficulty in making the junctions planar and parallel. The top view (magnified 150 times) shows a large area junction in silicon which has an uneven front at equilibrium due to delayed wetting in alloying. Shown at the bottom (magnified 400 times) is a junction in silicon formed by the diffusion technique. This junction is flat, the planarity being limited only by the wafer surface. The edges of this sample are uneven due to the metallurgical stain-etch.

The second basic condition to be met in a high frequency transistor is that the RC (resistance-capacitance) time constants associated with the transistor of mobile charges be smaller than the transit time. A first order approximation to the high frequency equivalent circuit[4] (Fig. 3) shows that the parameters of major interest are the emitter transition capacitance C_{te}, collector capacitance C_c, and a series resistance r_{bb}, between the internal junction areas and the external base connection. These must be minimized. A low value of both C_{te} and C_c is obtained by using a base region of high resistivity—that is, a region between the emitter and collector of a transistor having a low impurity density. The resistance r_{bb} is reduced by increasing the base width and decreasing the base resistivity. Obviously not all of these requirements are compatible.

To overcome some of these inconsistencies in design, proposals[5] were made to use a non-homogeneous base structure which had a low resistivity base of thin width adjacent to the emitter with an abrupt transition to a base region of high resistivity on the collector side. With the application of a reverse voltage across the collector and base contacts (normal bias condition), this region of high resistivity is depleted of carriers and an accelerating electrical field exists there. Consequently, the effective base width for the transit time is only that of the thin, low resistivity region.

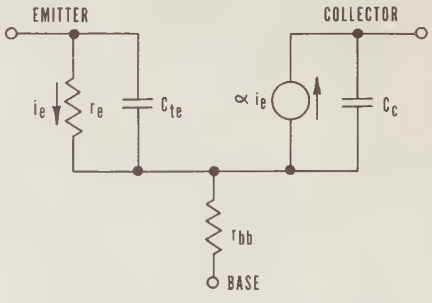

Fig. 3—Some of the problems in circuit design can be analyzed in this equivalent circuit of a high frequency transistor. The emitter transition capacitance C_{te} effectively loads the emitter to base input. Similarly, the collector capacitance loads the output. Both capacitances are charged through the series resistance r_{bb}. The ratio of collector-to-emitter current is α. The resistance r_e is about 20 ohms at 1 ma.

This structure satisfies the theoretical requirements (except for C_{te}) but is impractical to fabricate by alloy methods alone.

Such ideas have since been manifested in the diffused base *drift* and *mesa* transistors (Fig. 4). Not only are the parametric conditions satisfied by the nonhomogeneous base resistivity resulting from the impurity distribution, but the fabrication process permits accurate control. This process is carried out by applying high temperature for a considerable length of time. Impurities can be placed to less than ± 0.000001 in. The high temperatures used in the process (800°C for germanium, 1,150°C for silicon) assure the permanence of the structure at operating temperatures.

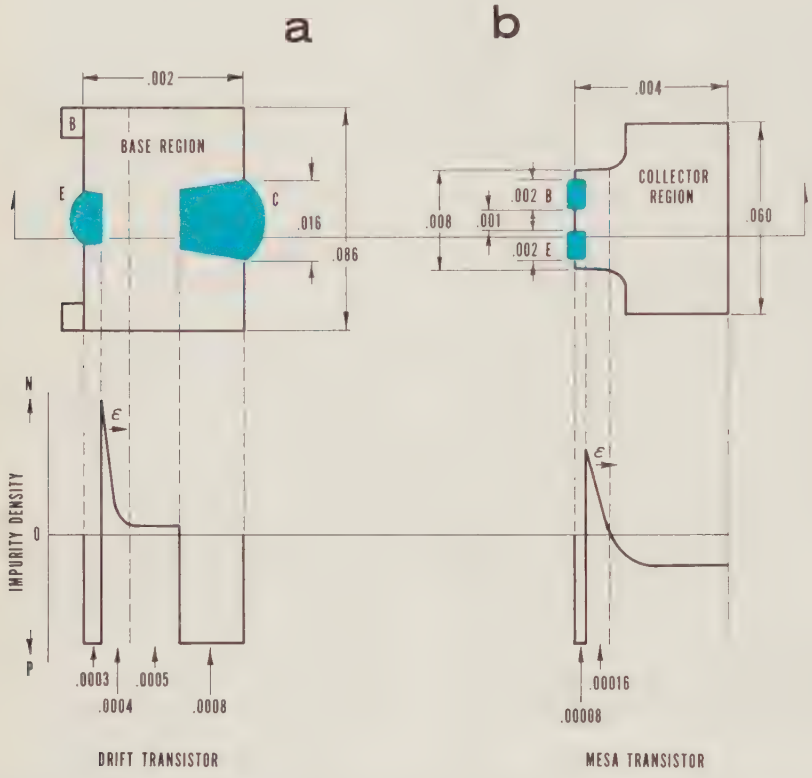

Fig. 4—A cross section view of two high frequency transistor structures is shown here. The bottom views through both units illustrate the relative impurity density. (A high impurity density corresponds to a low resistivity and vice versa.) The *drift* transistor (*a*) combines an alloyed emitter and collector with a diffused base[5]. *N* impurities are diffused into an *N* wafer forming a region of low resistivity adjacent to the emitter and a high resistivity region near the collector. The built-in field due to the impurity distribution ε is called a drift field. The *mesa* transistor (*b*), so named because of its geometric profile, is formed by diffusing *N* impurities into a *P* wafer. The collector thus is formed by diffusion. This transistor is inherently a very high frequency structure. An extremely narrow base region exists between the emitter and collector contacts on both units. The scale has been exaggerated to emphasize the impurity profiles. All dimensions are in inches.

Diffusion Depends on Thermal Motion of Molecules or Atoms

Diffusion theory is being studied and developed by many research workers. Some of the theory, as well as the processing technology, is complex and not completely understood. There are certain mathematical relationships, however, which apply in diffusion work.

Diffusion can be described as the mixing on an atomic scale of two molecular species due to the random thermal motion of the molecules or atoms. The host material as well as the diffusant can be in a solid, liquid, or vapor state. The diffusion effect is analogous to introducing a few drops of dye on the surface of a long column of water. Initially the dyed region forms a visible boundary with the water. After a period of time the dye penetrates to all parts of the column giving an even color. The motion of the dye is observed to be in the direction of its lowest concentration until complete equilibrium is reached.

Fick[6] put diffusion on a quantitative basis by utilizing the following equation of heat conduction:

$$\vec{F} = -D\overrightarrow{\nabla N} \qquad (1)$$

where

F = directed rate of transfer of diffusant
D = diffusion coefficient
∇N = concentration gradient of the impurities.

Germanium and silicon have a face centered cubic lattice structure whose symmetry permits the diffusion coefficient to be isotropic. Thus, D is independent of direction and a one-dimensional analysis can be applied with D treated as a scalar quantity. For diffusion along the x axis,

$$F = -D\left(\frac{dn}{dx}\right). \qquad (2)$$

The values of D differ for various impurities in the host material and, in turn, each D value is an exponential function of the host material's temperature. At a specified temperature and for a diffusant concentration small compared to that of the host material, D is a constant. Combining the law of continuity

$$\frac{\delta F}{\delta x} + \frac{\delta N}{\delta t} = 0, \qquad (3)$$

with equation (2), the following differential equation of diffusion is obtained:

$$\frac{\delta N}{\delta t} = D\frac{\delta^2 N}{\delta x^2}. \qquad (4)$$

For group IV elemental semiconductors, such as germanium and silicon, only the group III (P-type) and group V (N-type) diffusants are of interest. These impurities diffuse through the semiconductor lattice by a substantial mechanism where the impurity occupies a lattice vacancy and then exchanges its position with adjacent sites. Certain fast diffusants, like nickel and copper in germanium and gold in silicon, move in the actual spaces between the host atoms and are termed *interstitial*. For example, at 700°C copper atoms can pass through a ½-in. germanium slab in about 12 minutes. These interstitial diffusants not only contribute to the doping, but can have a deleterious effect on the carrier lifetime because they act as recombination centers. The values of D for many substitutional impurities in germanium and silicon have been published[7]. The comparative penetration of some impurities in germanium and silicon for different temperatures are shown in Table I.

Many solutions to equation (4) exist depending upon the boundary conditions assumed. This discussion will consider only the practical case where

PENETRATION DEPTHS OF VARIOUS IMPURITIES IN GERMANIUM AND SILICON

D (CM² PER SEC)	IMPURITY—DIFFUSION TEMPERATURE °C												PENETRATIONS (THOUSANDTHS OF AN INCH)			
	GERMANIUM						SILICON									
	Sb	As	P	B	In	Ga	Sb	As	P	B	In	Ga	100 SEC	1,000 SEC	10,000 SEC	100,000 SEC
10^{-10}	870	830	—	—	—	—	—	—	1,400	1,400	—	1,380	0.24	0.75	2.4	7.5
10^{-12}	675	640	740	810	880	900	1,280	1,280	1,155	1,155	1,210	1,130	0.024	0.075	0.24	0.75
10^{-14}	530	510	590	720	700	730	1,070	1,060	960	960	1,020	930	0.0024	0.0075	0.024	0.075

Table I—This table shows a comparison of the penetration depths of various impurities in germanium and silicon for a surface concentration N_o of 10^{18} atoms per cc diffused into an existing homogeneous level N_b of 10^{14} atoms per cc. These are theoretical depths based on the solution to equation (4). See equation (5) in Fig. 5. It is interesting to note that the diffusion depth of a 16-hour run would be only twice that of a 4-hour run.

impurities are diffused into a crystal which already has a homogeneous impurity concentration N_b (Fig. 5). The interface at $x = 0$ presents a discontinuity between the source of impurity atoms and the crystal. Therefore, at $t = 0$,

$N(x) = N_b$ for $x > 0$ (inside the crystal)

and

$N = N_s$ for $x < 0$ (outside the crystal).

On solving equation (4) subject to these conditions, the classical solution is obtained, equation (5) (Fig. 5). The implications of this solution are that the diffused distribution is superimposed on the existing distribution and the concentration at the crystal surface comes to an instantaneous equilibrium with the external impurity density N_s. The latter condition is not often found in practice. Smits and Miller[8] have shown that a rate limitation occurs where the actual surface concentration $N(0,t)$ slowly builds up to the limiting value N_o.

The solution for the rate limited case is found by modifying the boundary condition for N_o. If the actual surface concentration $N(0,t)$ differs from N_o, there will be a net flow of impurity

$$\left[N_o - N(0,t)\right] K$$

in or out of the crystal until

$$N(0,t) = N_o.$$

When equation (4) is subjected to this condition, a solution takes the form shown in equation (6) (Fig. 6). This solution contains equation (5) and a

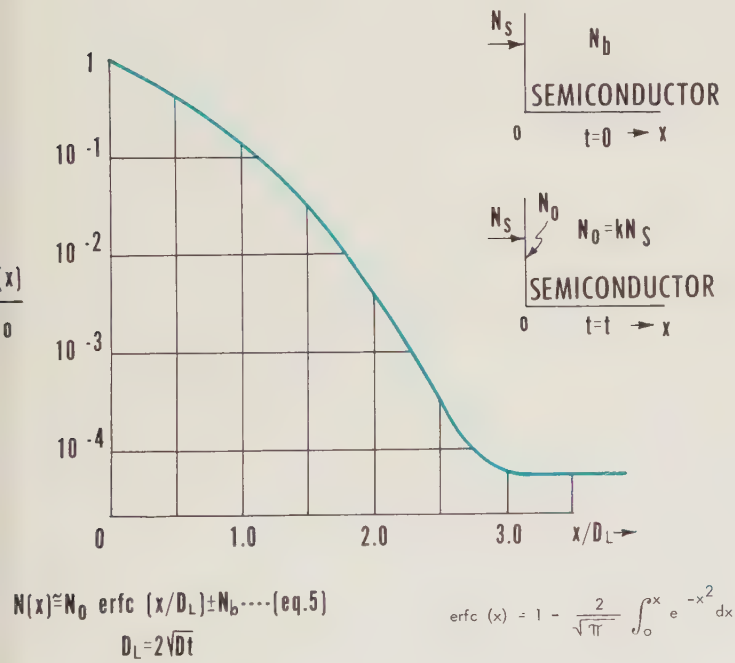

Fig. 5—The classical solution of the diffusion equation for a constant source concentration is a complementary error function. Note that N_o, the surface concentration, is considerably different from the external impurity concentration N_s. They are related by a partition coefficient k. Diffusion length D_L characterizes the curve for a given time and temperature.

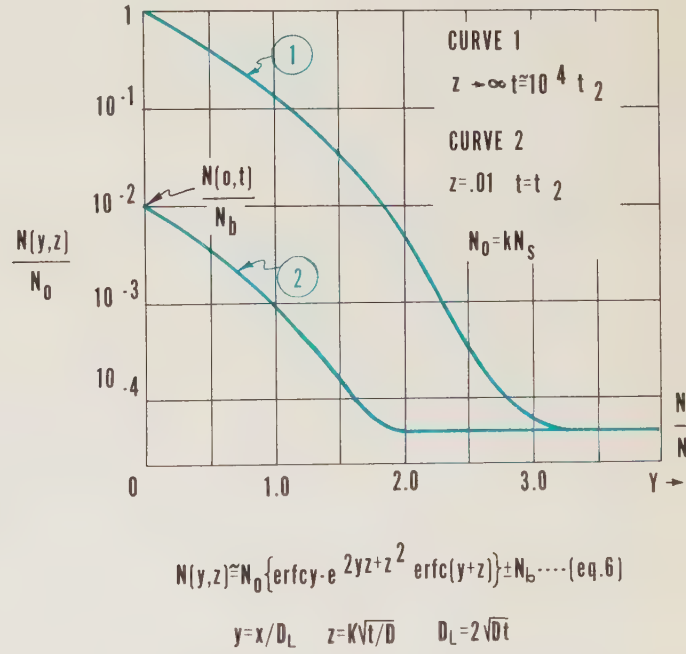

Fig. 6—The solution of the diffusion equation for the rate limited boundary condition is shown for two widely different time conditions. As the time increases, $z \rightarrow \infty$, and the solution approaches that of Fig. 5. For curve *2* insufficient time has elapsed for the surface concentration to have reached its limiting value N_o. For curve *1* the time has been increased by a factor of 10^4 over that of curve *2* and the surface concentration has stabilized at N_o. This value remains unchanged for a further increase in time.

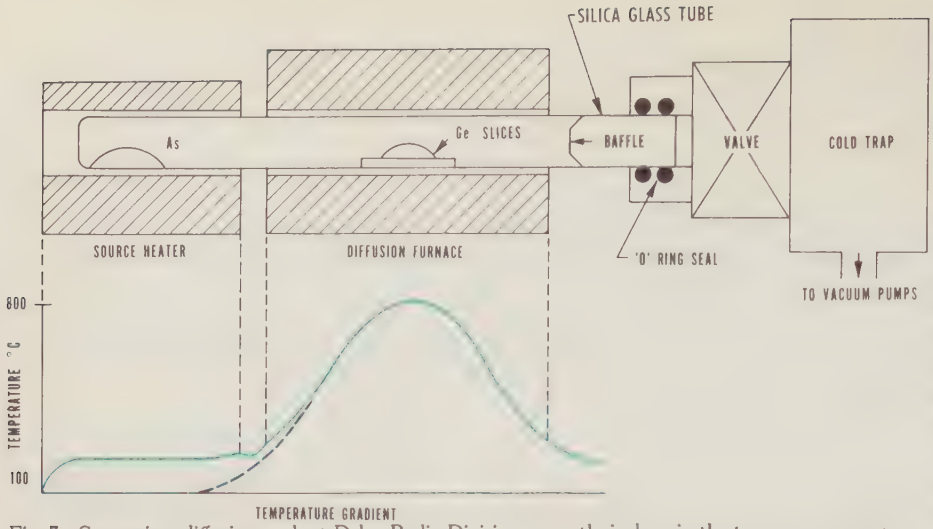

Fig. 7—Germanium diffusion work at Delco Radio Division currently is done in the two-zone, vacuum diffusion system shown here. A molybdenum baffle deflects the arsenic vapor and the cold trap condenses the spent vapors.

correction term which is a function of y and z (Fig. 6). As the length of diffusion time is increased, the rate limitation vanishes,

$$z \longrightarrow \infty ,$$

and equation (6) becomes effectively equation (5).

Germanium and silicon have a maximum solid solubility for a given impurity which, if exceeded, will cause the formation of a liquid alloy phase at the diffusion temperature. This solubility value must not be exceeded if the crystal surface is to be kept undamaged for further processing. For most impurities, this value is about 1 part in 10,000; therefore, only infinitesimal amounts can be used. A variety of processing methods will fulfill this solubility condition. For example, the impurity may be introduced by three methods: (a) in an inert solid and placed on the surface, (b) by a carefully controlled surface reaction, or (c) by the use of a dilute vapor.

Germanium Diffusion Technology

In the studies of diffusion at Delco Radio Division, some useful techniques have been developed applying to diffusion of impurities into germanium and silicon.

Arsenic was chosen as the impurity for diffusion into germanium because it is easily volatilized, it can be obtained in high purity form, and it is a fast diffusant. The Delco Radio studies established that a vapor pressure of about 10^{-5} mm Hg (1/100,000,000 of an atmosphere) is sufficient to give an ultimate N_o of about 10^{16} atoms per cc. This vapor pressure was maintained by keeping the arsenic zone of the diffusion furnace at 100°C (Fig. 7). The germanium was heated to 800°C in this vapor for 12 hours giving a usable diffused layer 0.0013 in. thick.

One of the problems which typifies those encountered in research leading to the present high vacuum diffusion technique was the conversion of N-type germanium to P-type. It was found that copper was entering the diffusion process as a P-type impurity and partially overcompensating the N diffusant. The amount involved was so tiny that only the change in resistivity of the material could be used for its detection. The copper was found to be normally present in the water and nitric acid used in the chemical etching of the wafer prior to diffusion. The problem has been virtually eliminated by the use of an agent which inhibits the deposition of copper and its salts on the wafer and associated handling equipment. In addition, the high vacuum used during the diffusion process caused the copper present in the bulk of the material to be diffused out to the surface where it evaporated.

The oxidation of germanium occurs quite readily at the high diffusion temperatures resulting in an eroded surface which is incapable of being further processed. The use of high vacuum (10^{-5} mm Hg) prevents such effects.

In the course of investigating the degree of oxidation damage done to the surface, it was observed that the impurity distribution obtained by a diffusion made in the presence of a trace of oxygen followed that of equation (5). On the other hand, the continuously pumped vacuum diffusion process (Fig. 7) gives distributions which exhibit rate limitation tendencies as in equation (6), thereby necessitating longer diffusion times for an adequate surface concentration. This possibility can be explained on the basis of a barrier presented to the impurities at

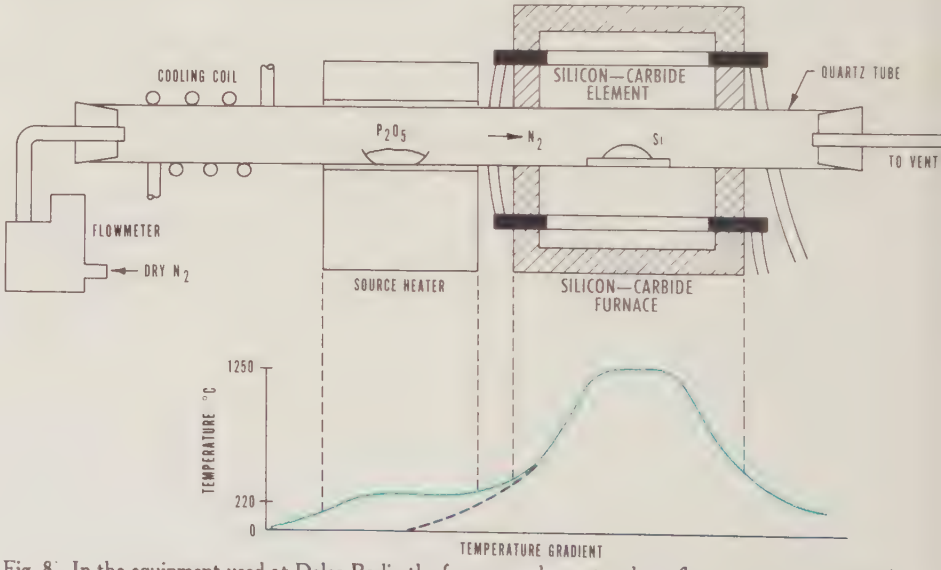

Fig. 8—In the equipment used at Delco Radio the furnace and a metered gas flow system are arranged so that the diffusant vapors are carried over the heated silicon wafers. The vapor source can be heated separately or simply placed in the temperature gradient near the edge of the furnace. It is important that the region between the source and host material be at a temperature higher than that of the source so the diffusant vapor does not condense. The cooling coil is used to prevent decomposition of the rubber stopper and the backflow of vapors.

The conditions for forming a thin P layer suitable for solar cells are to use boron oxide at 1,000° C as a source with the silicon at 1,125° C for two hours. A depth of about 0.00015 in. results. For a deeper N layer, phosphorous pentoxide is used at 220° C, with the silicon at 1,250° C for 12 hours, resulting in a depth of 0.001 in.

the crystal surface. Each atom striking the surface must have enough energy to overcome the barrier, if it is to enter the lattice. Normally, only a small fraction of the atoms have sufficient thermal energy to do this. When oxygen enters the system it forms arsenious oxide with the arsenic vapor. This decomposes at the germanium surface with the release of sufficient chemical energy for the arsenic atoms to instantly overcome the barrier. Conversely, in the high vacuum system, only the thermal energy of the arsenic atoms is available to surmount the surface barrier and a rate limitation results.

Silicon Diffusion Technology

The process technology for diffusion into silicon is simpler than that of germanium, but the theories involved are considerably more complex since they involve complicated surface reactions. Silicon oxidizes readily forming a protective silicon dioxide layer which is impervious to further oxidation up to the oxide evaporation point (1,350°C in a vacuum). The impurities are introduced as vapors of the oxides and chlorides of the group III and V metals. The oxides react with the silicon forming a glassy surface film containing the impurity. The chlorides react with the surface directly forming only an impurity film. Either type of film serves as an instantaneous source of impurity atoms needed for the diffusion. Consequently, the impurity profile is characterized by equation (5).

The temperature of silicon diffusion necessitates a high current, silicon-carbide-element furnace such as the one used at Delco Radio (Fig. 8).

The principal problem in silicon diffusion work is to avoid the deterioration of the electrical carrier lifetime in the bulk of the material. Whether such effects are produced by the introduction into the crystal of extraneous impurities or structural defects, or both, is not known. Regardless of the mechanism, it has been found at Delco Radio that slow cooling at the rate of 4°C per minute following the diffusion process is beneficial.

Measurement of Diffused Layers Is a Research Problem

The investigation of diffusion processes has been hampered by the lack of an easy means for determining the impurity distribution. The use of radioactive diffusants is possibly the only direct approach to locating minute amounts of impurities in a minuscule layer, and this requires highly specialized techniques. The surface concentration N_o and the diffusion depth x_o (this would be the depth where $N(x) \cong N_b$) characterize the profile to a high degree, even for perturbations of the complementary error function distribution.

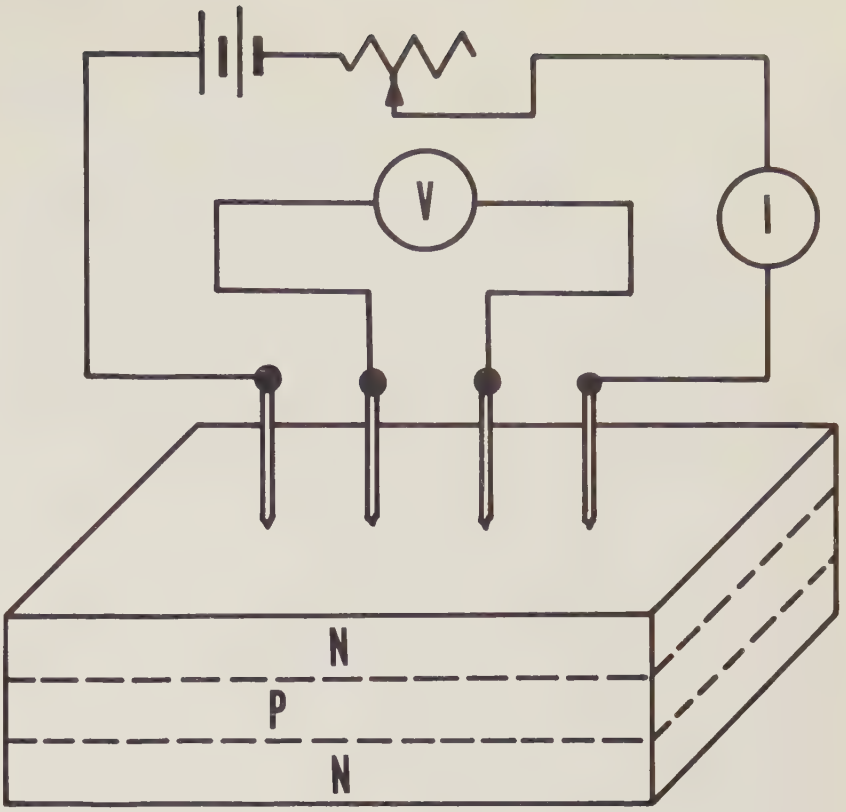

Fig. 9—An N diffused sample is shown in this schematic drawing of a four-point probe method for measuring resistivity. The probes consist of four tungsten points electrically connected. The outer pair permits the passage of current through the sample. The inner probes are placed sufficiently far from the current probes so that the measured voltage drop is only that of the sample resistance and not due to current contact effects. The sample is formed by diffusing into a P-type wafer and then trimming the edges so that a distinct P-N layer is formed. The two lower layers are isolated by the junction and do not enter into the measurement.

The usual practice has been to diffuse N impurities into a P wafer forming a P-N junction. The depth of the junction then can be determined by such methods as metallurgical cross sectioning and etching or by the use of a hot and cold probe connected to a galvanometer. Neither method is very accurate. If N_o is to be determined from x_o by an extrapolation of the theoretical profile, x_o must be known with great accuracy. A 5 per cent variation in x_o can lead to a 300 per cent variation in N_o. On the basis of this, it would be preferable to read N_o directly.

Various laboratory schemes were tried at Delco Radio Division to experimentally determine the impurity profile. All of these schemes involved the removal of thin layers and indirectly measuring the resistance of the layers. A difficulty common to these methods was experienced in measuring the thickness of the removed material (0.00005 in.) due to local surface variations.

As a means of overcoming these difficulties, a four-point probe procedure, which measures resistivity, is being studied further. This method permits the surface concentration to be measured directly and does not involve the removal of thin layers of material. Four tungsten points are used. The two outer points are electrically connected to permit passage of current through the test sample and the inner pair of points are connected to measure a voltage drop (Fig. 9). The sample is formed by diffusing an impurity of opposite type to that already within the host material. In this way the diffused layer is isolated electrically from the bulk of the sample by the P-N junc-

Fig. 10—Delco Radio engineers developed an accurate method for measuring junction depth using the equipment shown here. A toolmaker's microscope *A* is equipped with a hinged electrical probe *B* arranged at the point of focus. The transverse travel of the microscope is geared to a potentiometer *C* permitting distance to be linearly converted into a voltage output. When a small reverse voltage is applied to a P-N junction, practically all of it is sustained at the junction. Thus, if the probe is pulled across a junction, the output of the probe and potentiometer can be applied to an X-Y recorder *D* and a plot of sample voltage versus distance can be directly recorded. The junction is located by the voltage jump.

tion which is formed. The voltage and current readings on a given sample can be used with a correction factor to calculate the total resistance of the diffused layer[9]. The surface concentration is a known function of this layer resistance and, therefore, can be obtained directly without reference to the junction depth. A junction depth x_o can be inferred from the surface concentration by extrapolation along an assumed theoretical distribution pertinent to the actual diffusion conditions.

An accurate means of independently measuring junction depth x_o also has been developed at Delco Radio Division (Fig. 10). This method uses an electrical probe whose transverse travel is measured by a potentiometer to convert distance into a voltage output. The voltage output is shown on an X-Y recorder. The principle of operation is as follows: when a small reverse voltage is applied to a P-N junction of a sample, practically all of the voltage is sustained at the junction. Thus, if the probe is pulled across a junction, the output of the probe and potentiometer can be applied to the X-Y recorder and a plot of the sample voltage versus distance can be directly recorded. The junction is located by the voltage jump. For example, if an N-type layer is to be measured, it is first formed by diffusing into a P sample. The sample is beveled (by lapping) at a small angle such that the relatively narrow diffused region is revealed as an elongated layer almost parallel to the horizontal surface. Under these conditions the junction depth x_o is related to the probe travel L by $x_o = (\tan \Theta)L$. If $\Theta = 2°$ and $L = 0.028$ in., x_o will be 0.001 in. Since L is the measured quantity, small values of Θ permit x_o to be determined accurately. The angle of the bevel Θ is measured by the reflection angle of a narrow beam of light. Monochromatic (sodium vapor) light incident to the sample through a partially silvered optical flat produces interference lines. An even spacing of these lines indicates that the bevel is smooth.

Summary

Diffusion as a means of fabricating devices has two advantages: impurities can be precisely placed, even over large areas, and the nonhomogeneous impurity distribution can be used to advantage to obtain properties beyond the realm of homogeneous materials. The state of the art of diffusion is still in its infancy. As new techniques evolve, not only should many new devices appear, but some of the electrical capabilities of existing devices will be improved.

Bibliography

1. Schwarz, B. A., "A Survey of the Transistor," *General Motors Engineering Journal*, Vol. 2, No. 1 (January-February 1955), pp. 40-47.
2. Rittmann, A. D. and Heckert, W. F., "A Discussion of Transistor Action and Manufacture," *General Motors Engineering Journal*, Vol. 5, No. 3 (July-August-September 1958), pp. 28-33.
3. Rittmann, A. D., Messenger, G. C., Williams, R. A., and Zimmerman, E., "Microalloy Transistor," *I. R. E. Transactions on Electron Devices*, Vol. ED-5, No. 2 (April 1958), pp. 49-51.
4. Hunter, L. P., *Handbook of Semiconductor Electronics*, (New York: McGraw-Hill Book Co., Inc., 1956), pp. 12-3, 12-5.
5. Early, J. M., "P-N-I-P and N-P-I-N Junction Transistor Triodes," *Bell System Technical Journal*, Vol. 33, No. 3 (May 1954), pp. 517-33.
6. Crank, J., *The Mathematics of Diffusion*, (London: Oxford University Press 1956), pp. 2-37.
7. Biondi, F. J., *Transistor Technology*, Vol. III (New York: D. Van Nostrand Co., Inc., 1958), pp. 70-73, pp. 86-89.
8. Smits, F. M. and Miller, R. C., "Rate Limitation at the Surface for Impurity Diffusion in Semiconductors," *Physical Review*, Vol. 104, No. 5 (December 1, 1956), pp. 1242-45.
9. Smits, F. M., "Measurement of Sheet Resistivities with the Four-Point Probe," *Bell System Technical Journal*, Vol. 37 (May 1958), pp. 711-18.

Rolling Friction of Balls on Plates

By RICHARD C. DRUTOWSKI
General Motors
Research Laboratories

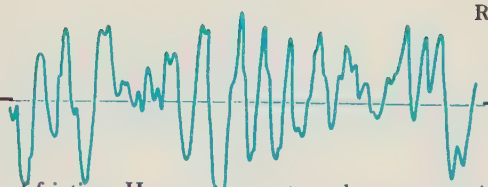

A small friction force, but it can be significant in some bearing designs

The rolling ball seemingly has only minor problems of friction. However, an extremely small rolling force exists which takes on importance in applications of ball bearings known as the instrument type. If the friction torque can be minimized in these bearings, the accuracy of the overall device can be improved. Thus, to learn more about the problems of the rolling ball, the GM Research Laboratories recently studied the energy losses of balls rolling on plates using specially constructed apparatus. Energy losses were shown as functions of load, material, and surface roughness. Confirmation was obtained of the theory that the energy lost in rolling a ball on a plate is dissipated in hysteresis losses of the elastically strained metals. An equation was derived relating the rolling force and the material damping capacity of the ball and plates. The results of this work provided information which was valuable in pursuing further studies and could be applied to bearing development.

BALL BEARINGS are accepted as very low friction devices. Because the friction is low, the greater part of ball bearing developmental work has been concerned with attaining longer bearing life. In most applications, the bearing is considered satisfactory if it has long life under the design conditions of speed and load. However, even this small amount of friction is significant in certain instrument type ball bearing applications where bearing torque is critical. An example of such a bearing is the gimbal mounting for a gyroscope. Thus, if a bearing can be improved by minimizing the friction torque, it will permit increased accuracy in the operation of the instrument. For many applications, both a low starting torque and a low running torque are desirable.

To obtain more information which might lead to minimizing friction torque in instrument ball bearings, the GM Research Laboratories made a study of the energy losses in rolling balls on plates. Such a study, in addition to having its practical values, is an interesting one to pursue in light of the information it may give on the way energy is lost during rolling. The rolling of a ball is a cyclic process since the stress field resulting from the ball contact moves with the ball. Relating the energy losses to this cyclic stressing may eventually increase the understanding of the inelastic behavior of materials.

Historically, the problem of the freely rolling ball, that is, one under almost no tangential traction, was not understood until a few years ago when D. Tabor published his work[1] on rolling friction. Prior to that time investigators tried to account for rolling friction in terms of surface interaction. Osborne Reynolds[2], in 1876, explained rolling friction in terms of microslip caused by differential elastic displacement in the contact area. H. L. Heathcote[3], in 1921, attributed the rolling friction of a ball in a groove to interfacial slip, the slip being caused by different parts of the contact area being different distances from the axis of rotation. G. A. Tomlinson[4], in 1929, proposed an explanation based on molecular adhesion. Tabor's experiments prove that none of these mechanisms is important except for Heathcote's and then only for balls in deep grooves. Tabor reached the conclusion that the energy required in rolling a ball on a plate is dissipated in hysteresis losses of the elastically strained metals. This conclusion is confirmed by the work done at the GM Research Laboratories.

The friction torque of a ball bearing is affected by two groups of variables. In the first group are those variables affecting the rolling itself, such as ball and race materials, surface finish, and contact stress. The second group includes additional variables inherent in the assembled ball bearing such as those resulting from ball-separator design and the degree of fit of the parts.

The work described in this paper is concerned with the first group of variables. Rolling was studied in the experimental arrangement of a ball of radius R rolling between two flat parallel plates under a load N (Fig. 1). To overcome the resistance to rolling at the contact areas of the ball and the plates, a torque must act on the ball. Assuming deformation of ball and plates is negligible, this torque is the force F times the diameter $2R$ of the ball. The frictional work for an advance s of the ball on the plates is then $2FR$ times the angular displacement of the ball s/R in radians. With identical plates this frictional work $2Fs$ is evenly divided between the two contact areas.

Rolling Ball Studied in a Laboratory Device

The laboratory apparatus and procedure used by the GM Research Labora-

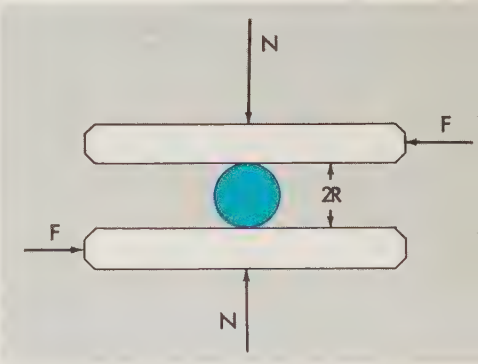

Fig. 1—The forces acting in the experimental arrangement of a ball rolling between two plates are shown here. N is the load acting on the plates, R is the radius of the ball, and F is the frictional force. The frictional work for an advance s of the ball on the plates is the torque $2FR$ multiplied by s/R, the angular displacement of the ball in radians.

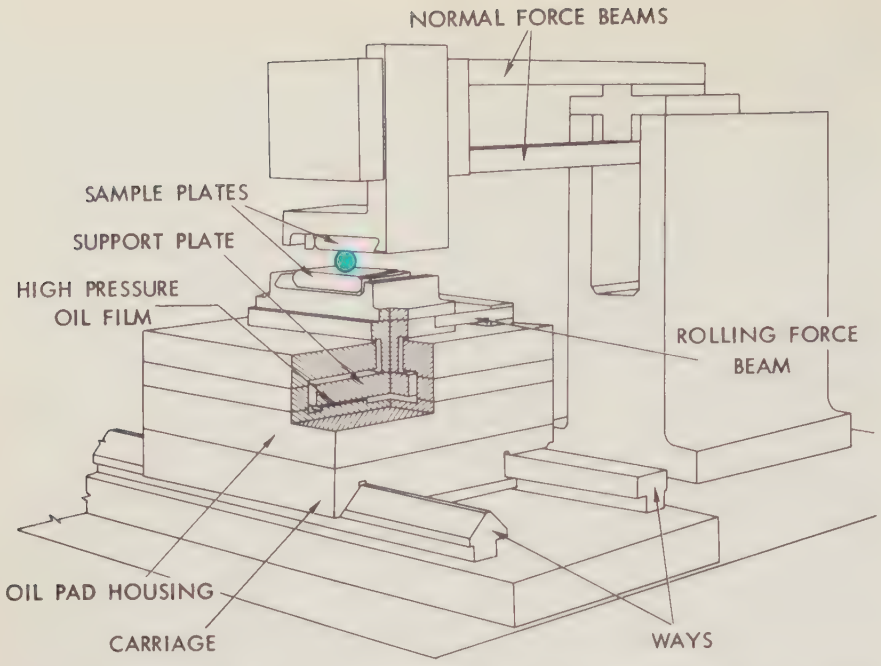

Fig. 2—The principal components of the laboratory apparatus used by the GM Research Laboratories to study rolling friction are illustrated here. In the rolling area, the upper plate of the material sample selected is held stationary by a pair of parallel beams while the lower plate moves with the carriage. The lower sample plate is located in a holder bolted to a support plate. The support plate is movable and rests on four, 3/4-in. by 1-1/4-in. oil pads, one at each corner. This oil-film support practically eliminates the resistance to lateral movement of the plate in response to the small rolling friction force encountered in the experimental work. The cutaway portion shows the interface at which the film is maintained. Elastic restraint of the lower plate holder is provided by two parallel beams, one of which is visible in the illustration. One end of each beam is fixed to the lower plate holder and the other end is fixed to the oil pad housing. Strain gages mounted on the beams measure deflection of the sample and transmit the signal to an oscillograph (not shown). To prevent interference from vibrations, rubber pads are placed between the floor and the support for the machine.

tories to make these studies had to have several special features to collect the data in usable form. For example, the normal force acting on the plates could not interfere with the measurement of the small rolling friction force. The condition of the surfaces of the ball and plates and any deviations from the true geometric shapes had to be accounted for. Also, suitable means had to be provided to measure and record the forces. The following description of the apparatus and the experimental work will help to explain the data obtained and the conclusions reached.

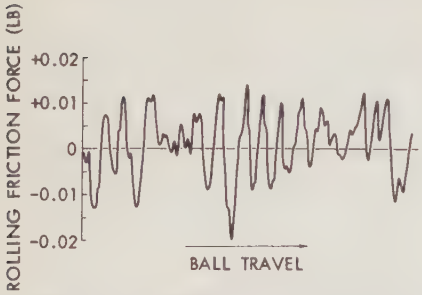

Fig. 3—The variation in the friction force encountered during rolling is shown by this reproduction of an actual trace. The conditions represented are for rolling a smooth, 1/2-in. diam hardened steel ball on a hardened steel surface of 15-microin. roughness at a load of 36 lb. The rolling distance is approximately 2 in. Rolling is perpendicular to the lay, that is, perpendicular to the direction of the surface scratches. For the test run in which this trace was obtained, an average rolling friction force of 0.0021 lb. was calculated.

The rolling friction force of the ball and plate arrangement is an extremely small quantity compared to the normal force. Measuring this rolling friction, therefore, requires a mechanical arrangement whereby the normal force acting vertically will not interfere with the measurement of the small friction force acting horizontally. This is done by supporting the bottom plate on a high-pressure film of oil. This oil film supports the load while offering practically no resistance (at the low shear rates encountered) to the lateral movement of the plate in response to the rolling friction force.

The means of providing the oil film support in the apparatus consists of a *support plate* resting on four, 3/4-in. by 1-1/4-in. oil pads, one at each corner. The lower *sample plate* on which the ball rolls is mounted in a plate holder on the support plate (Fig. 2).

To measure the rolling force, an elastic restraint in the form of two parallel beams is placed on the lower plate holder. One end of each beam is fastened to the holder while the other end is fixed to an oil pad housing. This parallel beam arrangement restricts rotation of the plate when displacement occurs. Deflection of the sample, which is proportional to the acting friction force, is measured by means of strain gages mounted on the beams. The signal from the strain gages is amplified and fed into an oscillograph.

The upper sample plate is held by the free end of a much stiffer pair of parallel beams. The vertical deflection of this upper sample plate, when contact is established between the ball and the plates, determines the normal loading. Strain gages mounted on these beams feed another channel of the oscillograph and give a continuous indication of the normal load during the course of a run.

Rolling the ball between the sample plates is accomplished by a hydraulic ram which moves a carriage and the oil pad housing along straight ways. The upper sample plate is stationary. The velocity of the carriage can be varied from 0.0001 to 1 in. per sec and controlled in either direction. The ball center moves at an average speed of one-half of the speed of the carriage. While the carriage and oil pad housing are moved uniformly the motion of the lower sample plate, which is elastically connected to the oil pad housing, is continuously modified by the action of the friction force. The difference in the displacement of the oil pad housing and the plate sample is measured. This difference is proportional to the acting friction force.

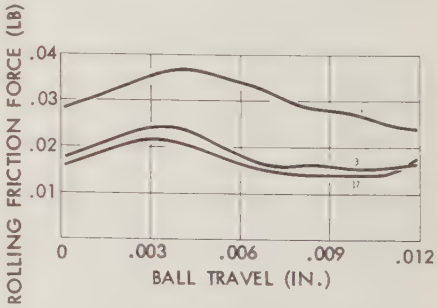

Fig. 4—This reproduction of rolling friction traces shows how friction varies after several passes of the ball rolling in the same direction over the same portion of the track. The friction force is greater on the first pass than on succeeding passes. Most of the reduction occurs between the first and third passes. Microscopic plastic deformation occurs during these beginning passes. After equilibrium conditions are reached, further deformations are elastic.

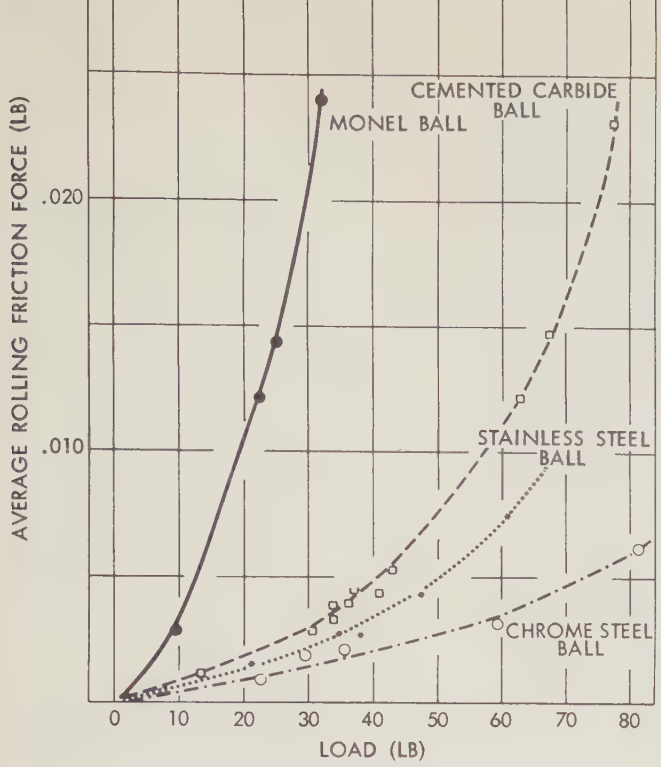

Fig. 5—The effects of using four different ball materials are shown in this plot of equilibrium values of rolling force and load, as observed in the rolling tests. The ball diameter is 1/2 in. and surface roughness is less than one microin. In all cases, the plate material is 52100 steel hardened to a value of Rc 50 and unidirectionally abraded on emery paper to a roughness of 15 microin. The balls are rolled perpendicular to the surface lay of the plates at an angular velocity of 0.12 radians per sec. The approximate loads at which plastic deformation starts for these ball materials are: monel, 10 lb; cemented-carbide, 30 lb; stainless steel and chrome steel, 60 lb.

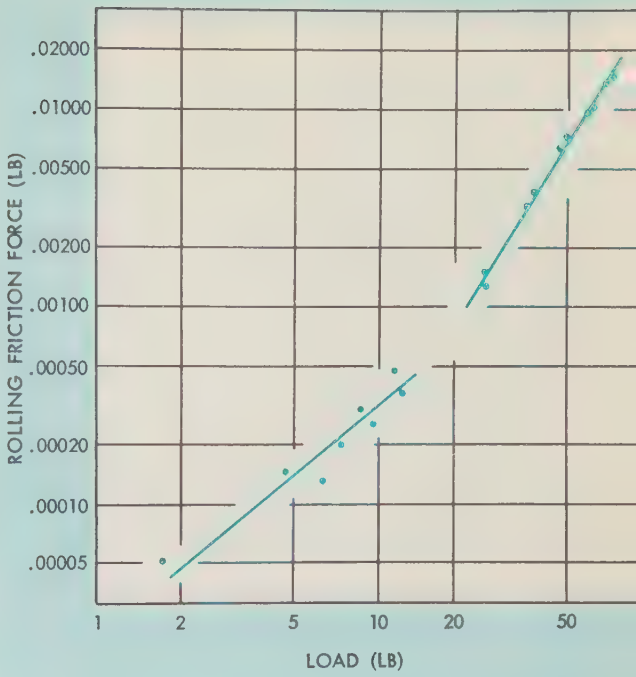

Fig. 6—A logarithmic plot shows a straight line relation of the observed rolling friction force and the load using a 1/2-in. diam cemented-carbide ball rolling on a polished 52100 steel plate hardened to Rc 60. For low loads, the equilibrium force increases as the 1.2 power of the load while at higher loads the equilibrium force increases as the 2.4 power. For this sample, plastic deformation occurs at a load of about 30 lb.

Characteristics of the Measurements

To measure rolling friction the ball is rolled back and forth over the same track. Because of the sensitivity of the friction force measurement and the large normal loads employed, small geometrical deviations of the ball from a perfect sphere, or the plates from perfect parallel planes, cause a horizontal component of the normal force to be added to the actual rolling force. To eliminate these geometrical force components, the determination of the average rolling resistance is based on two passes, one in each direction. Reversing the direction of rolling reverses the direction of the true rolling force, but does not affect the direction of the geometrical force components. Thus, the difference between the average recorded friction force for forward and reverse rolling is equal to twice the true rolling force. Instantaneous values of the measured force during the run, however, still will include these geometrical misalignment components.

A wide variation in the friction force is revealed in the reproduction of an actual friction trace (Fig. 3). This variation is due primarily to the roughness of the plates. The peaks in the trace are many times greater than the average value of the friction force. The number and size of these peaks define the force necessary to start rolling at any point on the sample surface and thus they are analogous to starting torque values for ball bearings.

Another type of variation in the friction force is shown after rolling the ball several times over the same track. For the first pass of a ball on new plates the friction force is greater than for succeeding passes over the same track (Fig. 4). Most of the reduction in the rolling force occurs between the 1st and 3rd passes. Any subsequent reduction is slight. The larger friction value for the beginning passes represents the work of plastic deformation in addition to the rolling work. After the surfaces become sufficiently deformed to carry the load, equilibrium conditions are reached and further deformations are all elastic. The results of this plastic work are plainly evident under large loads because a groove is actually formed in the plates. Even for light loads, however, where no apparent plastic deformation occurs, this larger force for the beginning passes is observed. For hardened steel, equilibrium values of the rolling forces are usually reached after just a few passes. Unless otherwise noted the equilibrium value is used in this paper.

How Materials, Conditions Affect Rolling

Using the procedures and equipment just described, observations were made of the rolling ball between plates. The results gave information on the effects of using various materials and the effects of material properties such as roughness, orientation of lay, and homogeneity.

Variation of Sample Material

Curves showing values of average friction forces plotted against load provide information on the use of different materials for balls and plates. The curves

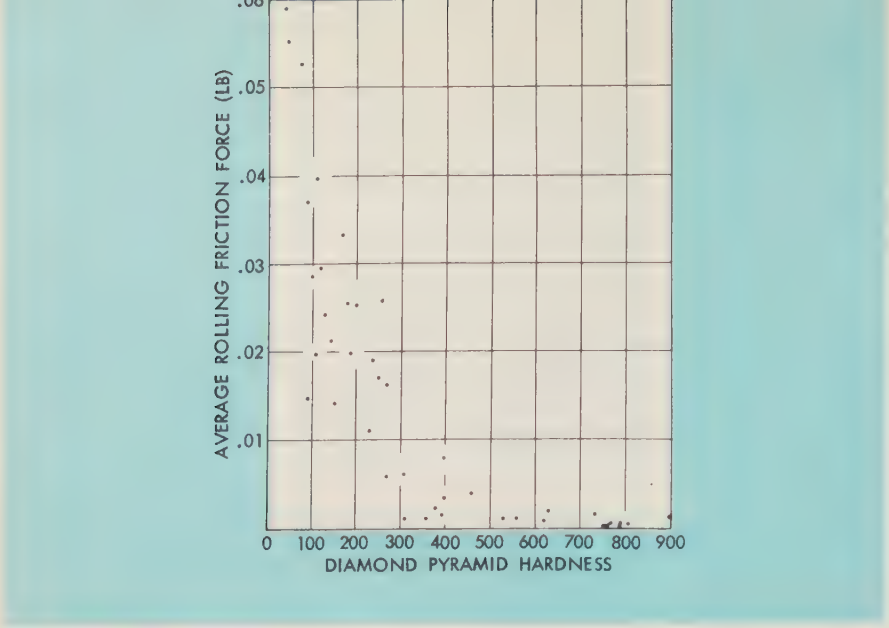

Fig. 7—The data plotted here show the results of rough determinations of equilibrium rolling forces for a large number of plate materials using a 1/2-in. diam ball of chrome alloy steel (700 diamond pyramid hardness *DPH*) at a load of 22 lb in all cases. The plate materials and their hardness values are shown in the tabulation. While the scatter in the data is appreciable, two definite regions are discernable: (*a*) for values less than 300 DPH, the rolling friction is high and increases rapidly with decrease of hardness, and (*b*) for values greater than 400 DPH, the rolling friction is low and is not affected greatly by changes in hardness.

also reflect material properties such as modulus of elasticity, hardness, and elastic hysteresis of the samples. The modulii of elasticity of the ball and plate affect the magnitude of the contact stress for a given load. The hardness determines the amount of plastic deformation at a given load before equilibrium rolling is established. Friction load curves for the use of balls made of monel, cemented carbide, stainless steel, and chrome-alloy steel illustrate this (Fig. 5). The plates are 52100 steel plates hardened to Rc 50 and abraded unidirectionally to a roughness of 15 microin. For the monel ball, plastic deformation starts at the lowest load employed; thus, the whole curve represents rolling at contact stresses which cause plastic deformation. For the cemented-carbide ball, plastic deformation starts at a load of approximately 30 lb so that the lower half of the curve represents elastic rolling while the upper half represents plastic deformation. For the stainless-steel ball and the chrome-steel ball, plastic deformation starts at approximately 60 lb so that almost the entire curve is for elastic rolling. The curve for the stainless-steel ball is higher than that for the chrome-steel ball because of the higher elastic hysteresis of the stainless steel. From these curves it is apparent that the equilibrium rolling force increases rapidly once the contact stress becomes large enough to cause plastic deformation on initial rolling.

In each of the curves of Fig. 5 the rolling force is a monotonically increasing function of load. To check possible relationships between these two variables, the data for a 1/2-in. diam cemented-carbide ball rolling on a polished 52100 steel plate (Rc 60) are plotted on logarithmic graph paper (Fig. 6). The data can be fitted by two straight lines indicating that for low loads the equilibrium rolling force increases as the 1.2 power of the load while for the higher loads the equilibrium rolling force increases as the 2.4 power of the load. For these particular samples, plastic deformation of the plate is observed at a load of approximately 30 lb. Thus, the increase of the equilibrium rolling force with an increase in load is greater in the plastic region than in the elastic region. It is felt that the difference between these two regions is primarily a function of the increase in stress amplitude, and thus of hysteresis, with load. The amount of plastic deformation even for the highest loads is very small and the groove thus formed is not sufficiently deep to bring into play slip of the Heathcote type.

Observation of the equilibrium rolling force using numerous other plate materials shows two definite patterns in the data (Fig. 7):

(a) For plate hardness values of less than 300 diamond pyramid hardness *DPH*, the rolling friction is high and increases rapidly with decrease of hardness

(b) For plate hardness values greater than 400 DPH, the rolling friction is low and is not affected greatly by changes in hardness.

For plate hardness less than 300 DPH, the plates are plastically deformed on initial rolling which means high equilibrium rolling forces. The amount of plastic deformation increases as plate hardness decreases. For plate hardness greater than 400 DPH the rolling is elastic thus giving a low friction force dependent primarily on elastic hysteresis of the samples.

Variation of Plate Roughness and Orientation of Lay

The effect of varying roughness and orientation of lay on a plate surface is shown in a force-load curve for 1/2-in. diam cemented-carbide balls rolling on hardened (50 Rc) plates of 52100 steel (Fig. 8).

While roughness and orientation of lay have only a small effect on the average rolling friction, they have a greater effect on the size and number of rolling friction peaks during a run. This is illustrated in histograms which are graphical representations of the frequency distributions of the friction peaks measured with respect to the average of the trace (Fig. 9). The histogram for rolling perpendicular to the lay of the 15-microin. plate surface covers the most area and is the broadest indicating the largest number of friction peaks per in. of rolling and the largest maximum peak (0.045 lb, ten times the average friction force for this run). The average peak value is 0.015 lb. Parallel rolling on the 15-microin. surface and on the 5-microin. surface and rolling on the random polished 1-microin. surface all have an average peak value of about 0.006 lb. When rolling parallel to the lay of a rough surface, the ball effectively sees a much smoother surface than when rolling perpendicular to the lay.

Effect of Material Homogeneity

The appreciable number of friction peaks measured for even the smoothest steel surfaces may indicate that the friction peaks are not only due to geometrical irregularities but may be due partly to

the inhomogeneity of the samples themselves. To test this hypothesis, comparisons are made with rolling tests using homogeneous samples of fused quartz and of synthetic sapphire for the ball and plate materials. A 1/4-in. diam synthetic sapphire ball rolling between quartz plates is compared with a 1/4-in. diam hardened 52100 steel ball rolling between the same plates. The friction peaks are much more pronounced in the case of rolling the steel ball (Fig. 10).

In making these test runs in the laboratory, all of the surfaces were highly polished equally so that if surface irregularities caused the variation in the rolling force for the steel ball they also should have caused the same variations for the synthetic sapphire. The fact that they did not is held as evidence that the inhomogeneous structure of the steel is the cause for the friction variations.

Rolling Force and Material Damping Studied Further

The rolling of a sphere on a plate is a cyclic process. The stresses resulting from the contact of ball and plate are carried along with the moving contact. Elements of volume in the samples are cyclically stressed as the stress field passes through them. This cyclic stressing is accompanied by a hysteresis loss which appears to be the primary source of energy dissipation during rolling.

The ball and the plate in the vicinity of the contact areas can be considered to be sub-divided into blocks of thickness Δx, each bounded by the material surfaces and by planes perpendicular to the direction of rolling (Fig. 11). The strain energy stored in each of these blocks is a function of the contact pressure and the elastic constants of the material. The stored strain energy in the blocks in the ball V_1 and in the blocks in the plate V_2 is plotted as a function of the distance of each block from the center of the contact area. The exact shape of these curves is not known but the essential fact is that the strain energy is a maximum for the block at the center of the contact area. As the ball rolls a distance Δx the energy dissipated is Δx times the friction force F, and the strain energy in the blocks is changed according to these curves. Effectively, this energy change between blocks is equivalent to one block in the ball and one block in the plane being subjected to a cycle of zero strain energy to maximum strain energy to zero strain energy.

By definition, the specific damping capacity *SDC* is the ratio of the energy dissipated during a cycle to the maximum strain energy stored during the cycle. Thus, the specific damping capacity for the rolling ball is:

$$SDC = \frac{F(\Delta x)}{V_1(\max) + V_2(\max)}. \qquad (1)$$

Since F is determined experimentally, all that is needed for calculation of the specific damping capacity is the value of V_{max} for the ball and plate. Choosing a co-ordinate system with the origin at the center of the contact area, the x-axis extending in the direction of rolling, and the z-axis extending into the sample, the complete stress distribution in the y-z plane for a sphere contacting a plane is given by Huber[5]:

$$\left.\begin{aligned}
\sigma_x &= q_o\left\{\frac{1-2\nu}{3}\frac{a^2}{y^2}\left[1-\left(\frac{z}{\sqrt{u}}\right)^3\right]\right. \\
&\quad + \frac{z}{\sqrt{u}}\left[2\nu + \frac{(1-\nu)u}{a^2+u}\right. \\
&\quad \left.\left. - (1+\nu)\frac{\sqrt{u}}{a}\tan^{-1}\frac{a}{\sqrt{u}}\right]\right\} \\
\sigma_y &= -q_o\left\{\frac{1-2\nu}{3}\frac{a^2}{y^2}\left[1-\left(\frac{z}{\sqrt{u}}\right)^3\right]\right. \\
&\quad + \left(\frac{z}{\sqrt{u}}\right)^3\frac{a^2u}{u^2+a^2z^2} + \frac{z}{\sqrt{u}}\left[\frac{(1-\nu)u}{a^2+u}\right. \\
&\quad \left.\left. + (1+\nu)\frac{\sqrt{u}}{a}\tan^{-1}\frac{a}{\sqrt{u}} - 2\right]\right\} \\
\sigma_z &= q_o\left(\frac{z}{\sqrt{u}}\right)^3\frac{a^2u}{u^2+a^2z^2} \\
\tau_{yz} &= q_o\frac{yz^2}{u^2+a^2z^2}\frac{a^2\sqrt{u}}{a^2+u}
\end{aligned}\right\} \qquad (2)$$

where u is defined by the equation

$$\frac{y^2}{a^2+u} + \frac{z^2}{u} = 1 \qquad (3)$$

and

$$q_o = \frac{3}{2}\frac{P}{\pi a^2}. \qquad (4)$$

In the preceding equations and those to follow,

P = force pressing the sphere against the plane

a = radius of the circular contact area

ν = Poisson's ratio

E = Young's modulus.

The strain energy in the element of volume

$$\Delta x\left(\int_0^\infty\int_{-\infty}^\infty dydz\right)_{x=0}$$

is V_{max} and is given by

$$V_{max} = \frac{\Delta x}{E}\int_0^\infty\int_{-\infty}^\infty\left[\tfrac{1}{2}(\sigma_x^2+\sigma_y^2 + \sigma_z^2 - \nu(\sigma_x\sigma_y+\sigma_y\sigma_z+\sigma_z\sigma_x) + (1+\nu)\tau_{yz}^2\right]dydz. \qquad (5)$$

Assuming $\nu = 0.3$ and substituting equations (2) and (4) into equation (5), the resulting double integral is evaluated by numerical integration on an electronic computer to give

$$V_{max} = 0.1315\frac{P^2}{a^2E}(\Delta x). \qquad (6)$$

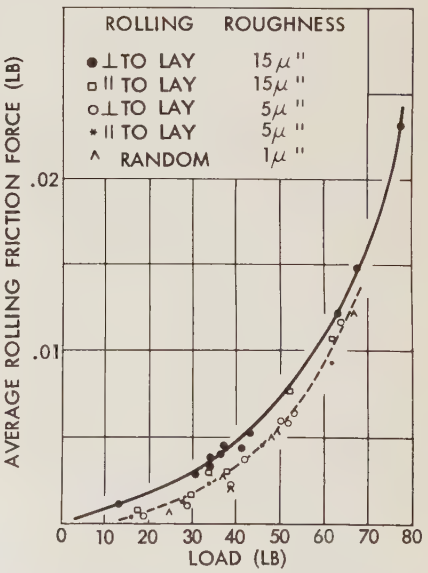

Fig. 8—These curves show the equilibrium rolling force versus load for plates of varying roughness and orientation of lay. One-half in. diam cemented-carbide balls, having a roughness of less than 1 microin., are rolled on hardened (50 Rc) plates of 52100 steel. The plates are polished undirectionally on varying grades of emery paper with the exception of the 1-microin. plate which was polished randomly on an abrasive-charged cloth wheel. Data for five combinations were obtained: rolling perpendicular and parallel to the lay of the 15-microin. surface; rolling perpendicular and parallel to the lay of the 5-microin. surface; and, rolling on the 1-microin. surface which had a random orientation of the roughness. For loads less than about 60 lb, the data divide themselves between two curves, one for perpendicular rolling on the 15-microin. surface, and the other for rolling on the 5-microin. and 1-microin. surfaces; the values for rolling parallel to the lay on the 15-microin. surface fall between these two curves. For higher values of the load the indication is that the two curves become one.

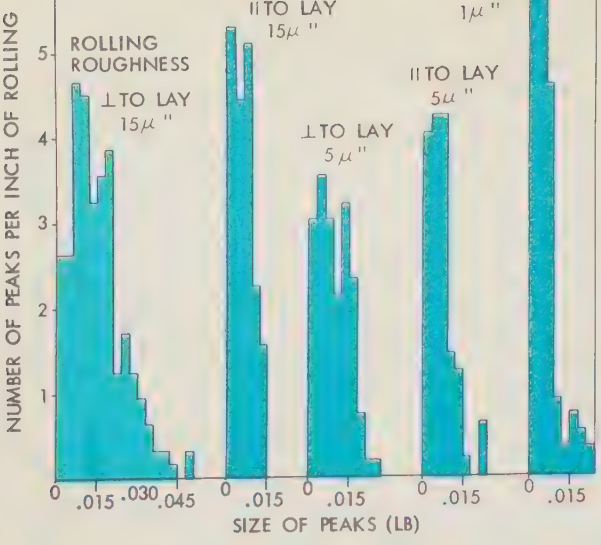

Fig. 9—Histograms showing the effect of plate roughness and orientation of lay during runs of balls on plates. Represented here are the frequency distributions of the friction peaks measured with respect to the average of the trace. The data are taken from runs made at about the same load (35 lb) on surfaces of varying roughness and orientation of lay as indicated. The largest number of friction peaks per inch of rolling and the largest maximum peak occur in rolling perpendicular to the lay of the 15-microin. surface (left histogram); the average peak value is 0.15 lb. Rolling perpendicular to the lay on the 5 microin. surface shows the next lower average peak value of 0.009 lb (center histogram). At the other conditions, the average value is about 0.006 lb.

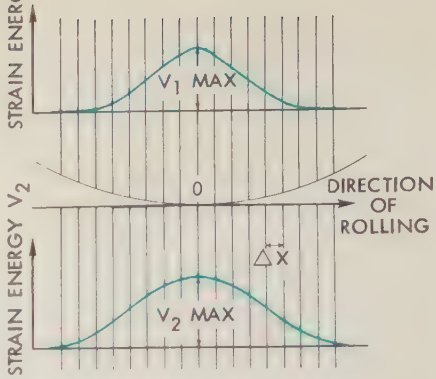

Fig. 11—The strain energy stored in the ball V_1 and in the plate V_2 in the vicinity of the contact area is represented in this graph. Blocks, of thickness Δx, are bounded by the material surfaces and by planes perpendicular to the direction of rolling. The curves show the strain energy plotted as a function of the distance of each block from the center of the contact area. The exact shape of these curves is not known.

Equation (1) for the specific damping capacity thus becomes

$$SDC = \frac{F}{0.1315 \frac{P^2}{a^2} \frac{1}{E_1} + \frac{1}{E_2}} \qquad (7)$$

where E_1 and E_2 are, respectively, the Young's moduli for ball and plate. Equation (7) is only applicable for values of the load which do not cause any plastic deformation. When plastic deformation does occur the geometry is no longer a sphere contacting a flat plate and equations (2) are no longer valid.

Specific damping capacities were calculated for three different materials, determined from rolling tests made at a mean compressive contact stress of 55,000 psi. These values were: 0.7 per cent for 52100 steel (Rc 60); 2.8 per cent for 1020 steel (Rb 80); and 14.9 per cent for manganese-copper alloy (Rb 70). The values calculated for 52100 steel and 1020 steel agree roughly with accepted specific damping capacities for alloy and mild steels determined from other tests. The agreement is not exact because the stress distribution for the rolling ball is different from that employed in the usual tests, and the SDC is known to depend on actual test configuration[6]. The high rolling force measured for the manganese-copper alloy with the consequent high SDC of 14.9 per cent is also to be expected. This alloy is a special type developed at the U. S. Bureau of Mines with an unusually high damping capacity.

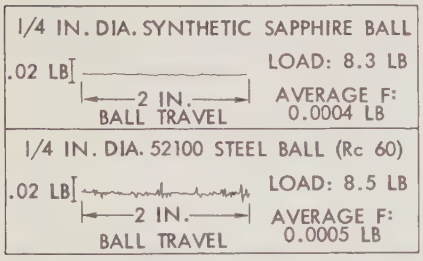

Fig. 10—These recordings compare the effects of rolling a 1/4-in. diam synthetic sapphire ball between fused quartz plates (top) and rolling a 1/4-in. diam hardened 52100 steel ball between the same plates (bottom). The results show evidence that the inhomogeneous structure of the steel balls causes variations in friction.

Conclusions

The conclusions observed from this work at the GM Research Laboratories are as follows:

(a) The hypothesis that the energy lost in rolling a ball on a plate is dissipated in hysteresis losses of the elastic strained metals is confirmed by the experimental results. Rolling-energy measurements can be translated into material hysteresis losses giving reasonable specific damping capacities

(b) The average rolling force is not very dependent on surface roughness and orientation of lay

(c) The frequency distribution of rolling-force peaks is a function of surface roughness, orientation of lay, and material homogeneity. These peaks are many times larger than the average rolling force

(d) The equilibrium rolling force increases more rapidly with load in the range where plastic deformation occurs than it does in the load range where only elastic rolling occurs.

Bibliography

1. Tabor, D., "The Mechanism of Rolling Friction—II The Elastic Range," *Proceedings of the Royal Society*, Series A, Vol. 229, (1955), pp. 198-220.

2. Reynolds, O., "On Rolling Friction," *Transactions of the Royal Society*, Vol. 166, (1876), pp. 155-74.

3. Heathcote, H. L., "The Ball Bearing: In the Making, Under Test and on Service," *Proceedings of the Institution of Automotive Engineers*, Vol. 15, (1921), pp. 569-662.

4. Tomlinson, G. A., "A Molecular Theory of Friction," *Philosophical Magazine*, Vol. 7, (1929), pp. 905-39.

5. Huber, M. T., "Zur Theorie der Berukrung Fester Elastischer Korper," *Annalen der Physik*, Vol. 14, (1904), pp. 153-63.

6. Freudenthal, A. M., *The Inelastic Behavior of Engineering Materials and Structures*, New York: John Wiley & Sons, Inc., 1950), p. 326.

7. Jensen, J. W. and Rowland, J. A., Jr., "Manganese-Copper High-Damping Alloys," *Product Engineering*, Vol. 27 (May 1956), pp. 135-37.

Radioisotope Techniques Applied to Fundamental Corrosion Studies of Spark Plug Ceramics

By WILLIAM E. COUNTS and DR. WILLARD E. HAUTH, JR.
AC Spark Plug Division

New knowledge gained on diffusion of lead compounds in ceramics

Lead compounds, formed as by-products of combustion in internal combustion engines, deposit on the tips of spark plugs. Depending on the temperature within the cylinder, different types of lead compounds, such as bromides and chlorides, are deposited. As temperatures within the cylinder increase, the lead compounds become electrically conductive and may short out the plug. Metal components of the plug, such as the electrodes and shell, as well as the ceramic insulator, are subject to possible corrosion by the hot deposits. The ionic diffusion of lead compounds into spark plug ceramics was the subject of a recent research program conducted by the AC Spark Plug Division to gain more knowledge on the complex diffusion mechanism involved. Radioisotope tracer techniques were used in the research program to study the diffusion of tracer ions into ceramics. Relative rates of diffusion of selected anions and cations were determined along with information regarding the influence of the ceramic structure and composition on the rate of diffusion of a selected anion.

LEAD COMPOUNDS, formed from the combustion of gasoline and anti-knock additives in internal combustion engines, are deposited on various parts inside the engine, particularly on the tips of spark plugs (Fig. 1). The way in which these compounds form and their effect on the life and performance of spark plugs has been the subject of continuous study by AC Spark Plug Division's Research Laboratory. Of major concern has been the effect of these compounds on the ceramic insulator of the spark plug. To gain further fundamental knowledge in this area, the AC Research Laboratory recently applied one of the most versatile of research tools—the radioisotope—to study the ionic diffusion of certain lead compounds into spark plug ceramics at high temperatures.

Automotive Spark Plug Subjected to Lead Oxybromide Compounds

The phenomenon of knock in internal combustion engines has long been recognized. Materials which promote knock include bromine, oxygen, ethyl nitrite, and ethyl nitrate. To counteract knock, chemical additives such as iodine, selenium diethyl, tellurium diethyl, tin tetraethyl, and lead tetraethyl may be added to the gasoline.

Lead tetraethyl is one of the most satisfactory anti-knock agents and is almost universally used in gasolines. By adding ethylene dibromide or ethylene dichloride as scavenging agents, it is possible to remove up to 99.5 per cent of the lead combustion products from automotive engine cylinders[1].

The small amount of lead compounds remaining is no serious problem as long as power output and engine temperatures are low. At higher power outputs, however, with correspondingly higher engine temperatures, there may be inherent deleterious effects which arise from lead compound deposits. Exhaust valves and exhaust systems become prone to corrosion. Also, spark plugs collect deposits which affect the insulator, causing possible short circuiting and fouling of the plug.

The way in which lead compounds diffuse into spark plug ceramics has not been well understood. The little information which has been available in the literature consists mainly of chemical analyses and X-ray diffraction data on the lead compounds formed.

The temperature ranges at which different types of lead compounds form, however, have been determined by Dr. Frances Lamb of Ethyl Corporation (Fig. 2). For the general operating temperature range of an automotive engine, the spark plug is subjected to inherent conditions within the engine which favor the formation of lead oxybromide compounds. Aircraft engines, which have higher operating temperatures, favor the formation of mixed oxybromides and sulfates (or silicates).

Many of the lead compounds found in spark plug deposits have been synthesized in the AC Research Laboratory and identified by X-ray diffraction. A typical deposit usually consists of more than one lead compound; frequently, five or six definite compounds are identified in a single deposit. Once the lead compounds present in a deposit are known, it is then possible to define the temperature range at which the deposit was formed. The

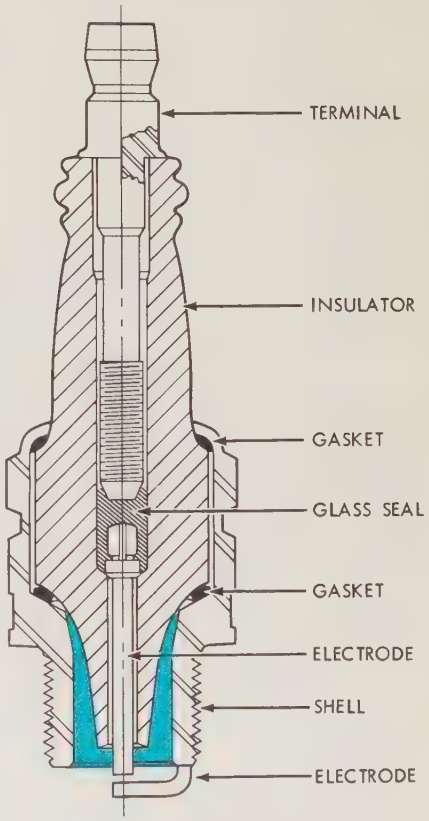

Fig. 1—This is a cross-sectional view of an AC automotive engine spark plug. Lead deposit, a by-product of combustion, collects on the cooler portion of the tip, between the centrally located ceramic insulator and the external metal shell. As the deposit becomes more extensive it becomes compacted between the insulator and shell (the area indicated by color) and grows toward the tip.

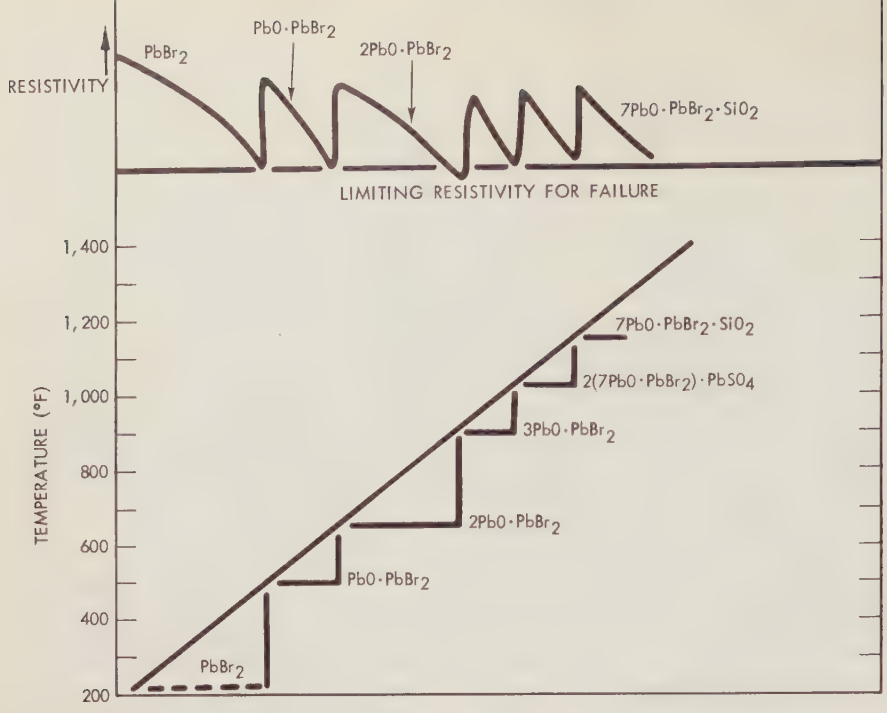

Fig. 2—This chart, developed by Dr. Frances Lamb of Ethyl Corporation, summarizes the temperature formation of various lead compounds commonly found in spark plug deposits and also indicates the limiting resistivity of the various lead compounds which may lead to electrical shorting of the plug. At low temperatures (approximately 700° F) the lead compounds occur as chlorides and/or bromides. At increasing temperatures these compounds are oxidized to form oxychlorides or oxybromides (up to approximately 1,400° F). Above these temperatures, the oxides, sulfates, sulfides, and mixtures of same are formed (up to approximately 2,000° F). Less frequently occurring, due to the higher temperatures involved, are the silicates and phosphates. In cases where reducing conditions are present, some metallic lead can be obtained from almost any of the lead compounds.

presence of lead indicates reducing conditions while oxy-compounds indicate oxidizing conditions. Thus, by analyzing these deposits, pertinent information concerning engine operating conditions can be obtained.

Diffusion Rate of Lead Compounds a Function of Time and Temperature

One of the major functions of a spark plug ceramic insulator is to prevent leakage of current from the electrode to the metal shell, thus assuring an adequate spark in the gap. This requires a ceramic material which has high bulk resistivity and high surface resistance at high temperatures. In addition, the ceramic material must have high resistance to the extreme thermal shock conditions which exist during ignition to prevent breakage and spalling of the thin insulator tip.

To meet these requirements, the insulator of the AC spark plug is made of a very strong alumina ceramic with high thermal conductivity and low electrical conductivity. This ceramic is composed of more than 90 per cent aluminum oxide bonded by a flux phase which contains siliceous glass and alkaline earth silicates.

The accumulation of lead deposits on the insulator tip during engine operation provides a potential source of contamination which with time, at elevated temperatures, may cause a decrease in the strength and electrical resistivity of the ceramic. Various methods have been used by the AC Research Laboratory through the years for studying and evaluating the accumulation and diffusion of lead compounds into spark plug ceramic insulators. The methods have been used to find the answer to two questions: (a) what compounds diffuse into the ceramic and (b) what influence does the ceramic composition and structure have on diffusion. Since the rate of diffusion is a function of time and temperature, both of these factors have had to be carefully controlled and experimental conditions selected which would be readily attainable in the laboratory and, simultaneously, result in reactions relevant to those found within an engine.

Initial research studies were made by immersing the ceramic in a molten lead oxide bath maintained at a specific temperature for the desired time. Later, at the suggestion of Dr. Lamb, part of the lead oxide was replaced by lead oxybromide. This gave a significant improvement in test efficiency.

Another phase in evaluating the diffusion of lead compounds concerned detecting the susceptibility of the ceramic to penetration by the reacting materials. It was observed, on sectioning an insulator, that a yellow discoloration had diffused into the insulator under fixed conditions of time and temperature. Penetration of several mils was observed optically. When X-ray photographic methods became available and were applied to the study, an even greater penetration under the same fixed time and temperature conditions was indicated.

Depth of Penetration Indicated by Radioisotope Tracers

With the advent of the industrial application of radioisotopes, a powerful research tool became available not only for studying the true depth of diffusion of contaminants but also for selectively observing the different components in the reactants. Facilities at the Isotope Laboratory of the GM Research Laboratories were utilized to develop a

PROPERTIES OF RADIOISOTOPES USED IN RESEARCH STUDY

ISOTOPE	CHEMICAL FORM	ENERGY OF RADIATION(MEV)		HALF-LIFE
		β	γ	
S-35	H_2S* in BaS Solution	0.167	0	87 Days
	$H_2S^*O_4$ Solution	0.167	0	87 Days
Cl-36	KCl* Solution	0.71, K	0	$3(10^5)$ Years
P-32	$H_3P^*O_4$ Solution	1.71	0	14.5 Days
Br-82	KBr* Solution	0.46	0.55, 0.77, 1.04	35.9 Hours
Pb-210	Pb* $(NO_3)_2$ Solution	0.020	0.047, etc.	20 Years

*Radioactive Tracer Element

Table I—This table summarizes the various properties of the radioisotopes used in the research study on the diffusion of lead compounds into ceramics. Radioactive isotopes, in solution form, were obtained for each of the elements commonly present in combustion deposits—lead, bromine, sulfur, and phosphorus.

radiotracer test method suitable for carrying out further studies on the diffusion of various ions into several ceramic materials.

Radiotracer Test Method

The elements commonly present in combustion deposits are lead, bromine, chlorine, sulfur, and phosphorus. Radioactive isotopes of these elements were obtained in solution form from the Oak Ridge National Laboratory and Atomic Energy of Canada, Limited (Table I).

The radiotracer test method developed consisted of placing a small quantity of $2PbO{\cdot}PbBr_2$ compound plus a tracer quantity of the isotope to be studied inside a small ceramic crucible and heating at a temperature of 1,500°F for two hours. The amount of isotope used gave approximately 10^7 counts per minute. The sample furnace was located in a glovebox. All isotope handling was done using conventional glovebox techniques.

After heating, the ceramic was sampled on a specially designed fixture (Fig. 3). Successive layers of ceramic, a few thousandths of an inch in thickness, were removed by grinding on a diamond wheel. The grindings which constituted each layer were flushed from the wheel with water and collected. The initial layer was removed from the exterior bottom surface. Successive layers then were removed and segregated until only a thin shell of crucible bottom remained.

Gamma emitting isotopes were used in the study for lead and bromine. Beta emitting isotopes were used for chlorine, sulfur, and phosphorus. Separate counting techniques were used for each type of isotope. For beta emitters, the grindings corresponding to each layer were collected in separate test tubes and transferred to stainless steel planchets. The samples then were dried and coated with a thin layer of collodion to seal the activity in place. Counting was done with either a Geiger-Mueller counter, a gas-flow proportional counter, or both, depending on the level of activity. The grindings containing gamma emitters were collected in test tubes, sealed, and counted in a well-type scintillation counter.

Experimental Results

The first phase of the study concerned investigating the diffusion of the lead, bromine, chlorine, sulfur, and phosphorus elements in the ceramic material used for AC spark plug insulators. The results of the study were plotted as the logarithm of the contaminant concentration (as indicated by the count rate) versus the square of the distance diffused (Fig. 4). This is the conventional way to display diffusion data and is derived from Fick's Law governing diffusion rates. This Law states that the change of concentration with time is proportional to the rate of change of the concentration gradient, the proportionality factor being the diffusion constant. The Law may be mathematically expressed as

$$\frac{\delta C}{\delta T} = D\left(\frac{\delta^2 C}{\delta t^2}\right) \qquad (1)$$

where

C = concentration factor
T = time
t = thickness of diffused layer
D = Fick's diffusion constant.

Assuming suitable boundary conditions, equation (1) may be integrated to give:

$$C = \frac{Co}{\sqrt{\pi D T}}\left(e^a\right)$$

where

C = concentration of tracer (at time T)
C_o = initial concentration

$$a = -\frac{t^2}{4DT}.$$

For simple diffusion, in situations which approximate the boundary conditions assumed in the integration, a plot of log C versus t^2 should result in a straight line, D and T both being constant.

A study of the relative diffusion curves (Fig. 4) shows that simple diffusion was not obtained in this system and that the process cannot be described by a single diffusion constant. There was a leveling of the count rate at a point above the background which was attributed to contamination of the external surfaces of the crucible by volatilization of the tracer at the high temperatures used in the experiment. To minimize the influence of this contamination when comparing the data,

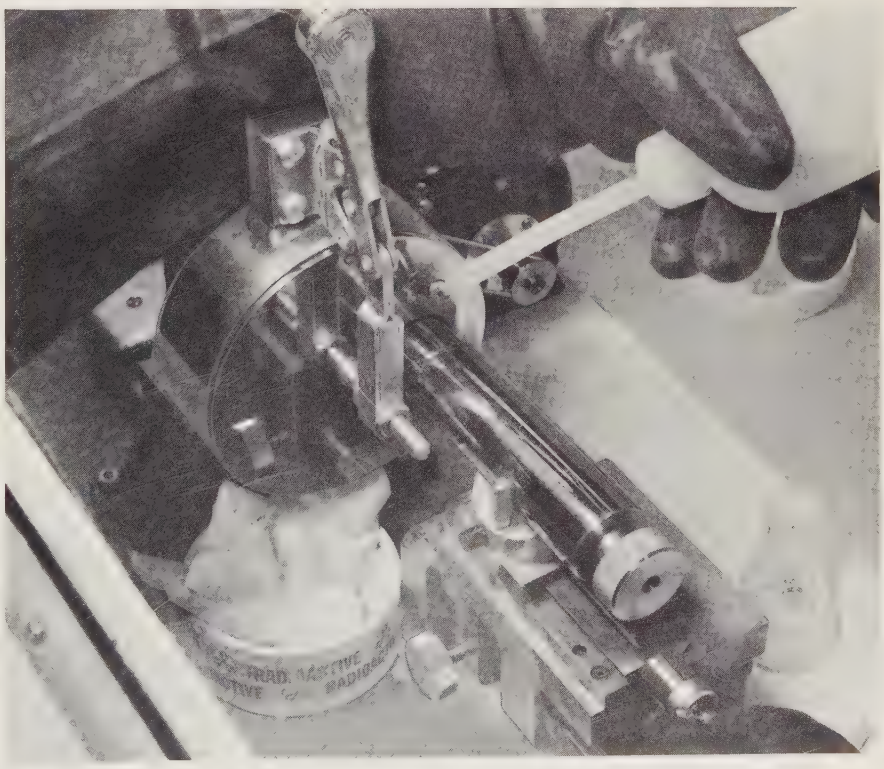

Fig. 3—The diffusion of lead compounds into several ceramic materials was studied by heating a small ceramic crucible containing a quantity of $2PbO{\cdot}PbBr_2$, plus a tracer quantity of the isotope to be studied, at a temperature of 1,500°F for two hours. The ceramic was then sampled on a specially designed fixture, located inside a glovebox as shown here. Successive layers of ceramic, a few thousandths of an inch thick, were removed by a diamond grinding wheel. The grinding fixture consisted of a collet for tightly gripping the ceramic specimens. The collet was mounted on a jeweler's lathe having a micrometer feed. The ceramic samples were fed to the diamond grinding wheel through a front plate having an "O" ring to seal the system against the spread of contamination. The grindings, which constituted each layer of ceramic, were flushed from the wheel with water. The water was inserted through an inlet in the front plate as shown. The outlet was at the bottom of the fixture. All parts of the fixture were made of polished stainless steel.

the steep slope portion of the curves was extrapolated to the background level line. This gave an approximate depth of tracer penetration, designated as the *relative penetration*, which was used as an indication of the tendency of the ion to diffuse into the ceramic. The value for the relative penetration, given below for the series of isotopes used, is unique for the particular ceramic investigated and the experimental conditions employed.

ISOTOPE	ACTIVITY	RELATIVE PENETRATION
Pb-210	γ	0.008 in.
Br-82	γ	0.015 in.
S-35($S^{=}$)	β	0.010 in.
S-35($SO_4^{=}$)	β	0.013 in.
P-32	β	0.008 in.
Cl-36	β	Negligible

Considerable care must be exercised in the use of this data. The count rates obtained on the lead tracer and the chlorine tracer were relatively low. Such a result may be caused by either a low diffusion rate or excessive loss of the tracer by volatilization during the heating, thereby reducing the initial concentration. Heats were made with these two tracers at 1,500°F with a soak period extended to four hours. It was found that practically all radioactivity had been volatilized by this treatment. It must be assumed, therefore, that the low diffusion rates observed for lead and chlorine must be due, in part at least, to an excessive loss of initial concentration by volatilization.

How Ceramic Composition and Structure Affect Diffusion

The next phase of the investigation was a study of the influence ceramic composition and structure had on diffusion. For this study, the S-35 tracer, added as the $SO^{4=}$ radical, was used.

To determine the effect of bonding phase and grain boundaries on the diffusion, experimental tests were made in crucibles prepared from pure sintered alumina and single crystal sapphire. The results of these tests (Fig. 5) showed that diffusion rates decreased with the elimination of the bonding phase and were very low in the single crystal material. This indicated that the major diffusion takes place intergranularly rather than through grains. Also, the diffusion through the ceramics that were free of bonding phase closely approached that expected from Fick's Law. The low diffusion rate in the single crystal sapphire was real since the volatile losses of the initial isotope were identical for all samples in this experiment.

Three oxide compositions were studied: alumina Al_2O_3*, beryllia BeO*, and magnesia MgO*. The alumina and magnesia were pure polycrystalline materials, while the beryllia contained 1.5 per cent bonding phase. The rate of diffusion through the BeO was high (Fig. 5). Diffusion through the MgO was low and, as for alumina and sapphire, approximated the straight line relationship predicted by Fick's Law.

The relative penetration values for S-35 from the $SO^{4=}$ ion determined for the various ceramics studied are shown below.

CERAMIC MATERIAL	RELATIVE PENETRATION
Polycrystal BeO	0.017 in.
Polycrystal MgO	0.006 in.
Polycrystal Al_2O_3	0.007 in.
Bonded Polycrystal Al_2O_3	0.011 in.
Single Crystal Al_2O_3 (sapphire)	0.006 in.

Values obtained in this experiment may be directly compared, since only a single isotope was used and volatilization was not a variable factor.

Conclusions

The results of the research study show that the diffusion of lead deposits in spark plug ceramic insulators can be studied in considerable detail by radiosotope tracer techniques. The diffusion of each element

*Crucibles of Al_2O_3, BeO, and MgO were obtained from the Aluminum Company of America, Coors Porcelain Company, and Corhart Refractories Division, respectively.

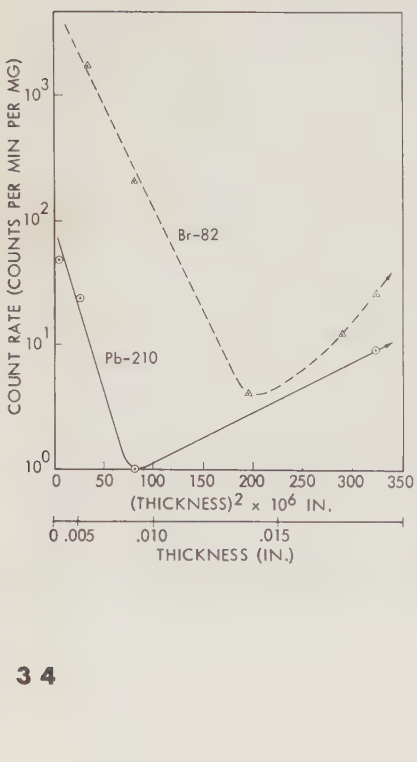

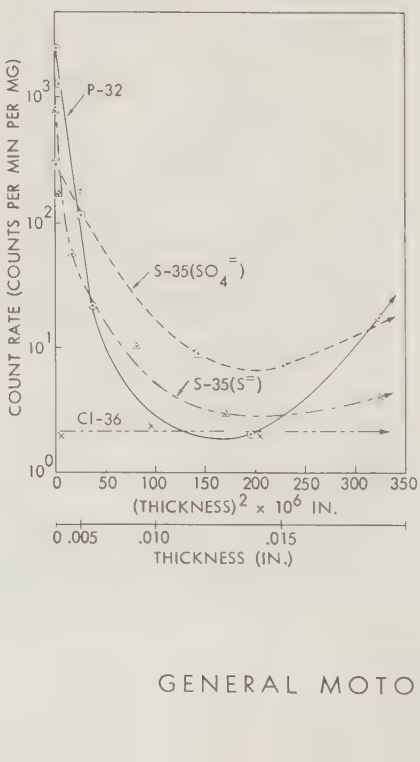

Fig. 4—These curves show the relative penetration of isotopes into a spark plug ceramic insulator material. Data are shown for radioactive isotopes of five elements commonly present in combustion deposits—lead, bromine, chlorine, sulfur, and phosphorus. Gamma emitting isotopes were used for lead and bromine (left). Beta emitting isotopes were used for chlorine, sulfur, and phosphorus (right). The reference background level for the gamma and beta emitting tracers is at the bottom of each diagram.

The slight rise in count rate for each curve on the right of each diagram indicates some contamination due to volatilization of the tracers. The Br-82 tracer showed far more penetration into the ceramic and did not seem to be as volatile as the Pb-210 tracer. The small amount of Pb-210 penetration was somewhat unexpected, since it always had been assumed that the attack on a spark plug insulator ceramic was caused by the lead ion. The S-35 tracer (as sulfate) diffused more readily into the ceramic than did the S-35 tracer (as sulfide). There was apparently very little diffusion of the Cl-36 due to its tendency to volatilize at elevated temperatures.

It appears from these curves that anions, such as bromine, sulfide, sulfate, and phosphate, play a much more important role in the so-called "lead attack" than lead.

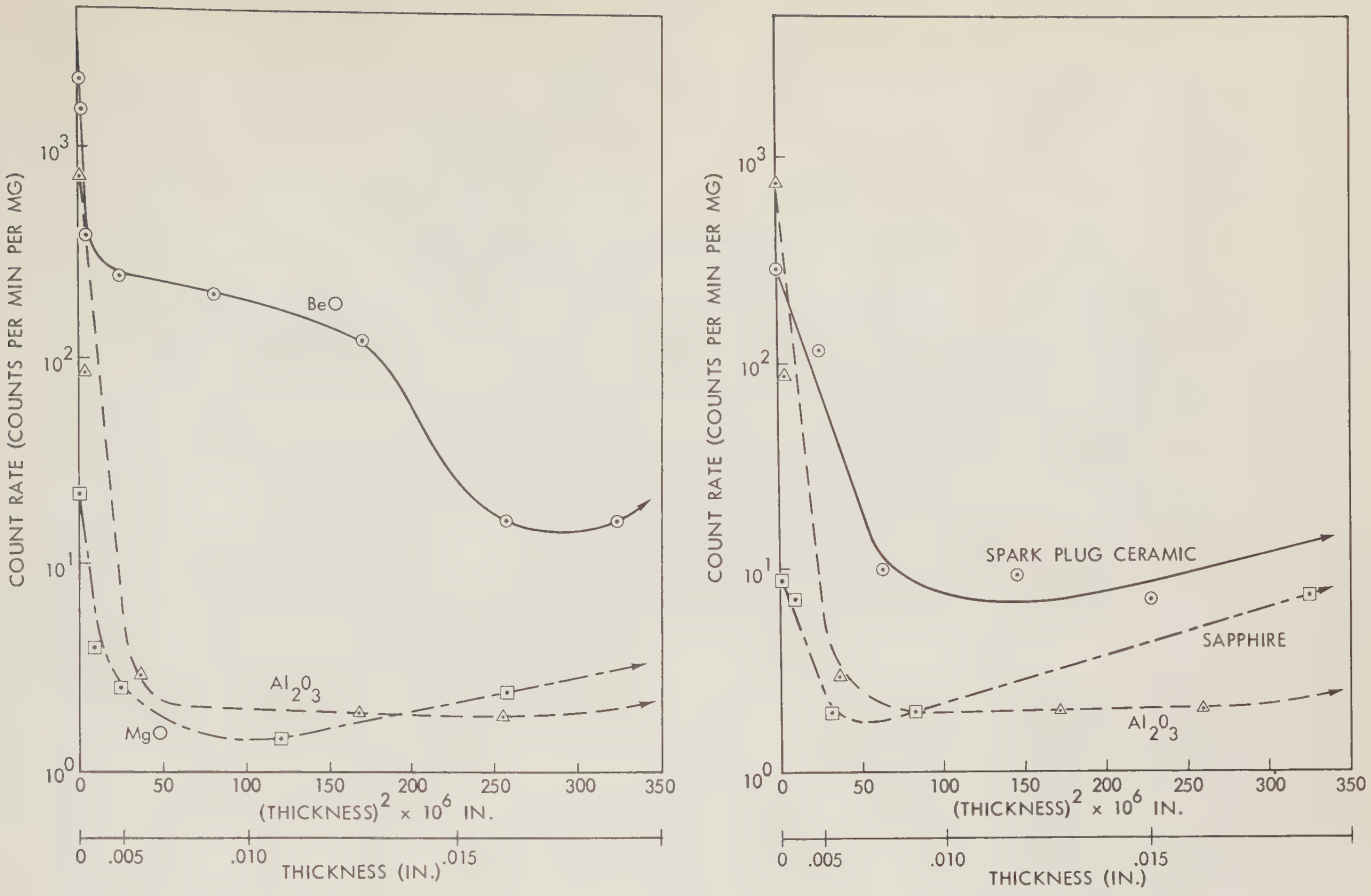

Fig. 5—The relative diffusion of a single isotope (S-35 as sulfate) into various ceramic materials is shown by these curves. The diagram at the left shows the relative diffusion of S-35 in three different polycrystalline oxide ceramics—beryllia BeO, alumina Al_2O_3, and magnesia MgO. The diagram at the right shows the relative diffusion of S-35 in three alumina-containing ceramics—that is, single crystal sapphire, polycrystalline sintered Al_2O_3, and polycrystalline bonded Al_2O_3. The reference background level is at the bottom of each diagram.

The slight rise in count rate for each curve on the right of each diagram indicated some contamination due to volatilization of the S-35 tracer. The BeO appeared to be more permeable to the S-35 tracer than did Al_2O_3 and MgO. The polycrystalline alumina bodies exhibited more diffusion than did the single crystal alumina.

found in the deposits can be uniquely determined by this method. The study is complicated, however, by the volatility of the compounds used at the necessarily high experimental temperatures. Also, the data gathered are valid for only one time-temperature relationship and the diffusion rates will change as experimental conditions are changed.

The studies also showed that the source of the diffusion ion influences the rate at which it penetrates into the ceramic. In future studies, therefore, particular attention will be paid to the careful choice of both the elements used and their source material.

Both the composition and structure of the ceramic have a profound effect on the rate of penetration of the elements tested. The presence of a bonding phase increases the rate of diffusion and results in a complex diffusion mechanism. Diffusion rates along grain boundaries are much higher than through a crystal. Additional work is needed to establish whether the relative rates of diffusion are different for different ceramic materials.

In conclusion, radioactive tracer techniques provide the best means available to date for determining the susceptibility of a ceramic insulator to the penetration of elements from complex salt mixtures used to simulate engine deposits. This research program is being continued to define the reactions involved and gain further knowledge on the complex diffusion mechanism.

Bibliography

1. *X-Ray Diffraction Patterns of Lead Compounds*, Published by the Shell Petroleum Company, Ltd., Product Development and Research Department, Thornton Research Center, Chester, England.

Other related literature in this area includes the following:

Bonner, N. A. and Wahl, A. C., *Radiation Applied to Chemistry*, (New York: John Wiley and Sons, Inc.).

Fara, H. and Balluffi, R. W., "On the Effect of Non-Equilibrium Vacancies on the Kinetics of Kirkendall Diffusion," *Journal of Applied Physics*, Vol. 30, No. 3 (1959), pp. 325-29.

Malkovich, R. SH., "On the Calculation of the Diffusion Coefficient in Solids," *Soviet Physics—Solid State*, Vol. 1, No. 4 (1959), pp. 548-54.

Pines, B. YA., "The Problem of the Mechanism of Diffusion in Crystals of Chemical Compounds and the Kinetics of Reactive Diffusion," *Soviet Physics—Solid State*, Vol. 1, No. 3 (1959), pp. 434-38.

Acknowledgment

The authors acknowledge the help and suggestions of Karl Schwartzwalder, director of research, AC Spark Plug Division, and Dr. Alexander Somerville, John P. Danforth, Dr. William J. Mayer, Walter H. Lange, and Caleb P. Moore of the General Motors Research Laboratories.

The Effects of Lubricant Composition on Sliding Friction of Steel on Steel

By FRED G. ROUNDS
General Motors
Research Laboratories

Bench test machine aids in evaluating friction properties of lubricants

For many years, the General Motors Research Laboratories has been engaged in fundamental and applied research dealing with various aspects of lubrication. These studies enabled the Research Laboratories to actively participate in such developments as detergent motor oils, multi-viscosity oils, and hypoid gear lubricants. Recently, the Fuels and Lubricants Department of the Research Laboratories completed a study on one more aspect of lubrication—the effect of lubricant composition on sliding friction. A bench test machine was developed to aid in evaluating the friction properties of over 100 lubricants. This machine, which uses two thrust bearings as test elements, simulated conditions occurring at the rubbing surfaces of many mechanical devices. Information gained from this study has served to further knowledge on sliding friction and has provided additional data on how straight mineral oils, synthetic fluids, and lubricant additives affect friction.

THE POWER TRANSMITTED by lubricated friction drive units and lubricated plate clutches is proportional to the product of the coefficient of friction and the applied load. Since the fatigue life of the drive members varies inversely as the cube of the applied load, it is generally desirable that the maximum kinetic coefficient of friction be present between the mating parts.

Three factors contribute to the kinetic coefficient of friction for lubricated friction drive units and lubricated plate clutches[1]: (a) the materials used for the two mating surfaces, (b) the type and velocity of motion, and (c) the composition of the lubricant. Although the first two factors are generally fixed by the design, the lubricant composition often can be altered to obtain the desired friction characteristics. Curves have been developed showing coefficient of friction versus contact velocity for different lubricants (Fig. 1). These representative curves indicate the type of lubricant preferred for friction drive units and for lubricated plate clutches.

Bench Test Machine Simulates Conditions at Rubbing Surfaces

To obtain friction data directly applicable to actual service conditions, a bench test machine was developed to measure the friction of lubricated steel on steel (Fig. 2). This machine, which simulated the conditions occurring at rubbing surfaces in many mechanical devices, used two thrust ball bearings as test elements. When such bearings were rotated under load, the individual balls tended to spin on an axis through the center of the ball as well as roll around the race. This spinning motion caused sliding of the balls relative to the race. As a result, both rolling and sliding friction contributed to the observed friction, with the latter being the most important. Because of the combined rolling and sliding, the observed coefficients of friction were not the same as values previously reported for pure sliding. Of greater importance was the fact that the observed friction values were comparable to those measured in actual mechanical devices.

The procedure for evaluating the friction properties of a lubricant consisted of first breaking in a new set of thrust ball bearings in the test lubricant and then measuring the torque transmitted through the bearings as a function of load, speed, and oil temperature. To eliminate the possibility of carry-over from one lubricant to the next, a new set of bearings was used for each test. During break-in, the machine was run at the test loads and temperatures until stabilized friction values were obtained. This took from a few minutes to several hours depending on the lubricant. All lubricants were evaluated in the "as received" condition.

Friction properties were investigated at loads from 300,000 to 500,000 psi Hertz, oil temperatures from 100 to 300°F, and speeds from 0 to 1,000 ft per min. Only the results at 200°F oil temperature and 400,000 psi Hertz load are presented in this paper, since these data are representative of that for the other loads and temperatures. Repeatability data obtained over a nine-month period using bearings from several lots showed that differences in the measured coefficient of

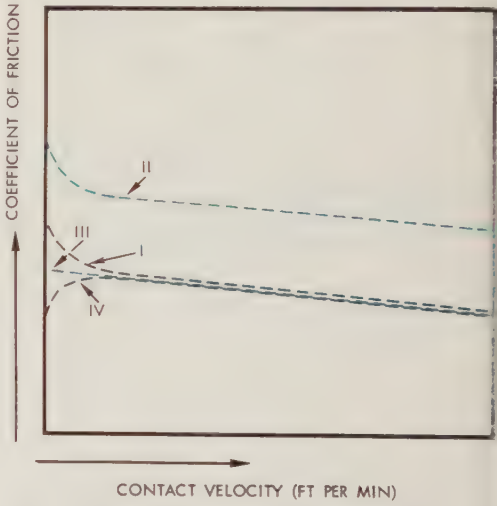

Fig. 1—These are representative curves which show the effect of different lubricants on coefficient of friction versus contact velocity. The majority of oils give curves similar to *I* or *II* which differ in friction by an essentially constant amount over the entire velocity range. A few oils give curves similar to *III* or *IV* which differ from curve *I* only in the low velocity region below 100 ft per min. For a friction drive unit, an oil giving a curve similar to *II* would be preferred.

The use of a lubricant in lubricated plate clutches, such as those used in automatic transmissions, which gives a curve similar to *I* or *II* may lead to objectionably noisy or harsh clutch engagements. The noise is believed to be the result of a stick-slip type motion caused by the rapid increase in friction as the velocity approaches zero. If the lubricant gives curves similar to *III* or *IV* the clutch engagement is silent and smooth. In some clutch applications, however, a lubricant giving a curve similar to *IV* will allow excessive plate slippage causing damage to the clutch plates. Thus, a lubricant giving a curve similar to *III* is generally preferred for lubricated plate clutches.

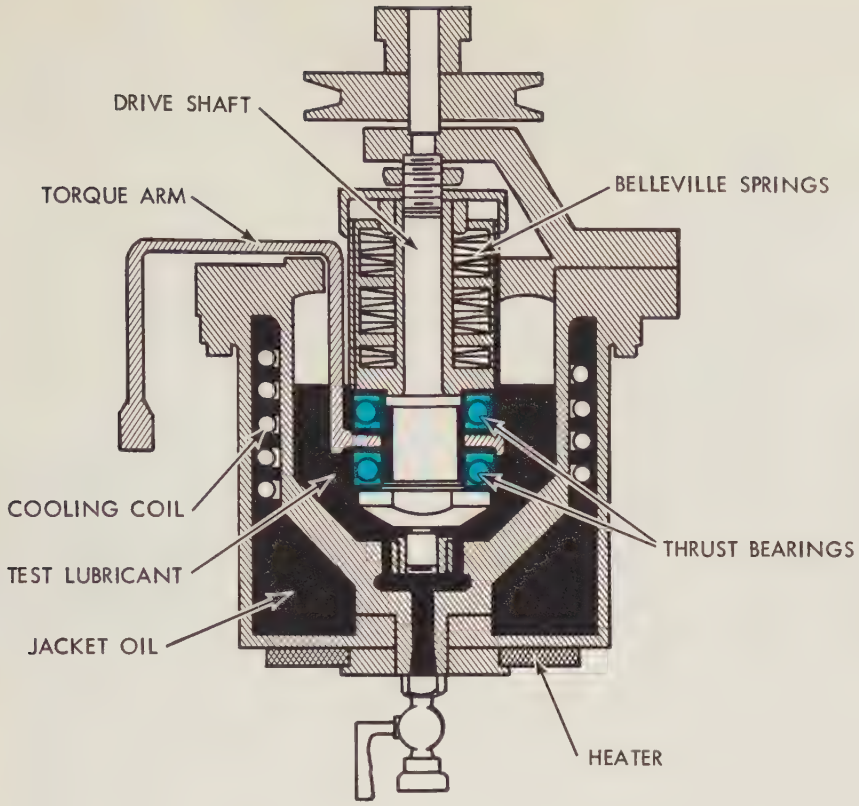

Fig. 2—To simulate the conditions occurring at rubbing surfaces in many types of mechanical devices, the GM Research Laboratories developed a bench test machine, shown here in cross section, to measure the friction of lubricated steel on steel. Two thrust ball bearings are used as the test elements. Torque, proportional to the coefficient of friction, is transmitted from the drive shaft to the torque arm through the test bearings. Loads are applied by compressing the calibrated Belleville springs. Temperature of the test lubricant is held constant by heating or cooling the jacket oil. To evaluate the friction properties of a test lubricant, the torque transmitted through the bearings is measured as a function of load, speed, and oil temperature.

friction of less than 10 per cent should not be considered significant.

Viscosity and Surface Coating Affect Friction

The lubrication conditions present at the sliding surfaces of mechanical devices determine the lubricant factors affecting friction. Such factors include viscosity and the presence or absence of surface coatings formed by the lubricant.

Under hydrodynamic lubrication conditions, the coefficient of friction is proportional to the lubricant viscosity and speed but inversely proportional to load[1]. As a result, viscosity is the only lubricant factor which controls friction. Under boundary lubrication conditions, on the other hand, fluid viscosity ceases to be important and the presence or absence of surface coatings formed by the lubricant controls friction.

Test results for the more than 100 lubricants evaluated indicated that friction and oil viscosity were independent in these tests. Oil additives were found to reduce friction at all test conditions by as much as 40 per cent without significantly changing the lubricant viscosity. These and other observations indicated that boundary lubrication conditions were present in these tests.

Components in Straight Mineral Oils May Control Friction

To determine the effect of base oil type on friction, tests were run on five straight mineral oils from widely different crudes. Naphthenic base oils caused substantially higher coefficients of friction than did paraffinic base oils (Fig. 3). This effect of base oil type also had been observed by Lane[2] and others. The five oils were analyzed by the method of van Nes and van Westen[3] to determine their hydrocarbon type composition. Little or no correlation was found between the composition of the oils as measured by the hydrocarbon type analyses and the friction data.

The lack of correlation between friction and the gross hydrocarbon type analyses suggested that friction may be controlled by specific components or limited groups of components in the oil. For example, it has been theorized by Zisman[4] that the friction caused by mineral oils depends on small amounts of fatty acids either present naturally or formed by oxidation.

In an attempt to concentrate the components that may be controlling friction, typical naphthenic base oils were fractionated by two methods—thermal diffusion and chromatography—and were hydrogenated. The two methods of separation, as well as hydrogenation, yielded products differing appreciably from each other and from the original oils in composition. However, none of the products gave friction values significantly different from the original oil.

Synthetic Fluids Have Varied Friction Characteristics

Results from a study of 25 different synthetic fluids showed that kinetic friction values obtained with the fluids varied from high values obtained with fluoroalkyl camphorate to very low values obtained with ethylene glycol (Fig. 4).

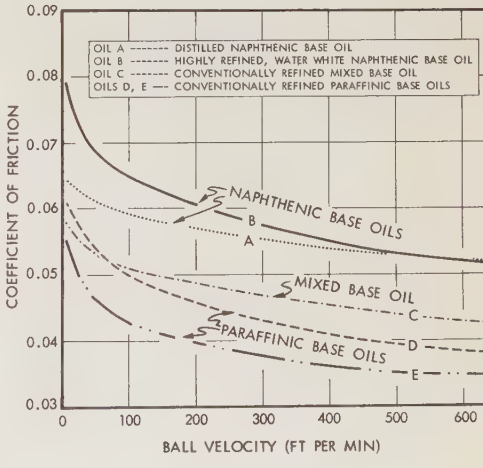

Fig. 3—The effect of base oil composition on friction was determined by running tests on five straight mineral oils. The results showed that the naphthenic base oils *A* and *B* caused substantially higher friction than did the paraffinic base oils *D* and *E*.

For static friction, the fluids giving the high and low friction values were ethylene glycol and oleic acid, respectively.

The friction characteristics for most of the synthetic fluids evaluated can be related to the chemical characteristics of the fluid. For example, both fluoroalkyl camphorate and a Kel-F fluid gave friction values falling above the mineral oil range (Fig. 4). Since these fluids are quite unreactive and essentially non-polar, the friction results with the fluorinated fluids have been considered to typify the friction results to be expected when fluids neither react with nor adsorb on the rubbing surfaces. Fatty acids such as oleic acid, on the other hand, are known to be adsorbed on metal surfaces and under favorable conditions to react with the surface to form a soap film[1]. Such materials can give friction values somewhat below the mineral range. However, tests on a series of fatty acids having different alkyl group chain lengths demonstrated that a C_9 acid (pelargonic acid) did not give as low friction values as did two C_{18} acids tested. These results were consistent with data obtained by other investigators studying the effect of carbon chain length on friction [5,6].

Alcohols May Reduce Friction

Since alcohols are less polar and less reactive than fatty acids and thus less likely to form an adherent surface coating, it would be anticipated that alcohols would reduce friction less than would the corresponding fatty acids. Tests on cyclohexanol and oleyl alcohol indicated that such was the case. However, increasing the number of OH groups in the alcohol molecule from one to the two or three in ethylene glycol and glycerol not only reduced kinetic friction radically but also raised static friction. The kinetic friction values obtained with ethylene glycol and glycerol were by far the lowest observed in these tests. Similar effects of glycerol have been observed by others[7,8]. Evaluation of several modifications of the ethylene glycol molecule indicated that the static and kinetic friction values could be greatly changed by varying the location of the OH groups and the size of the molecule.

To determine whether bearings conditioned by running in ethylene glycol would retain the low coefficient of friction when the lubricant was changed, a test was run with a naphthenic base mineral oil using bearings that had been used previously for an ethylene glycol test. The bearings were cleaned with solvents to remove any materials that were not strongly adherent to the surface prior to the second test. The results of this study indicated that the coefficient of friction obtained at 500 ft per min with the mineral oil after the ethylene glycol test (0.032) was intermediate between that for ethylene glycol alone (0.004) and the mineral oil alone (0.053). These results illustrate the magnitude of the carry-over effects that can be encountered in friction studies.

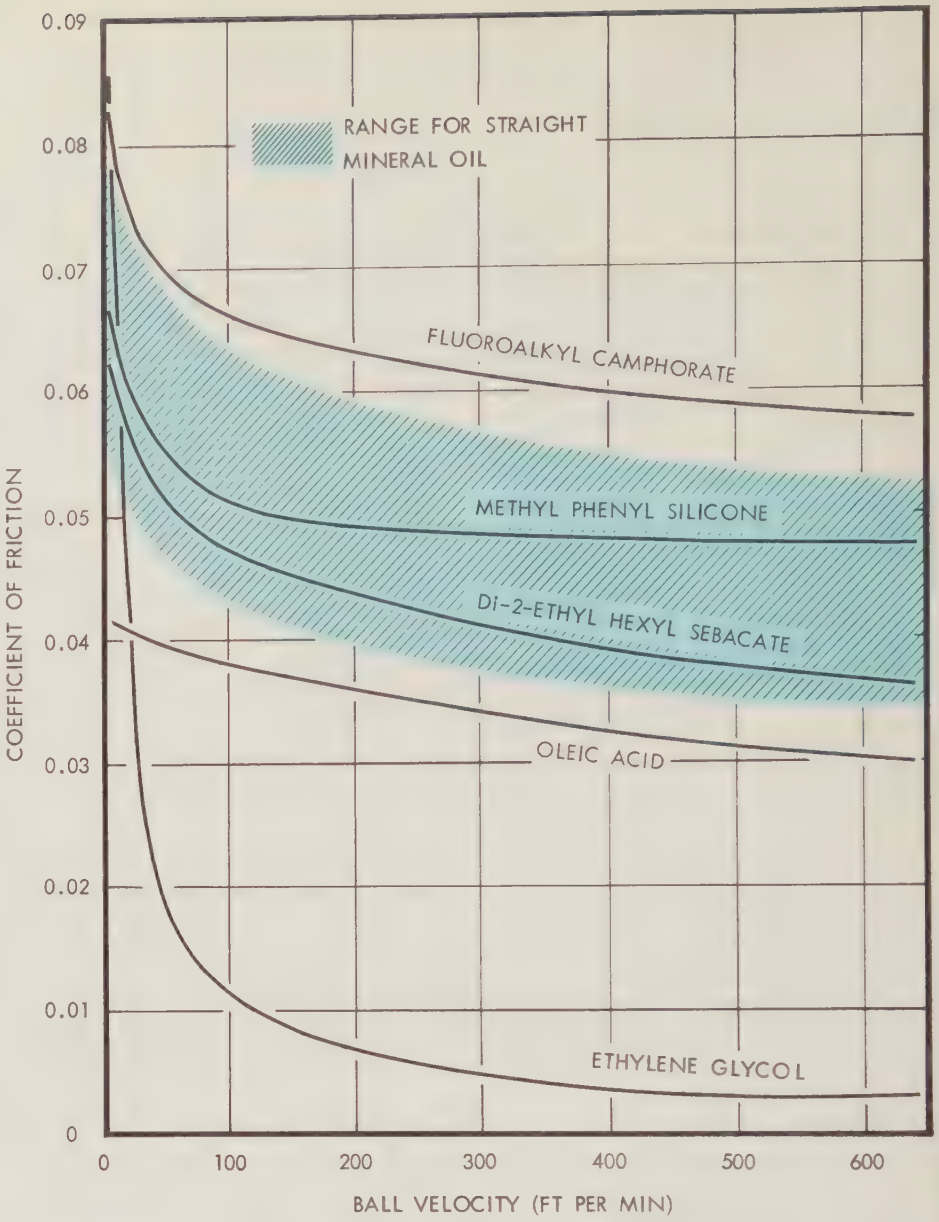

Fig. 4—This graph summarizes the results obtained when 25 different synthetic fluids were tested in the bench test machine to determine their effect on friction. For kinetic friction, high coefficients were obtained with fluoroalkyl camphorate and low coefficients with ethylene glycol. For static friction, ethylene glycol gave a high coefficient and oleic acid gave a low coefficient. Other types of synthetic fluids such as silicones, polybutenes, polyglycols, and diesters generally gave friction values which fell inside the mineral oil range indicated by the shaded area.

Considering the effectiveness of some fatty acids and alcohols in reducing friction, it was of interest to determine whether esters (in which the polar hydroxyl and carboxyl groups have been neutralized) would also be effective. Tests on six basically different ester fluids including a silicate ester and a phosphate ester indicated that all except one (dipropylene glycol dipelargonate) gave friction values similar to di-2-ethylhexyl

sebacate (Fig. 4). A possible explanation for this observation suggested by Murray, Johnson, and Bisson[9] is that the presence of free fatty acids in the esters determines their friction characteristics. These acids may be present as impurities or as oxidation or hydrolysis products.

Lubricant Additives Affect Both Static and Kinetic Friction

If friction under boundary lubrication conditions is controlled by coatings on the rubbing surfaces, many lubricant additives might be expected to have a pronounced effect on friction. Such lubricant additives could be anti-wear agents, rust inhibitors, and detergents which are surface active or react with the surface to perform their function.

Nearly 40 representative additives of various types normally used in finished lubricants were evaluated by blending them individually into a highly refined naphthenic base oil. The additive concentrations tested (one to three per cent depending on the additive) were representative of those used in finished lubricants.

All of the additives were found to have one of the five following friction characteristics (Fig. 5):

- Type I Additives—no effect on friction
- Type II Additives—preferentially lowered friction ratio at velocities below 100 ft per min
- Type III Additives—lowered the friction ratio at all velocities
- Type IV Additives—preferentially lowered friction ratios at velocities above 100 ft per min
- Type V Additives—preferentially raised the friction ratio at low velocities.

The type of friction characteristics obtained with the various additives were generally related to the additive composition and use. For example, the long hydrocarbon chain fatty acids which are used as friction modifiers all had a Type II effect. Changing the polar group in the molecule from the carboxylic acid group, such as that in oleic acid, to the phosphoric acid group in dilauryl phosphate did not change the type of friction effect. The tertiary amine rust inhibitors were also effective Type II or Type III additives. Octadecyl nitrile, oleyl alcohol, and a perfluoro acid are examples of polar molecules that did not affect friction. This pointed out that not all long chain polar molecules are adsorbed strongly enough to form a protective coating in the contact area.

The sulfur and chlorine additives used as anti-wear and extreme pressure agents are known to react with steel surfaces to form iron sulfides and iron chloride, respectively[10,11,12]. In comparing the friction effects of typical sulfur and chlorine additives, it was noted that three sulfur additives or two chlorine additives had quite different friction characteristics even though one might expect the coatings formed by the sulfur or chlorine additives to be the same. For example, sulfurized sperm oil preferentially reduced static friction (Type II effect) whereas a sulfurized terpene oil had a greater effect on kinetic friction (Type IV effect). Hexadecyl chloride also had a Type IV effect whereas a chlorinated wax reduced friction over the entire velocity range (Type III effect). These differences in the friction characteristics for the sulfur or chlorine additives suggest that the coatings formed with these additives are not the same and thus may be something other than iron sulfides or iron chloride.

Phosphorus additives such as tricresyl phosphate which are used as anti-rumble additives in gasoline as well as anti-wear agents in lubricants are reported to reduce friction by the formation of a phosphide which acts as a polishing agent for improving surface finish[13]. The friction tests showed that the phosphorus additives differed widely in their effect on friction. A dialkyl phosphate and a dialkyl phosphite both reduced static friction (Type II effect) whereas the corresponding trialkyl compounds, including tricresyl phosphate, had no effect. If it is assumed that tricresyl phosphate is typical of the compounds that form polishing agents, the results suggest that dialkyl phosphates and phosphites reduce friction through the formation of a protective coating rather than by changing the surface finish.

Twelve metal-organic additives also were evaluated. Each additive had one of three effects on friction. Barium and calcium detergents, believed to perform their function through physical adsorption on surfaces[14], generally had a Type

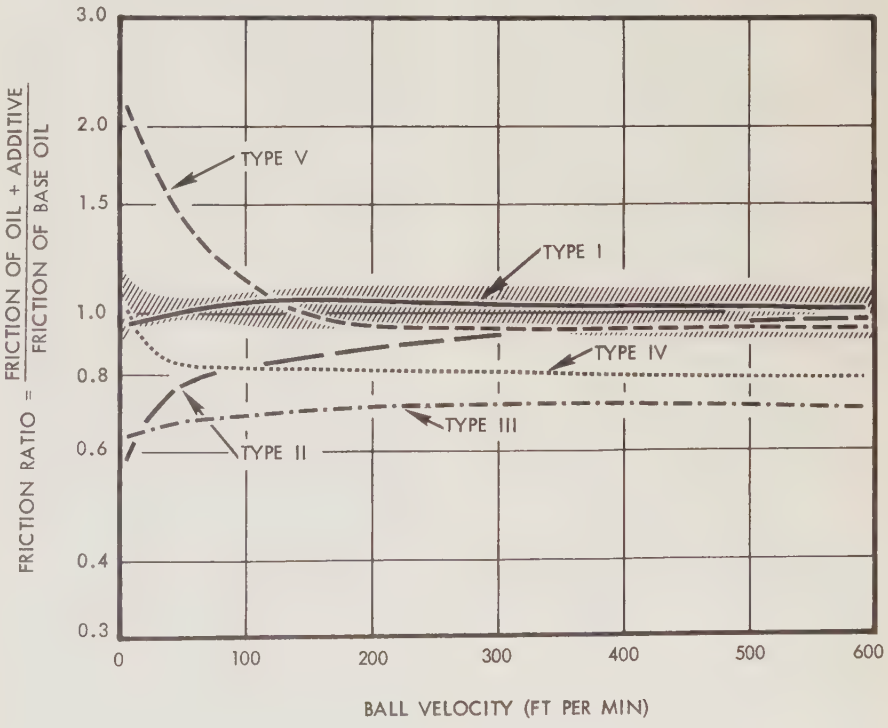

Fig. 5—Tests also were run to determine the effect lubricant additives have on friction. Nearly 40 representative types of additives normally used in finished lubricants were evaluated by blending them individually into a highly refined naphthenic base oil. All additives tested had one of five friction characteristics. In general, the *Type I* additives had no effect on friction. *Type II* additives preferentially lowered the friction ratio at velocities below 100 ft per min. *Type III* additives lowered the friction ratio at all velocities. *Type IV* additives preferentially lowered the friction ratio at all velocities above 100 ft per min while *Type V* additives preferentially raised the friction ratio at low velocities.

V effect. Similar results were obtained with some dithiocarbamate oxidation inhibitors. On the other hand, lead naphthenate and dithiocarbamate anti-wear agents had a mild Type II effect as did many of the anti-wear agents previously discussed. In contrast, the dithiophosphate anti-wear agents had no effect on friction. These studies demonstrated that both the metal and the organic portions of the molecule are important in controlling friction.

The non-metallic oxidation inhibitors and polymeric V.I. (Viscosity Index) improver additives were all found to have little or no effect on friction in these tests. This behavior was not surprising, since these additives primarily affect the bulk oil properties rather than the surface acitivity of the lubricant.

Oil Composition Has Pronounced Effect on Friction

The results of the studies described so far show that oil composition has a pronounced effect on the friction of lubricated steel on steel. Although a change in the base oil generally tended to raise or lower the entire coefficient of friction-velocity curve, a few base oils preferentially increased static friction. Additives, on the other hand, lowered the high velocity portion of the friction-velocity curve, raised or lowered the low velocity portion of the curve, or affected both the low velocity and the high velocity portions of the curve. No additives raised kinetic friction. A summary of the more effective base oils and oil additives for changing friction of steel on steel is given in Tables I and II. The use of different construction materials in the rubbing surfaces may significantly alter the lubricant effectiveness.

Only two synthetic oils gave kinetic coefficient of friction values higher than those for the straight mineral oils. Both of these synthetic oils were low viscosity index materials—that is, they experienced a large change in viscosity with temperature. Further, low viscosity index naphthenic base mineral oils gave higher friction values than the higher viscosity index paraffinic base mineral oils or diesters. Therefore, one might postulate with Lane[2] that kinetic friction is associated with the viscosity-temperature properties of the fluid. However, a chlorinated biphenyl which is also a very low viscosity index material gave values for friction which were quite low. This observation plus the fact that the measured friction with mineral oils is essentially independent of viscosity tends to refute Lane's suggestion. A more reasonable explanation is that the high kinetic coefficient of friction obtained with the fluorinated materials is related to the reduced reactivity of these fluids with steel surfaces.

Low kinetic coefficients of friction were obtained with both base oils and additives. In comparing Tables I and II, it will be noted that the most effective materials for lowering kinetic friction are materials that readily react with steel with the possible exception of the polyhydroxy alcohols. Many of the less effective additives also are capable of reacting with the surface.

In wear studies, it has been observed that the chemical activity of the additive must be adjusted so that the wear preventive coating is formed rapidly enough to replace the coating as it is worn away but not so rapidly as to corrode the metal parts excessively[1,2]. Thus, the rate at which the various additives react with the surface may determine their effectiveness in reducing friction. If so, this implies that the additives which are effective under one set of conditions may not be effective under another set of conditions.

EFFECTIVE BASE FLUIDS FOR CHANGING THE FRICTION OF STEEL ON STEEL

(In Order of Decreasing Effectiveness)

BASIS OF COMPARISON: OIL B

HIGHER KINETIC COEFFICIENT OF FRICTION

Trifluorochloroethylene Polymer
Fluoroalkyl Camphorate Ester
Naphthenic Mineral Oils

LOWER KINETIC COEFFICIENT OF FRICTION

Ethylene Glycol
Glycerol
Diethylene Glycol
Triethylene Glycol
Chlorinated Biphenyl
Oleic Acid
Saturated Fatty Acid (C_{24} est.)
2, 3 Butanediol
Paraffinic Mineral Oil

HIGHER STATIC COEFFICIENT OF FRICTION

Chlorinated Biphehyl
Glycerol
Ethylene Glycol
Diethylene Glycol
Pelargonic Acid
Trifluorochloroethylene Polymer
Methyl Phenyl Silicone

Table I—This table summarizes the effective base fluids which can be used to change the friction of steel on steel.

To reduce static friction, additions of fatty acids and related long hydrocarbon chain polar materials were most effective. It is interesting to note that the fatty acid type additives which were most effective for reducing static friction were not as effective as chlorine, sulfur, and phosphorus additives for reducing kinetic friction.

For an additive to be effective in reducing friction, it appears that the additive must form a suitable coating on the metal surface. As the relative velocity of the two rubbing surfaces increases from zero, the temperature in the contact area which tends to decompose these coatings increases. At the higher velocities, only the more stable coatings would be expected to maintain an effective coating between the metal surfaces. Consequently, the reduced effectiveness of fatty acid type materials at the higher velocities as compared to some chlorine, sulfur, and phosphorus additives may be due to the poorer stability of the films formed by fatty acid type materials.

High static friction was obtained with both selected base oils and certain metal-organic additives. The base oils that gave high static friction are generally considered to be rather poor in their anti-wear performance. Other studies have shown that the addition of metal-organic detergents to a base oil increases wear as compared to that for the base oil alone. Since both wear and friction are believed to depend on surface films, these observations suggest that high static friction results from failure by certain lubricant compositions to maintain a low friction coating under low velocity, low surface temperature conditions.

During limited friction studies conducted in the bench test rig and in full scale equipment, it was observed that the effects of one additive, such as the use of a fatty acid to reduce static friction, can be cancelled by the addition of a second, more reactive additive. Thus, in a finished lubricant containing several additives, the friction characteristics of the lubri-

EFFECTIVE ADDITIVES FOR CHANGING THE FRICTION OF STEEL ON STEEL

(In Order of Decreasing Effectiveness)

BASIS OF COMPARISON: OIL B

INCREASE COEFFICIENT OF FRICTION

(0 to 100 Ft Per Min)

Zinc Diamyl Dithiocarbamate
Cadmium Diamyl Dithiocarbamate
Barium Sulfonate
Barium Phenate
Calcium Sulfonate

(100 to 600 Ft Per Min)

None

DECREASE COEFFICIENT OF FRICTION

(0 to 100 Ft Per Min)

Dilauryl Phosphate
Oleic Acid
Stearic Acid
Tallow Fat Diamine
Saturated Fatty Acid (C_{24} est.)
Sulfurized Sperm Oil
Chlorinated Wax

(100 to 600 Ft Per Min)

Bis Beta Chloroethyl Vinyl Phosphonate
Sulfurized Terpene Oil
Dibutyl Phosphite
Dilauryl Phosphate
Chlorinated Wax
Hexadecyl Chloride
Oleic Acid

Table II—Approximately 40 representative lubricant additives, such as anti-wear agents, rust inhibitors, and detergents, were evaluated for friction characteristics. The additives were evaluated by blending them into a highly refined naphthenic base oil (Oil B). This Table summarizes those lubricant additives which were found to be effective in changing the friction of steel on steel.

cant are the net result of competition by the additives for the surface.

Summary

The bench test machine employed by the GM Research Laboratories to determine the effects of lubricant composition on the friction of lubricated steel on steel has facilitated the development of lubricants for use in devices such as lubricated plate clutches and friction drive units. From tests on straight mineral oils, synthetic oils, and oil additives, it was observed that both the base oil and the additive treatment have a pronounced effect on friction. Naphthenic base oils gave higher friction values than paraffinic base oils, but no correlation with hydrocarbon type analyses was found. Limited attempts to change the friction properties of a naphthenic base oil by fractionation and hydrogenation were unsuccessful.

Most of the more commonly used synthetic fluids had friction characteristics similar to straight mineral oils. Kel-F fluid and a fluoroalkyl camphorate ester gave higher kinetic friction values than those for naphthenic base oils. Several synthetic fluids gave lower kinetic friction values than those for paraffinic base oils with ethylene glycol and glycerol being by far the most effective.

Additives were found that would lower kinetic friction and/or raise or lower static friction. For preferentially lowering static friction, fatty acids and related compounds were most effective. To lower kinetic friction at velocities above 100 ft per min, reactive chlorine and sulfur compounds were required. Some metal-organic compounds raised static friction.

The data presented support the theory that films formed by lubricants on rubbing surfaces control the friction of steel on steel under boundary lubrication conditions.

Bibliography

1. Bowden, F. P. and Tabor, D., *The Friction and Lubrication of Solids* (London: Oxford University Press), 1954.
2. Lane, T. D., "The Lubrication of Friction Drives," *Lubrication Engineering*, Vol. 13 (1957), pp. 85-88.
3. van Nes, K. and van Westen, H. A., *Aspects of the Constitution of Mineral Oils* (Amsterdam: Elsevier Publishing Company), 1951.
4. Zisman, W. A., "Present Problems and Future Trends in Lubrication," *Naval Research Laboratories Report 4080, Chemical Division*, Washington, D. C., (November 26, 1952).
5. Bowden, F. P. and Leben, L., "The Friction of Lubricated Metals," *Transactions of the Royal Society* (London), Vol. A239 (1940), pp. 1-27.
6. Murray, S. F. and Burwell, J. T., "Measurement of the Incremental Friction Coefficient of Several Homologous Series of Straight Chain Hydrocarbon Compounds," *Annals of the New York Academy of Sciences*, Vol. 53 (1951), pp. 906-18.
7. Neeley, G. L., "Friction Testing Methods," *American Petroleum Institute Proceedings (Division of Refining Meeting)*, June 1-3, 1932, pp. 60-73.
8. Wolf, H. R. and Mougey, H. C., "New Aspects of the Free-Wheeling Lubricant Problem," *American Petroleum Institute Proceedings (Division of Refining Meeting)*, June 1-3, 1932, pp. 75-84.
9. Murray, S. F., Johnson, R. L., and Bisson, E. E., "Effect of High Bulk Temperatures on Boundary Lubrication of Steel Surfaces by Synthetic Fluids," *National Advisory Committee for Aeronautics Technical Note 2940* (1953).
10. Davey, W., "The Extreme Pressure Lubricating Properties of Some Chlorinated Compounds as Assessed by the Four-Ball Machine," *Journal of the Institute of Petroleum*, Vol. 31 (1945), pp. 73-88.
11. Davey, W., "Some Observations of the Mechanism of the Development of Extreme Pressure Lubricating Properties by Reactive Sulfur in Mineral Oils," *Journal of the Institute of Petroleum*, Vol. 31 (1945), pp 154-58.
12. Prutton, C. F., Turnbull, D., and Dlouhy, G., "Mechanism of Action of Organic Chlorine and Sulfur Compounds in Extreme Pressure Lubrication," *Journal of the Institute of Petroleum*, Vol. 32 (1946), pp. 90-118.
13. Beeck, O., Givens, J. W., and Williams, E. C., "On The Mechanism of Boundary Lubrication, II. Wear Prevention by Addition Agents," *Proceedings of the Royal Society* (London), Vol. A177 (1941), pp. 103-118.
14. Bondi, A., *Physical Chemistry of Lubricating Oils*, (New York: Reinhold Publishing Corporation, 1951).

Acknowledgment

The author acknowledges the help of Messrs. Charles R. Begeman, Stanley G. Anderson, and Michael J. Tyro, Fuels and Lubricants Department, GM Research Laboratories, in performing the studies described in this paper.

Patents and Basic Research

By PETER P. KOZAK
Patent Section
Detroit Office

The discoverer of a principle may immediately sense a practical use

An issue of *Chemical Week** magazine opened its editorial column with the following paragraph: "Thoughtful executives agree that we need more basic research—the pursuit of new knowledge solely for knowledge's sake—but we're still not getting enough of it. What is holding it up? The question of who will pay for it."

The philosophical approach to the definition of basic research in the above quotation may leave doubt as to precisely what type of knowledge flows from research which is conducted solely for knowledge's sake. The results of basic research are generally thought to consist largely of the discovery of new scientific principles or concepts, facts regarding the physical and chemical properties of physical things and answers to why physical things behave as they do. The basic researcher may be interested in discovering, for example, what causes cancer, which is of vital interest to everyone, or what causes rust spots over a painted surface of the body of a new car, which is of particular interest to those interested in attractive automobiles. In contrast, the applied researcher is interested in devising some machine, process, substance, or article which will perform some useful function.

The question of who will pay for it seldom arises in relation to applied research because the industry conducting such research expects the fruits of the research to provide it with a significant advantage in the competition of the market place and, in fact, considers applied research to be essential to survival in a competitive economy.

It is generally accepted that the patent system promotes technical development because a patent provides the inventor or his assignee with a proprietary interest in his invention (in the form of a right to exclude others from practicing it for a limited period of time) and encourages others to make inventions which satisfy the same need as the patentee's invention but which fall outside the patent monopoly staked out by the claims in the patentee's patent.

There appears to be a common public concept that the results of applied research stem from prior basic research and that the two types of scientific activity are performed separately by different types of scientific workers. While, of course, there is considerable truth to this concept, it is also true (a) that basic and applied research are tied closely together, (b) that the discoverer of a new principle may immediately sense a practical application of it, and (c) that the discovery of the cause is frequently accompanied by an obvious solution. In these instances the abstract fruits of basic research may be expressed in terms of practical applications which are properly the subject matter of patents, and to this extent, at least, the patent system promotes basic research. The principal aim of this article is to discuss this relationship.

In the interpretation of the patent statutes, the United States Patent Office and the courts have established definite limits concerning the subject matter which is patentable. The pertinent statute, 35 U. S. Code, Section 101, reads as follows: "Whoever invents or discovers any new and useful process, machine, manufacture or composition of matter, or any new and useful improvement thereof, may obtain a patent therefor . . ." At various times, beginning shortly after Congress passed the first *Patent Act* in 1790, the courts have construed this language to exclude from the purview of a patent, mere ideas, mental theories, and principles or laws of nature. The following statements of law taken from court decisions are representative:

> "While the means by which an idea may be made practically useful may be the subject matter of a patent, the idea itself is not patentable, however new and useful or even revolutionary or beneficial to humanity it may be or regardless of its importance or the ingenuity by which it was conceived."

> "The mere existence of an intellectual notion that a certain thing could be done and, if done, might be of practical utility does not furnish a basis for a patent. Mere mental theories or plans of action are not comprehended within the subject matter described by Congress."

> "An idea of means whereby a principle or law of nature is utilized to effect a practical result may be the subject matter of a patent, but no patent can be obtained for the discovery of an abstract principle or a law or phenomenon of nature."

> "The mere discovery of the principles on which a device or process operates or the mere discovery of the cause for the production of a particular effect is not patentable. The principle or law of nature must be embodied in some practical mode of carrying the principle or law of nature into effect. A principle in the abstract is a fundamental truth; an original cause; a motive; these cannot be patented because no one can claim an exclusive right in any of them."

In short, these statements of law indicate that the mere discovery of a new principle, force, or law of nature will not, in itself, entitle the discoverer to a patent. It is only when he has gone beyond the point of mere discovery and has devised some particular process, physical medium, or machine by which he may employ or control the new principle, force, or law to some useful end that he may obtain a patent. His patent is for the resulting process, physical medium, or machine rather than the principle, force, or law.

For example, the discovery that a substance known as Elastin, when separated from other substances, possessed sensitivity and uniformity of action in

*April 9, 1960

determining relative humidity of the atmosphere, was found patentable by the courts when claimed as a "hydroscopic element in a humidity responsive apparatus consisting of a piece of animal membrane composed substantially of Elastin."

In general, statements with reference to the unpatentability of laws of nature, principles of nature, fundamental truths, or mere ideas are words of broad meaning and it is not always easy to deduce from the court decisions where the unpatentable principles or laws of nature, mental ideas and the like end and where the patentable means by which these may be utilized to effect a practical result begin. It seems clear, however, that the instant the mental process passes from the mere idea or the concept of the fundamental principle or law of nature to some specific means for putting it to use, a patentable invention may be involved.

A scientific investigator may discover that the presence of ingredient "A" in a lead alloy has the effect of markedly reducing the surface tension of the lead. This effect is, of course, a law of nature and as such is not patentable. However, the alloy of lead plus the ingredient "A", if novel, may be patentable. And even if the lead alloy containing the ingredient "A" was previously known, the development might be patented in terms of a specific type of alloy, such as a solder, where the resulting low surface tension of the lead may be beneficial.

The basic research conducted by a particular industrial concern tends to be directed along lines of its commercial interest, and the scientific workers should keep in mind the applicability of their basic discoveries to the company's products. It is perhaps seldom that a scientist engaged in basic research discovers some new principle or property of a known material without turning his mind immediately to some useful or practical application of his discovery. If there is only one economically practical means whereby a new principle may be utilized, a patent directed to such means may have the same effect as claiming the principle which is employed.

Notes About Inventions and Inventors

Contributed by
Patent Section
Detroit Office

THE following is a general listing of patents granted in the names of General Motors employes during the period January 1, 1960 through March 31, 1960.

AC Spark Plug Division
Flint, Michigan

• **Argyle G. Lautzenhiser,** (*B.S.E.E., Tri-State College, 1940*) experimental engineer, inventor in patent 2,921,160 for an electric switch.

• **John L. Dart,** junior designer, inventor in patent 2,924,642 for a spark plug and method for forming same.

• **Norbert Sem,** (*B.S.E.E., Marquette University, 1943*) head, test equipment engineering, and **John E. Lynott,** (*B.S.E.E., Marquette University, 1951*) test equipment engineer, inventors in patent 2,924,998 for a differential gear reducer.

• **Wilfred A. Bychinsky,** (*B.S.E.E., 1930; M.S.E., 1931; and Ph.D., 1933, University of Michigan*) chief engineer, automotive products, inventor in patent 2,927,144 for a spark plug engine seal construction.

• **Alfred Candelise,** (*Ph.D. in electrical-mechanical engineering, University of Naples, 1923*) staff engineer, inventor in patent 2,927,238 for a spark plug.

• **Gordon W. Harry,** (*B.S.M.E., University of Michigan, 1923*) staff engineer, inventor in patent 2,929,333 for a fuel pump with pulsator.

Allison Division
Indianapolis, Indiana

• **R. Donald Tyler,** (*B.S.E.E., Rose Polytechnic Institute, 1947; B.S. in Bus. Adm., Butler University, 1955*) superintendent, controls and instrumentation development, and **John M. Whitmore,** (*B.E.E., The Ohio State University, 1936*) head, Electronics and Parts Test Department, inventors in patent 2,922,931 for a torquemeter and control means.

• **Earl J. Clark,** (*B.S.M.E., Purdue University, 1941*) head, Engineering Section, Bearings Department, and **Leonard J. Schmid,** (*B.S.Met.E., South Dakota School of Mines and Technology, 1942*) senior experimental metallurgist, inventors in patent 2,923,987 for a method of making bearings.

• **John R. Hayes,** (*General Motors Institute, 1944*) senior project engineer, and **Stephen C. Lampman,** (*B.S.M.E., Iowa State College, 1943*) senior project engineer, inventors in patent 2,925,998 for turbine nozzles.

• **Arthur W. Gaubatz,** (*B.S., University of Wisconsin, 1920*) senior project engineer, inventor in patent 2,926,899 for a counterbalanced speed switch and in patent 2,926,900 for a speed switch lubricating system.

• **Earl J. Clark*,** inventor in patent 2,926,970 for a journal bearing assembly.

• **James J. Mooney, Jr.,** (*B.S.M.E., Georgia Institute of Technology, 1948*) senior project engineer, and **Robert M. Tuck,** (*B.M.E., General Motors Institute, 1947*) chief development engineer, inventors in patent 2,929,270 for a transmission.

• **Mark E. Fisher,** (*B.S.M.E., Purdue University, 1937*) senior project engineer, and **Robert M. Tuck*,** inventors in patent 2,929,478 for a transmission control system.

***Inventors' names marked with an asterisk have biographical listings noted previously in this issue's Notes About Inventions and Inventors.**

Aeroproducts Operations
Allison Division
Vandalia, Ohio

• **Roy H. Brandes,** senior project engineer; **Richard A. Hirsch,** (*University of Dayton and Sinclair College*) section head, Electra propellers; and **Darrell E. Royer,** (*Sinclair College and University of Dayton*) senior designer, inventors in patent 2,919,752 for a fluid pressure system and control valve assembly therefor.

• **Calvin C. Covert,** (*B.S.M.E., University of Cincinnati, 1950*) senior engineer, and **Dale W. Miller,** (*B.S., Wittenberg College, 1934*) assistant chief engineer, inventors in patent 2,924,940 for a pump control system.

Buick Motor Division
Flint, Michigan

• **Lloyd E. Muller,** (*B.S.M.E., University of Kansas, 1929*) director, Experimental Engineering, inventor in patents 2,921,528 for an air compressor lubrication and power steering system; 2,922,485 for a muffler; and 2,929,232 for a torque ball assembly.

• **Carlton H. Holtslander,** senior layout man; **Roy S. Thornburgh,** (*B.S.E.E., Purdue University, 1925*) staff engineer—electrical; and **John C. Yurk,** senior designer, AC Spark Plug Division, inventors in patent 2,925,061 for an indicator mechanism.

• **Harold Fischer,** (*B.M.E., General Motors Institute, 1947*) section engineer, inventor in patent 2,926,737 for a transmission cooling system.

• **William C. Edgley,** (*General Motors Institute*) assistant chief draftsman, inventor in patent 2,926,762 for a control mechanism.

• **Nelson W. Kunz,** (*B.S.M.E., Michigan College of Mining and Technology, 1948*) senior project engineer, and **Joseph D. Turlay,** (*B.S.M.E., Oregon State College, 1928*) director, Power Plant Activities, inventors in patent 2,927,564 for a charge forming apparatus.

• **George C. Wilson,** (*B.S.M.E. and E.E., Michigan College of Mining and Technology, 1951*) project engineer, inventor in patent 2,929,267 for a transmission.

Cadillac Motor Car Division
Detroit, Michigan

• **Casimer J. Cislo,** (*Wayne State University and University of Michigan*) senior project engineer, inventor in patents 2,919,930 and 2,919,931 for a height extending control apparatus for air suspension and a dual trim height leveling valve mechanism for air suspension, respectively.

• **Bruce M. Edsall,** (*B.S.M.E., Wayne State University, 1942*) staff engineer, inventor in patent 2,924,992 for a parallel torque path transmission.

Chevrolet Motor Division
Warren, Michigan

• **Chester H. Fehlberg,** design engineer, and **William A. Lerg,** (*B.M.E., General Motors Institute, 1949*) design engineer, inventors in patent 2,919,760 for an adjustable suspension for vehicle driving wheels.

• **George H. Primeau,** (*Northern State Teachers College*) design engineer, inventor in patents 2,922,315 and 2,924,988 for a transmission control and transmission, respectively.

• **Richard L. Keinath,** (*B.S.M.E., Michigan State University, 1950; M.B.A., University of Detroit, 1960*) senior project engineer, inventor in patent 2,925,071 for a combined splash guard and oil separator.

• **Frank K. Berry,** foreman, inventor in patent 2,926,689 for an air supply system.

• **Maurice S. Rosenberger,** (*Nebraska Wesleyan University*) assistant chief engineer in charge of engine and passenger car chassis design, inventor in patent 2,927,808 for a seal.

• **Eugene B. Etchells,** (*B.S.E.E., University of Michigan, 1932*) assistant staff engineer, and **Edward Gray,** (*B.S.M.E., U. S. Military Academy, 1935; M.S.M.E., Massachusetts Institute of Technology, 1938*) director of quality control, inventors in patent 2,929,591 for a resilient mounting.

• **Adelbert E. Kolbe,** (*University of Michigan*) assistant staff engineer, inventor in patent 2,930,366 for an internal combustion engine.

• **Adelbert E. Kolbe*,** and **Jack M. Roberts,** (*Wayne State University and The Ohio State University*) senior designer, inventors in patent 2,930,367 for a heat valve.

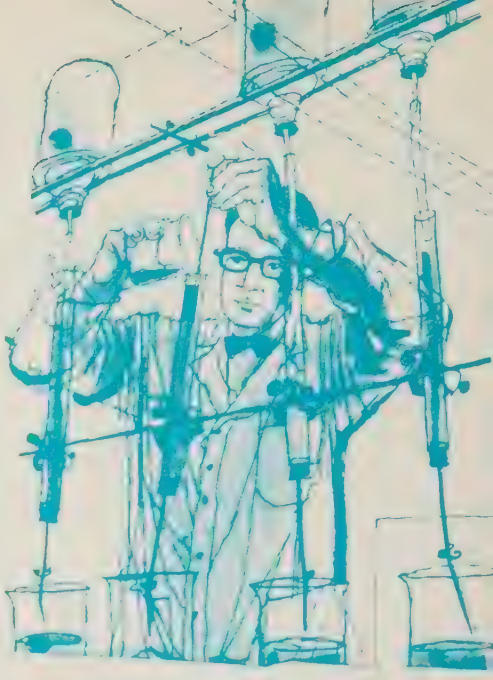

Delco Appliance Division
Rochester, New York

• **Francis M. Ryck,** (*B.S., University of Rochester, 1950*) assistant supervisor, windshield wiper applications, inventor in patent 2,920,335 for a windshield wiper blade.

• **Eugene R. Ziegler,** design engineer, inventor in patents 2,925,618 and 2,926,693 for a windshield cleaning system and windshield washer valve, respectively.

Delco Moraine Division
Dayton, Ohio

• **Frederick W. Sampson,** (*M.E., Cornell University, 1924*) section engineer on special assignment, inventor in patent 2,924,303 for a brake structure.

• **James O. Helvern,** (*B.A., Wittenberg College, 1927*) senior designer, and **William F. Erickson,** (*General Motors Institute, 1943*) section engineer, inventors in patent 2,928,511 for a fluid pressure control for circulating fluid in a brake.

• **De Loss D. Wallace,** (*B.M.E., The Ohio State University, 1926*) section engineer, inventor in patent 2,929,329 for a constant pressure variable displacement pump.

• **Roland P. Koehring,** (*Earlham College*) research engineer, inventor in patent 2,930,521 for a gas turbine structure.

Delco Products Division
Dayton, Ohio

• **George W. Jackson,** (*B.S.M.E., Purdue University, 1937*) assistant chief engineer, inventor in patents 2,919,929 and 2,927,801 for a closed air suspension and air supply system and a hydraulically actuated trim height control, respectively.

• **Charles E. Huggins,** (*B.S.E.E., Rose Polytechnic Institute, 1943*) general supervisor, Process Department; **Gerald F. Munn,** (*B.S. Ed., Ohio Northern University, 1940*) mechanical engineer; and **Robert W. Smith,** (*B.S.E.E., University of Southern California, 1950*) electrical engineer, inventors in patent 2,928,932 for a sheet metal weld assembly.

• **Ralph K. Shewmon,** (*General Motors Institute, 1934*) assistant chief engineer, electrical products, inventor in patent 2,929,944 for a dynamoelectric machine.

Delco Radio Division
Kokomo, Indiana

• **Charles W. Kay,** (*B.S.M.E., Purdue University, 1946*) senior project engineer, inventor in patent 2,922,860 for an automatic headlight beam control.

• **Thomas H. Lee,** (*University of Akron*) senior project engineer, and **Edward G. Stedry,** (*University of Kentucky*) senior layout man, inventors in patent 2,924,801 for an electrical contact spring.

• **Manfred G. Wright,** (*B.S.M.E., Purdue University, 1938*) head, Mechanical Engineering Section, and **Bertram A. Schwarz,** technical assistant to the general manager, inventors in patent 2,924,980 for a means for tuning a radio receiver.

• **James H. Guyton,** (*B.S.E.E., 1934, and M.S.E.E., 1935, Washington University*) chief engineer, radio, and **Kenneth S. Vogt,** (*The Ohio State University*) senior project engineer, inventors in patent 2,925,560 for a transistor power oscillator.

Delco-Remy Division
Anderson, Indiana

• **Thomas C. Heath,** (*E.E., M.E., Tri-State College*) regulator and relay engineer, inventor in patent 2,920,160 for a regulator.

• **John E. Irwin,** (*B.S.E.E., Purdue University, 1952*) sales engineer, inventor in patent 2,921,554 for an air horn.

Detroit Diesel Engine Division
Detroit, Michigan

• **John Dickson,** (*diploma, Royal Technical College, Glasgow, Scotland*) staff engineer, and Harvey G. Humphries, retired, inventors in patent 2,922,408 for a toxic exhaust gas preventing device for an internal combustion engine.

• **Charles T. Gruner,** (*Purdue University*) senior engineer—mechanical, inventor in patent 2,922,488 for a filter device.

• **Stephen A. Larkin,** senior special tester, and **Gordon W. Phillips,** (*B.A., Albion College, 1948; B.S.M.E., University of Michigan, 1950*) senior engineer, inventors in patent 2,929,467 for a lubricating device.

• **William R. Fox,** (*B.M.E., General Motors Institute, 1952*) group leader—drafting, inventor in patent 2,929,616 for a droop control for governor mechanism.

Detroit Transmission Division
Ypsilanti, Michigan

• **August H. Borman, Jr.,** (*Detroit Institute of Technology and Wayne State University*) senior designer, inventor in patent 2,919,597 for a throttle valve control for automatic transmissions.

• **Kenneth E. Snyder,** senior project engineer, inventor in patent 2,925,897 for a torque transmitting device.

• **Darrel R. Sand,** (*B.M.E., General Motors Institute, 1949*) assistant staff engineer, inventor in patents 2,927,671 and 2,927,-673 for a sprag clutch and energy transmitting device, respectively.

Electro-Motive Division
La Grange, Illinois

• **James E. Hencken,** (*University of Missouri, Iowa State University, and Illinois Institute of Technology*) motor and generator mechanical design engineer, and **Walter H. Merker,** (*B.S.M.E., University of Illinois, 1948*) senior project engineer, inventors in patent 2,919,962 for a shaft support and lubricating arrangement.

• **Earl D. Smith,** project engineer, inventor in patent 2,922,895 for an induction generator system.

• **Benjamin C. Liebenthal,** (*B.S.E.E., University of Wisconsin, 1949*) senior project engineer, inventor in patent 2,924,762 for a generator motor power selection system.

• **Kenneth D. Swander, Jr.,** (*B.S.M.E., Purdue University, 1942*) assistant air brake engineer, inventor in patent 2,926,966 for a brake system.

• **Earl T. Seley,** experimental test mechanic, inventor in patent 2,927,540 for a bolster friction snubbing device.

• **Hugh C. Lafferty,** (*B.S.M.E., Purdue University, 1941*) combustion control development engineer, and Ottar Tuxen, no longer with GM, inventors in patent 2,927,562 for an engine fuel control means.

• **James J. Kotlin,** (*B.S.M.E., Massachusetts Institute of Technology, 1948*) senior project engineer; Ottar Tuxen*; and **Rolland B. Wallis,** now with Cleveland Diesel Engine Division, inventors in patent 2,929,366 for a fuel control mechanism for dual fuel engine.

GM Engineering Staff
Warren, Michigan

• **Gilbert K. Hause,** engineer in charge, Transmission Development Group, inventor in patent 2,919,608 for a transmission.

• **Stanley H. Mick,** (*B.M.E., General Motors Institute, 1955*) project engineer, inventor in patents 2,919,686 and 2,930,-368 for a split engine and an economy control for split engine, respectively.

• **John M. Winston,** (*U.S. Naval Academy and B.S.E.E., A & M College of Texas, 1938*) senior design engineer, and **Lothrop M. Forbush,** (*B.S., Harvard University, 1939, and Massachusetts Institute of Technology*) engineer in charge, Vehicle Development Group, inventors in patent 2,924,307 for a brake adjusting device.

• **William H. Kolbe,** (*B.S.M.E., University of Michigan, 1950*) section engineer, Power Development Group, inventor in patent 2,926,775 for a gear lubricating mechanism.

• **Alexander J. Sagady,** (*B.S.M.E., Detroit Institute of Technology, 1945*) senior design engineer, inventor in patent 2,927,568 for a signal modifier valve.

• **James H. Stone,** (*B.S.M.E., Wayne State University, 1946*) section engineer, inventor in patent 2,927,825 for a bearing support.

Fisher Body Division
Warren, Michigan

• **Everett B. Arnold,** senior project engineer, inventor in patent 2,919,460 for a hinge cover.

• **William E. Sehn,** (*B.M.E., General Motors Institute, 1951*) engineer in charge, Product Evaluation Department, and **James H. Wernig,** (*Johnson School of Body Design and Engineering, and Alexander-Hamilton Institute*) general director of engineering and related activities, inventors in patent 2,919,478 for a weather strip structure.

• **Ralph M. Stallard,** (*B.S.E.E., Michigan College of Mining and Technology, 1949*) senior production engineer, inventor in patent 2,920,172 for a dielectric heating and pressing die structure.

• **John Kalvaitis,** (*University of Detroit*) design leader, inventor in patent 2,922,462 for a four way seat actuator.

• **Aloys C. Hollerbach,** engineer in charge, Body Engineering Department, inventor in patent 2,922,674 for an arm rest assembly.

• **James H. Wernig*,** inventor in patent 2,922,675 for a self-draining weatherstrip for vehicle closure.

• **Wilburn A. Schattler,** (*B.S. Math, Eastern Michigan College, 1934; University of Michigan*) senior production engineer, and **Ralph M. Stallard*,** inventors in patent 2,922,865 for a process and apparatus for dielectric heating.

• **James D. Leslie,** (*B.M.E., University of Detroit, 1939*) engineer in charge, Mechanical Department, and **Raymond G. Steffes,** senior project engineer, inventors in patent 2,926,943 for a closure latch.

• **Charles P. Hooverson,** design leader, Experimental Department, inventor in patent 2,926,950 for a vehicle seat.

Frigidaire Division
Dayton, Ohio

• **Richard E. Gould,** (*B.S.M.E., 1923, and M.S.M.E., 1927, University of Illinois*) chief engineer, inventor in patent 2,920-463 for refrigerating apparatus.

• **George B. Long,** (*B.S.E.E., Purdue University, 1937*) supervisor of major product line, inventor in patents 2,921-171 and 2,921,459 for a domestic appliance and a combined clothes washer and extractor, respectively.

• **Millard E. Fry,** (*B.S.M.E., University of Pittsburgh, 1931*) senior project engineer, inventor in patent 2,921,575 for a domestic appliance.

• **John J. Preotle,** (*B.M.E., The Ohio State University*) senior project engineer, inventor in patent 2,923,135 for an open top refrigerator display case.

• **Verlos G. Sharpe,** (*B.S.M.E., Purdue University, 1948*) section engineer, inventor in patent 2,923,139 for an ice block releaser and storage element.

• **George C. Pearce,** (*B.S.M.E., Stanford University, 1924*) section head, Non-Refrigerated Appliances Engineering Department, and **Verlos G. Sharpe*,** inventors in patent 2,925,204 for a storing and dispensing device.

• **Leonard J. Mann,** (*M.E., University of Cincinnati, 1940*) senior project engineer, and John C. Miller, not with GM, inventors in patent 2,928,258 for an evaporator defrosting means.

GMC Truck and Coach Division
Pontiac, Michigan

• **Hans O. Schjolin,** (*B.S. degree, Karlstad College, Sweden, 1920, and Polytechnical Institute, Mittweida, Germany, 1923*) staff engineer, and **Donald K. Isbell,** senior engineer, inventors in patent 2,920,722 for a brake-adjusting device.

• **George H. Wetterhahn,** (*B.M.E., Clarkson College of Technology, 1943; M.A.E., Chrysler Institute of Technology, 1945*) senior project engineer, inventor in patent 2,921,641 for an engine speed governing means.

• **Ralph H. Bertsche,** (*Colorado School of Mines*) head, Electrical Department, and **Eldred E. Gegenheimer,** (*B.M.E., General Motors Institute, 1950*) laboratory supervisor, inventors in patent 2,928,963 for a dynamoelectric machine.

Guide Lamp Division
Anderson, Indiana

• **David P. Clayton,** designer, and Robert N. Falge, retired, inventors in patent 2,920,188 for a sealed beam headlamp mounting.

• **Richard M. Goodwin,** (*B.S.M.E., Purdue University, 1932*) senior engineer, and **Frank J. Rada,** (*B.S.Ch.E., University of Illinois, 1936*) director, Facilities and Services, inventors in patent 2,922,259 for a lamp aim correction device.

• **Harry E. Welker,** senior process engineer, inventor in patent 2,924,916 for an endless buffing and polishing belt.

• **George W. Onksen,** (*B.I.E., General Motors Institute, 1956, and Purdue University*) staff engineer—reliability, inventor in patent 2,927,244 for a reversing switching circuit for automatic headlight control.

Harrison Radiator Division
Lockport, New York

• **Adolf Schwarz,** senior product designer, inventor in patent 2,929,396 for shaftless valve structures.

• **Robert A. Herberger,** chief draftsman, inventor in patent 2,930,206 for vehicle air conditioning systems.

Hyatt Bearings Division
Harrison, New Jersey

• **Willard Bayre,** (*B.S. in Physics, Rensselaer Polytechnic Institute, 1951*) experimental metallurgist, inventor in patent 2,922,681 for anti-friction bearings.

Inland Manufacturing Division
Dayton, Ohio

• **Allen L. Everitt,** (*M.S.M.E., Purdue University, 1931*) section engineer, inventor in patents 2,919,737 and 2,927,674 for a wheel cushioning structure and clutch structure, respectively.

• **Edward P. Harris,** (*M.E., Cornell University, 1931*) section engineer, and **James R. Wall,** (*B.Ch.E., University of Dayton, 1937 and M.Ch.E., Cornell University, 1939*) supervisor, Advanced Development Laboratory, inventors in patent 2,923,029 for a foamed rubber strip manufacturing process.

• **Russell J. Bush,** (*B.S.Ch.E., Purdue University, 1925*) project engineer, inventor in patent 2,924,472 for a pipe joint seal.

• **Harold E. Schweller,** (*B.S.Chem., University of Dayton, 1951*) supervisor, Latex Laboratory, and William L. Pearson, no longer with GM, inventors in patent 2,925,396 for method of manufacture.

• **George Rappaport,** (*B.S. in Chemistry, University of Miami, 1944, and M.S. in Chemistry, The Ohio State University, 1950*) senior chemist; **Joseph A. Szaruga,** (*B.S. in Agricultural Biochemistry, The Ohio State University, 1953*) development chemist; and **James R. Wall*,** inventors in patent 2,926,147 for composition containing polyester, organic polyisocyanate, tertiary amine salt, and alkali metal carbonate and process of preparing foam therefrom.

New Departure Division
Bristol, Connecticut

• **Wallace F. Dunn,** (*B.M.E., Pratt Institute, 1927*) manager, Product Engineering Design Section, inventor in patent 2,923,582 for a separator.

Oldsmobile Division
Lansing, Michigan

• **Robert Seyfarth,** (*B.S.M.E., Princeton University, 1936*) senior engineer, inventor in patent 2,926,895 for automatic choke improvement.

• **Gilbert Burrell,** (*B.S.E.E., Michigan State University, 1928*) motor engineer, inventor in patent 2,926,972 for crankshaft lubricating means.

• **Albert D. Baker,** (*B.S.M.E., Purdue University, 1926*) heating, cooling, and ventilating engineer and **Henning W. Rundquist,** (*B.S.M.E., Michigan State University, 1929*) senior project engineer, inventors in patent 2,929,226 for a throttle control mechanism.

• **Kenneth E. Faiver,** (*B.S.E.E., Notre Dame University, 1924 and Ph.D., Rensselaer Polytechnic Institute, 1927*) senior project engineer, inventor in patent 2,929,640 for a height adjuster for automobile suspension.

GM Overseas Operations Division
New York, New York

• **David Gormley,** (*Higher National Certificate in Electrical Engineering, Luton College of Further Education, 1952*) senior engineer, Vauxhall Motors, Ltd., Luton, England, inventor in patent 2,929,982 for electrical power supply units.

Pontiac Motor Division
Pontiac, Michigan

• **John Z. DeLorean,** (*B.S.I.E., Lawrence Institute of Technology, 1948; M.S.A.E., Chrysler Institute, 1952; M.B.A., University of Michigan, 1957; and Detroit College of Law*) assistant chief engineer, inventor in patents 2,919,604 for a transmission; 2,922,635 for vehicle suspension; and 2,926,510 for a universal joint.

• **George T. Timoff,** (*B.S.E.E. and B.S. in Mathematics, University of Michigan, 1953*) senior project engineer, and George E. McGill, retired, inventors in patent 2,920,186 for a vehicle dome light.

• **Richard E. Hulten,** (*B.M.E., University of Minnesota, 1955*) senior designer, inventor in patent 2,922,493 for an oil pump mounting.

GM Manufacturing Staff
Warren, Michigan

• **Charles A. Nichols,** (*B.S.M.E., Carnegie Institute of Technology, 1923*) technical assistant to the vice president, inventor in patent 2,919,611 for cold forming apparatus and method.

• **William A. Fletcher,** (*General Motors Institute, 1930*) director of advanced development; **Charles A. Nichols*; Carl L. Clevinger,** senior engineer, Delco-Remy Division; and **Forest L. Zion,** special machine builder, Delco-Remy Division, inventors in patent 2,920,378 for manufacture of commutators.

• **Robert B. Colten,** (*B.S., University of Michigan, 1939*) staff engineer; **Robert G. Pfetsch,** now with Detroit Transmission Division; and **Ralph B. Sylvester,** (*B.S.E.E., Wayne State University, 1960*) project engineer, inventors in patent 2,924,968 for press load measuring apparatus.

• **Otto W. Brandt,** (*University of Detroit*) process engineer, and **Philip West,** (*B.I.E., General Motors Institute, 1949*) senior project engineer, inventors in patent 2,929-120 for a method of defining sand cores.

GM Research Laboratories
Warren, Michigan

• **Worth H. Percival,** (*B.S., Iowa State College, 1942, and M.S., Massachusetts Institute of Technology, 1947*) assistant head, Mechanical Development Department,

inventor in patent 2,919,540 for a mechanism for utilizing waste heat.

• **Edward F. Weller, Jr.,** (*B.S.E.E., University of Cincinnati, 1943*) assistant head, Physics Department, and **Albert S. Lecky,** (*Akron University*) assistant head, Technical Facilities Department, inventors in patent 2,919,576 for an engine indicator apparatus.

• **Joseph F. Lash,** (*B.S.M.E., Michigan State College, 1938*) supervisor, Special Problems Department, inventor in patent 2,919,581 for a component transformation network.

• **Donald R. Whitney,** (*B.S.M.E., University of Michigan, 1942*) supervisor, missile system bearings, Special Problems Department, inventor in patent 2,919,960 for a precision spindle.

• **Frederick W. Bowditch,** (*B.S.M.E., University of Illinois, 1943; M.S.M.E., 1947, and Ph.D., 1951, Purdue University*) senior research engineer and **Lloyd L. Withrow,** (*A.B. in Chem., Oberlin College, 1922; M.A. in Chem., 1923, and Ph.D., 1925, University of Wisconsin*) head, Fuels and Lubricants Department, inventors in patent 2,919,688 for a cylinder and piston assembly.

• **Eugene A. Hanysz,** (*B.S.E.E., 1945, and M.S.E.E., 1948, University of Michigan*) supervisor of electro-physical research section; **Clark E. Quinn,** senior research engineer; and **Edward F. Weller, Jr.*,** inventors in patent 2,920,269 for a coating thickness gage.

• **Robert F. Thomson,** (*B.S.M.E., 1937; M.S.M.E., 1940; and Ph.D., 1941, University of Michigan*) head, Metallurgical Engineering Department, inventor in patent 2,923,989 for self lubricating shell molds.

• **James C. Holzwarth,** (*B.S.M.E., 1945, and M.S.M.E., 1948, Purdue University*) assistant head, Metallurgical Engineering Department and **Robert F. Thomson*,** inventors in patent 2,924,517 for copper base alloy.

• **Joseph T. Wentworth,** (*B.S.M.E., University of Michigan, 1952*) senior research engineer, inventor in patent 2,926,892 for fuel shut off mechanism.

• **Albert F. Welch,** (*B.S.E.E., Tufts College, 1948*) head, Electronics Instrumentation Department, and **Robert F. Thomson*,** inventors in patent 2,927,461 for a fuel metering system.

• **John S. Collman,** (*B.S., Naval Architecture and Marine Engineering, University of Michigan, 1940*) assistant head, Engineering Development Department, inventor in patent 2,929,217 for a working medium control system for a closed circuit gas turbine power plant.

Rochester Products Division
Rochester, New York

• **Donald D. Stoltman,** (*B.S.M.E., Rensselaer Polytechnic Institute, 1947, and M.S. in automotive engineering, Cornell University, 1948*) senior project engineer, inventor in patent 2,922,630 for a fuel injection cranking signal modifying device.

• **Ronald C. Groves,** (*B.E.E., 1936 and B.M.E., 1937, Lawrence Institute of Technology*) staff engineer, inventor in patent 2,924,206 for a fuel injection system.

• **Adolph F. Braun,** (*B.S.M.E., University of South Dakota, 1928*) chief engineer, inventor in patent 2,929,613 for a carburetor.

Saginaw Steering Gear Division
Saginaw, Michigan

• **Philip B. Zeigler,** (*B.S.M.E., Purdue University, 1941*) chief engineer, Product Engineering Department; C. W. Lincoln, retired; and Henry D. Spiekerman, no longer with GM, inventors in patent 2,919,600 for a transmission control external tube.

• **Philip B. Zeigler*,** and C. W. Lincoln*, inventors in patent 2,919,679 for a fluid power steering gear with damping feature.

• **Donald P. Marquis,** (*B.S.Chem.E., 1934 and M.S., 1939, Wayne State University*) assistant chief engineer, Engineering Department, and **Raymond J. Schultz,** (*B.S.M.E., University of Michigan, 1950*) senior project engineer, inventors in patent 2,922,680 for a bearing support.

GM Styling Staff
Warren, Michigan

• **John Himka,** (*diploma in Aero.E., Academy of Aeronautics, 1941*) general supervisor, inventor in patent 2,924,265 for a vehicle seat.

• **Anthony J. Ingolia,** (*M.S. in product design, Illinois Institute of Technology, 1952*) senior designer, inventor in patent 2,926,507 for a refrigerating apparatus.

• **Hans O. Koplin,** (*Diploma, Technical Institute—Art School, Berlin, Germany, 1926*) senior project engineer; **Ted Stewart,** (*Lawrence Institute of Technology*) senior design engineer; **John O. C. Pietsch,** (*General Motors Institute, 1939*) senior project engineer, Fisher Body Division; and **Harry W. Roach,** senior designer, Fisher Body Division, inventors in patent 2,926,948 for a folding seat structure for a vehicle body.

• **Rudolph H. Ferrara,** (*Knox College*) senior project engineer, inventor in patent 2,927,818 for a vehicle seat.

Ternstedt Division
Detroit, Michigan

• **Akira Tanaka,** (*B.S.M.E., Michigan State University, 1949*) group leader, design, inventor in patent 2,919,744 for a seat adjuster mechanism.

• **John P. Bogater,** (*B.S.M.E., Detroit Institute of Technology, 1937*) design group leader, inventor in patent 2,922,184 for a lid hinge and counterbalance.

• **Thomas E. Lohr,** (*Tri-State College*) senior design engineer, inventor in patent 2,927,627 for a vehicle seat adjuster.

• **Thomas E. Lohr*; George W. Sierant,** (*B.M.E., Lawrence Institute of Technology, 1947*) design group leader; and **Akira Tanaka*,** inventors in patent 2,929,439 for a vehicle seat adjuster.

• **William G. Hoag,** (*B.S.C.E., University of Michigan, 1929*) design group leader, and **Paul Widmer,** (*Machine Design Diploma, Niedernzwil, Switzerland, 1936*) senior designer, inventors in patent 2,929,528 for a telescopic stay for automotive vehicle lift gate and the like.

Solution to the Previous Problem:

Determine the Basic Design Parameters for a Strain Gage, Shaft-Type Torquemeter

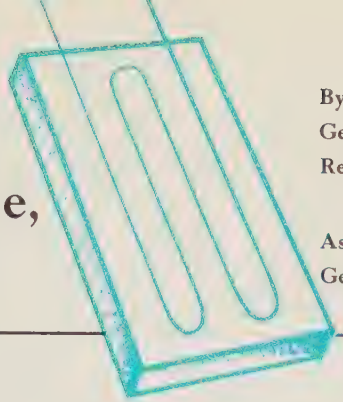

By ROBERT W. CAMPBELL
General Motors
Research Laboratories

Assisted by James Bay
General Motors Institute

In an electro-mechanical transducer using strain gages, the mechanical member(s) should be designed so that maximum strain is obtained for the given maximum load without exceeding the physical limitations of the material. The larger the strain, the greater the signal output and, therefore, the greater the sensitivity. This is the solution to the problem presented in the April-May-June 1960 issue of the GENERAL MOTORS ENGINEERING JOURNAL in which basic design parameters were to be established for one type of electro-mechanical transducer—a strain gage, shaft-type torquemeter. The parameters established were as follows: (a) the diameter of the gage section of the shaft should be *1.425 in.*, (b) four active strain gages should be used in a Wheatstone bridge circuit arrangement with the gages mounted at 45° angles with the shaft axis, and (c) the maximum and minimum signal output voltages should be *9.1* (10^{-3}) *volts* and *2.41* (10^{-3}) *volts*, respectively.

THE solution to the problem is divided into three parts: (a) calculations to determine the gage section diameter of the shaft, (b) selection of the proper type of strain gage to use from the four types available and specifications relating to the proper positioning of the gages on the shaft, and (c) calculations to determine the signal output voltages.

Part (a)—Gage Section Shaft Diameter

To determine the diameter of the gage section of the shaft requires, first of all, calculating the torque at the maximum and minimum load points in the operating cycle. The torque, in terms of horsepower and shaft speed, can be expressed as

$$T = \frac{(63{,}000)(hp)}{N} \qquad (1)$$

where

T = torque (in-lb)

hp = horsepower

N = shaft speed (rpm).

Substituting values for hp and N at the specified maximum and minimum load points into equation (1) gives the following maximum and minimum values for torque:

$$T_{max} = \frac{(63{,}000)(350)}{1{,}850} = 11{,}910 \text{ in-lb}$$

$$T_{min} = \frac{(63{,}000)(20)}{400} = 3{,}150 \text{ in-lb.}$$

Since it was assumed that no axial forces act on the shaft, the maximum tensile forces will occur in planes inclined at 45° with respect to the shaft axis. At this angle the tensile stress S_t, or compressive stress for inclined planes at 135° from the shaft axis, is equal to the shear stress S_s. The maximum shear stress limit of 30,000 psi, therefore, is the more critical stress condition.

The next step is to determine if the maximum shear stress or the maximum angle of twist Θ is the more severe limitation. The unit shearing stress in the outer fibers of the shaft can be expressed as

$$S_s = \frac{(E_s)(r)(\Theta)}{L_g} \qquad (2)$$

where

S_s = shear stress (psi)

E_s = modulus of elasticity in shear (psi)

r = shaft radius (in.)

Θ = angle of twist (radians)

L_g = length of gage section of shaft (in.).

Wheatstone bridge with four active strain gages gives maximum signal from transducer

Solving equation (2) for S_s, using the given maximum allowable angle of twist Θ of 4° in 20 diameters of length ($r = D_g/2$, $L_g = 20D_g$), gives:

$$S_s = \left[\frac{(12)(10^6)(1)}{(20)(2)}\right]\left[\frac{4\pi}{180}\right] = 20{,}940 \text{ psi.}$$

Since this design stress is within the shear stress limit, the angle of twist is the more restrictive limitation.

Using the new design stress of 20,940 psi and the maximum torque of 11,910 in-lb, the minimum shaft diameter D_g for the gage section can be calculated using the following basic relationships:

$$S_s = \frac{Tr}{J} = \frac{16T}{\pi(D_g)^3}$$

or

$$D_g = \sqrt[3]{\frac{16T}{\pi S_s}} \qquad (3)$$

where

T = torque (in-lb)

r = shaft radius (in.)

J = polar moment of inertia (in.^{4})

D_g = gage section diameter of shaft (in.).

Substituting the calculated values for T and S_s into equation (3) and solving gives the following value for the gage section diameter of the shaft:

$$D_g = \sqrt[3]{\frac{(16)(11{,}910)}{\pi(20{,}940)}} = 1.425 \text{ in.}$$

Part (b)—Strain Gage Selection, Installation, and Wiring

Four types of strain gages were given as available for use—A-7, C-7, AB-1, and CB-11. The type AB-1 strain gage should be used because of the oily atmosphere and duration of the test conditions[1]. Types A-7 and C-7 are paper-backed gages and would not be dependable enough for tests of long duration where accuracy is important. The iso-electric type gages (prefix letter C) are primarily intended for making dynamic measurements only, such as instantaneous torque measurements.

In general, when a test is to be of long duration, or when both static and dynamic values are to be observed and the strains to be measured are of sufficient magnitude, the constantan gages (prefix letter A) are recommended because of their smaller temperature coefficient (less zero shift).

Actually, there are many factors which influence the selection of a strain gage, such as available mounting area, ambient temperature conditions during the test, accuracy requirements, types of strain (uni-directional, bi-directional, static, dynamic), sensitivity requirements, and gage resistance. For example, all other factors being acceptable, the use of a higher resistance gage is desirable because of the greater allowable excitation voltage and consequent larger signal voltage for the same magnitude of strain. A thorough discussion of all factors which influence strain gage selection can be found in the literature[2,3].

To obtain a maximum signal from the transducer (torquemeter), a Wheatstone bridge circuit arrangement with four active gages should be used (Fig. 1). This arrangement will provide an output signal voltage four times greater than that provided by a single strain gage.

The gages should be mounted at 45°-angles with the shaft axis. Gages R_1 and R_3 and R_2 and R_4 should be mounted diametrically opposite each other on the shaft surface. This method of gage mounting will provide automatic temperature compensation and also eliminate the effects of all strains other than torsional strains. After installation, the gages and leads should be moisture proofed. Electrical balancing of the bridge can be done by a bridge balance box to which the bridge is wired through the slip rings.

Part (c)—Signal Voltage Output

A shaft in torsion is actually a special case of a two-dimensional strain where the strains are equal but of opposite sign. It would be incorrect to calculate shaft strain by dividing shaft stress by the modulus of elasticity, because of the effect of Poisson's ratio. The shaft stress, therefore, can be calculated by the following equation:

$$S = \frac{\varepsilon E}{1 + \mu} \qquad (4)$$

where

S = shaft stress (psi)

ε = strain (in. per in.)

E = modulus of elasticity (psi)

μ = Poisson's ratio.

For steel, $E = 30(10^6)$ and $\mu = 0.303$.

From Part (a), $S = S_s = 20{,}940$ psi (maximum). Equation (3) can be used to determine the minimum value for $S = S_s$ as follows:

$$S_{s(min)} = \frac{16(T_{min})}{\pi(D_g)^3} = \frac{16(3{,}150)}{\pi(1.425)^3}$$

$$S_{s(min)} = 5{,}540 \text{ psi.}$$

From equation (4):

$$\varepsilon = \frac{S(1 + \mu)}{E}.$$

Maximum and minimum values of strain can now be calculated by substituting into equation (4) the maximum and minimum values for shaft stress S.

$$\varepsilon_{max} = \frac{(20{,}940)(1.303)}{30(10^6)} = 910(10^{-6}) \text{ in. per in.}$$

$$\varepsilon_{min} = \frac{(5{,}540)(1.303)}{30(10^6)} = 241(10^{-6}) \text{ in. per in.}$$

The following strain gage bridge circuit indicates that gages R_1 and R_3 are in tension (increasing gage resistance) for the direction of shaft rotation specified.

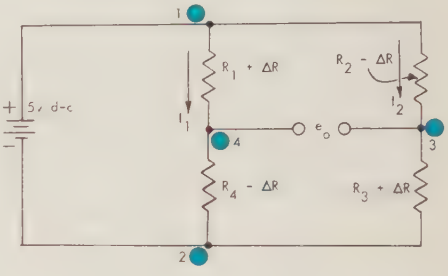

The gage resistance for the type AB-1 strain gage, as specified by the manufacturer[1], is 350 ohms. Therefore,

$$R_1 = R_2 = R_3 = R_4 = R = 350 \text{ ohms.}$$

If it is assumed that the impedance of the instrumentation is much larger than the bridge impedance, thereby causing negligible loading effect on the bridge,

$$e_{o(4\text{-}3)} = I_1(R_4 - \Delta R) - I_2(R_3 + \Delta R)$$

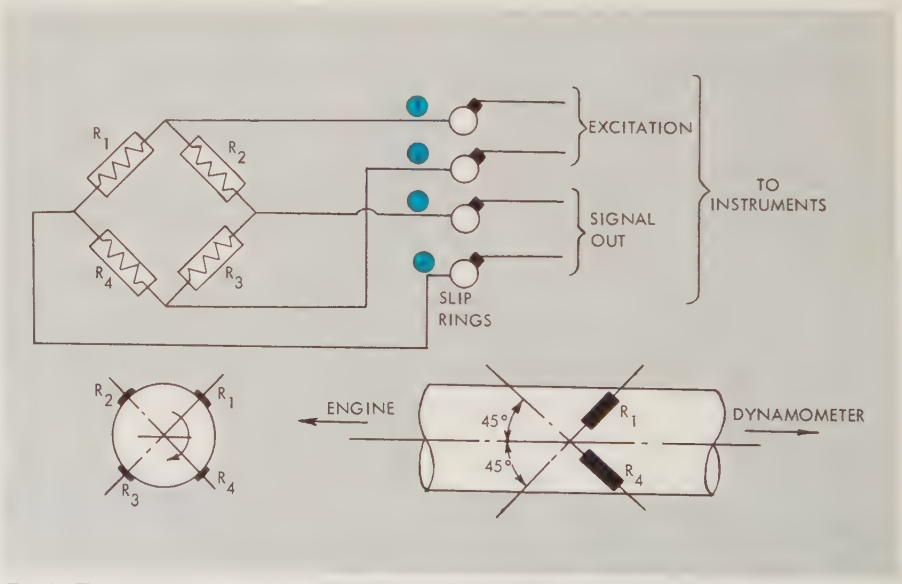

Fig. 1—To provide maximum signal output, four strain gages should be used in a Wheatstone bridge circuit arrangement. The gages should be mounted at 45° angles with the shaft axis, as shown, and gages R_1 and R_3 and R_2 and R_4 should be mounted diametrically opposite each other.

where

ΔR = change in gage resistance R due to strain

$$I_1 = \frac{V}{2R} = I_2$$

$$e_o = \frac{V}{2R}\left[(R - \Delta R) - (R + \Delta R)\right]$$

$$e_o = \frac{-V(\Delta R)}{R}. \qquad (5)$$

The minus sign in equation (5) means that point *3* is more positive than point *4*, for the battery polarity shown. To determine ΔR, the gage factor equation given in the problem can be used as follows:

$$G.F. = \frac{\frac{\Delta R}{R}}{\varepsilon} \qquad (6)$$

The gage factor equation is a dimensionless relationship between the change in resistance of the gage and the change in length, or strain. The gage factor, therefore, is a measure of gage sensitivity.

The gage factor for the type AB-1 gage, as specified by the manufacturer[1], is 2. Substituting this value plus the resistance R value of 350 ohms and the calculated maximum and minimum values for ε into equation (6) and solving for ΔR gives the following values for the maximum and minimum change in gage resistance due to strain.

$$\Delta R = (G.F.)(R)(\varepsilon)$$

$$\Delta R_{max} = (2)(350)(910)(10^{-6}) = 0.637 \text{ ohm}$$

$$\Delta R_{min} = (2)(350)(241)(10^{-6}) = 0.169 \text{ ohm}.$$

The signal voltages can now be calculated by applying equation (5).

$$e_{o(max)} = \frac{(5)(0.637)}{350} = 9.1(10^{-3}) \text{ volt}$$

$$e_{o(min)} = \frac{(5)(0.169)}{350} = 2.41(10^{-3}) \text{ volt}.$$

Summary

The signal voltages (Part c) were obtained by using nominal numbers—that is, gage resistance is actually 350 ohms ± 8 ohm, ignoring such factors as lead wire resistances. Therefore, these voltages are only close approximations and are intended to help the engineer determine the requirements for the instruments to be connected to the strain-gage bridge. From these values it can be determined how much, if any, signal amplification is needed. The polarity of the output signal also can be determined. Final calibration—that is, a known galvanometer deflection for a known load—is made in the instrument controls.

Actually, the bridge output voltage could have been obtained very quickly with the following equation[2]:

$$e_o = \frac{(V)\ (G.F.)\ (\varepsilon)}{4} \qquad (7)$$

where

e_o = output voltage

V = excitation voltage

$G.F.$ = gage factor

ε = strain.

Equation (7) is an equation for the output voltage of a Wheatstone bridge circuit arrangement using only one active strain gage. However, if $\Delta R/R$ divided by ε is substituted for $G.F.$ in equation (7) and the result multiplied by 4 (for four active gages) the result will be the same as equation (5). The longer method was used in the solution to illustrate the principles involved.

For greater accuracy, it is desirable to have as large a signal-to-noise ratio as possible. For this reason, the gage section diameter of the shaft was made as small as the material limitations permitted to provide maximum allowable strain at maximum load.

A somewhat arbitrary shaft-twist limit was imposed in the problem specifications to illustrate the need for the designer to consider the complete system in which the transducer is to be used. Not only the magnitude of the forces must be considered, but also the dynamic characteristics of the masses causing the forces. In actual practice, the engineer designing the torquemeter must consider the dynamic effect of the dynamometer on the response of the torquemeter. For this particular problem, the effect of the masses was simulated with the imposition of the twist limit.

Even with a safe shaft diameter determined by the twist limit, it is still prudent to keep the gage section of the shaft as short as possible while still allowing sufficient area for gage installation. This is to keep shaft twist, or windup, as small as possible. There are two reasons for doing this: (a) to maintain good transient response of the torquemeter and (b) to keep the possibility of shaft fatigue to a minimum by limiting the flexing of the shaft. In regard to transient response of the torquemeter, the combination of shaft windup and dynamometer-rotor mass could act as a spring-mass system and cause spurious oscillations in the mechanical system, thereby affecting the accuracy of the strains being measured.

Although slip rings are part of the torquemeter, the actual details of the slip ring assembly were omitted from the problem. The design of slip ring assemblies for sensitive measurements, especially at higher rpm, is more of an art than a science. This is especially so in the case of strain measurements, because of the very low resistance changes in the strain gages. Poor design and/or selection of slip ring assemblies can easily result in contact resistances larger than the resistance change being measured. Although good design information is available in the literature, experience is still a most important factor in the design of an acceptable slip ring assembly.

This problem has dealt with the design of the first primary functional component in a measuring system—the transducer. To complete the design of a measuring system, two other primary components must be considered—the matching network and the recorder. On pages 52 through 57 is presented a problem dealing with the design of the matching network and recorder needed to complete the torque measuring system discussed here.

Bibliography

1. "SR-4 Strain Gages, Instruments, and Accessories," Specification and Price List No. 4310, February 1, 1959, Baldwin-Lima-Hamilton Corporation, Electronics Instrument Division, Waltham 54, Massachusetts.

2. Perry, C. C., and Lissner, H. R., *The Strain Gage Primer* (New York: McGraw-Hill Book Co., Inc., 1955).

3. Murray, William M., and Stein, Peter K., *Strain Gage Techniques, Parts I and II*, published by the Massachusetts Institute of Technology, 1956.

A Typical Problem in Engineering:

Complete the Design of a Torque Measuring Instrumentation System

By LESTER V. OSTRANDER, JR.
General Motors
Research Laboratories

Assisted by James Bay
General Motors Institute

Instrumentation is of paramount importance to nearly all basic and applied research activities. Of special significance is instrumentation used to measure dynamic phenomena. Such instrumentation is comprised of three functional units: a transducer, a matching network, and a recorder. Each unit must be designed to be compatible with the others to meet requirements of frequency response, sensitivity, and impedance matching. In the April-May-June 1960 issue of the GENERAL MOTORS ENGINEERING JOURNAL, the typical problem in engineering presented dealt with determining the basic design parameters of a strain gage, shaft-type torquemeter. This torquemeter, or transducer, was to measure the instantaneous fluctuations of load on an automatic transmission. The problem presented here represents a continuation of the strain gage torquemeter problem in that design parameters for the remaining two units of the torque measuring system—the matching network and recorder—are to be determined.

Establish design parameters for the matching network and recorder components

TODAY, very few basic and applied research programs can proceed without the use of instrumentation to provide measurements of physical phenomena. The application of instrumentation to make accurate measurements of phenomena during a test of experimental working models is an important step in indicating what the actual operating characteristics will be. Comparison of measured values with theoretical values provides information needed by the scientist or research engineer to evaluate the accuracy of his predictions. In some cases, new theories may evolve as a direct result of measurements made during controlled test conditions.

To obtain the desired information from rapidly varying phenomena during a test, several variables must be measured simultaneously. If test records are to be used for analyzing the operation of a system, each measured variable must have some parameter in common with each of the other variables to provide a basis for comparison. For most measurement systems, this common parameter is time. The time reference is obtained by recording each of the measured variables on the same record. The recording medium, such as paper or tape, is driven at a constant speed past a recording pen, tape recorder head, or light beam. The length of the recording medium, therefore, is a direct measure of time for the test.

A separate instrumentation channel is required for each variable to be measured, except for some special cases such as time integration of acceleration to obtain velocity rather than directly measuring the velocity. Each channel of instrumentation is composed of units whose functions are compatible with the characteristics of the varying parameter, such as frequency and amplitude.

The type of information desired at the output is an important consideration in the selection of instrumentation making up the measurement channel. This instrumentation must be selected primarily on the basis of impedance considerations to insure that it has, at most, only a negligible effect on the operating characteristics of the device being tested.

Measuring System Must Not Affect Operation of Test Unit

The application of instrumentation to the measurement of dynamic phenomena[1] requires careful consideration of the characteristics of each component in the test unit whose variables are to be measured and proper selection of components for the measuring system according to the type of information desired. The physical characteristics of the overall test unit establish the limits of frequency and transient response required in the measuring system.

The fundamental requirement of any measuring system is that it should not noticeably alter the operating characteristics of the test unit. The measuring instruments must not add or remove any appreciable amount of energy to or from the test unit being measured. This requires that loading of any type be kept to a minimum.

In the torque measuring system used as the basis for the typical problem in engineering presented in the April-May-June 1960 issue of the JOURNAL*, the electrical portion of the test unit had no direct interaction with the electrical portion of the measuring system; therefore, no electrical loading occurred. Physical loading was present in the weight added to the test unit by the installation of the strain gages and slip rings. The added weight involved, however, was negligible when compared with the larger weight values for the moving parts of the engine, transmission, and dynamometer. Most of the weight added was balanced by the reduced diameter of the coupling shaft between the transmission and the load. Friction of the brushes on the slip rings contributed some loading. The friction forces involved, however, were quite small in comparison to the forces acting within the test unit.

Measuring System Comprised of Three Functional Units

Any measuring system can be reduced to three functional units, although several components may be required to accomplish each desired function. The three functional units are:

- A transducer, or sensing element
- A matching network
- An indicator, or recorder.

*Please see "*A Typical Problem in Engineering:* Determine the Basic Design Parameters for a Strain Gage, Shaft-Type Torquemeter," pp. 55-58, April-May-June 1960 issue. The solution to this problem appears on pp. 49-51 of this issue.

The function of a transducer is to sense the quantity being measured and provide an output which varies in proportion to this quantity. For example, the strain gage, shaft-type torquemeter of the torque measuring system sensed the torque transmitted from an automatic transmission to a dynamometer. The output from the transducer was an electrical signal proportional to the torque transmitted through the shaft.

The function of a matching network is to transfer the transducer signal to the recorder. The matching network must have a sufficiently high impedance to prevent loading of the transducer and also must provide a signal at the power level required to drive the recorder. This drive signal may require amplification or attenuation of the transducer signal.

The function of a recorder is to convert the electrical drive signal to a proportional physical motion of a meter pointer, pen or light beam, or a proportional tape head current. The recorder is selected to provide the required frequency response and number of channels for simultaneous recording of several variables.

Problem

The problem is to determine the necessary parameters for a matching network and recording unit needed to complete the design of a torque measuring instrumentation system initiated with the typical problem in engineering presented in the April-May-June 1960 issue of the JOURNAL. It will be required to determine the necessary relationships between the parameters of the transducer, matching network, and recorder to provide an accurate measurement of both static and dynamic torque between the transmission and dynamometer. The strain gage, shaft-type torquemeter, the design parameters of which are presented on pages 49-51 of this issue, is to be used as the transducer for the measuring system.

The parameters to be determined are:

(a) Bridge excitation voltage for highest signal-to-noise ratio
(b) Effect of excitation voltage drift
(c) Output impedance of strain gage bridge
(d) Effect of electrical loading on bridge output voltage
(e) Required frequency response needed to select a galvanometer
(f) Resistance values in galvanometer circuit to provide the required damping and required gain or attenuation of the matching network for desired galvanometer deflection.

Strain Gages Limit Bridge Excitation Voltage

The maximum limit of bridge excitation voltage is primarily dependent on the power dissipation capabilities of the strain gages. Experience has indicated that a good "rule of thumb" is to limit the current through any strain gage to 25 milliamperes. For the strain gage bridge described in the solution to the shaft-type torquemeter problem, each gage had a nominal resistance of 350 ohms, as shown in the following circuit diagram.

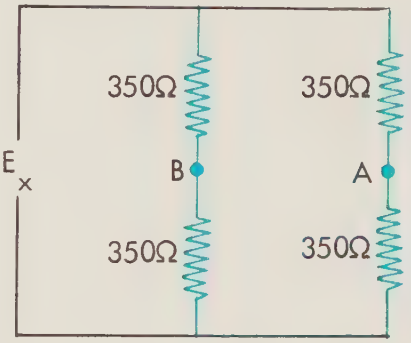

It is desirable, particularly when working through slip rings, to have as high a signal level as possible to maintain a good signal-to-noise ratio. The bridge output signal amplitude for a particular value of torque is directly proportional to the bridge excitation voltage amplitude.

Part (a)—Determine Maximum Bridge Excitation Voltage

For Part (a) of the problem determine the value of the bridge excitation voltage E_x to provide maximum output voltage within safe operating limits of strain gage power dissipation. To allow a safety factor for loading, the excitation voltage is to be specified to the next lowest value in terms of five-volt increments. For example, if $E_x = 29.8$ volts, specify 25 volts. If $E_x = 11.2$ volts, specify 10 volts.

At the value of excitation voltage determined from these calculations, calculate the bridge output voltage at maximum torque (point A with respect to point B in the following circuit diagram) for the values solved for in the solution to the shaft-type torquemeter problem. These values are:

R = 350 ohms

ΔR = 0.637 ohms.

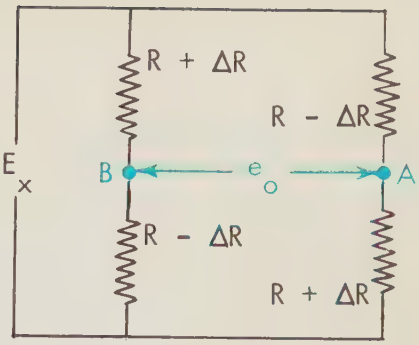

In this circuit diagram,

E_x = excitation voltage
R = strain gage resistance at no load
ΔR = change in strain gage resistance due to load
e_o = output voltage.

The general equation for the open-circuit output voltage e_o may be written by referring to the circuit diagram shown above.

Although d-c values will be used in the calculations and discussion of this problem and solution, the bridge excitation could be an a-c voltage. The equations would remain the same except that a-c rms values of current and voltage would be used in place of d-c values. When a-c is used for bridge excitation, it is usually provided by an oscillator in a carrier-amplifier systen. The carrier-amplifier also provides the necessary adjustments for phase balancing both the bridge and demodulating circuit to provide a d-c output proportional to the strain on the bridge strain gages. The carrier or bridge-excitation frequency imposes definite limits on the high-frequency response of the amplifier system. In general, the highest frequency to be amplified should not be greater than one-fifth of the carrier frequency.

Part (b)—Determine the Effect of Excitation Voltage Drift

A substitution of different values for E_x into the general equation which is to be written for the open-circuit voltage e_o in Part (a) will show the effect of excitation voltage drift. This effect will be reasonably apparent from the form of the equation for e_o when R and ΔR are held constant.

Part (c)—Determine Output Impedance of Bridge

First, assume that the strain gage bridge is perfectly balanced. Determine

the output impedance of the bridge in terms of gage resistance R. Replace the excitation source by a general term for its internal impedance Z_x. Note the effect of Z_x on the output impedance when the bridge is balanced.

Next, assume that the bridge is unbalanced due to a torque load. Again, calculate the output impedance. Substitute the following values into the equation to determine the magnitude of the effect of the unbalance on the output impedance:

R = 350 ohms
ΔR = 1 ohm
Z_x = 1 ohm.

Eliminate any terms having a negligible effect on the result and compare the value of the output impedance obtained with the balanced bridge to that obtained for the unbalanced bridge.

Part (d)—Determine the Effect of Electrical Loading on Bridge Output Voltage

Connecting a load across the bridge output terminals will have a direct effect on the output voltage amplitude. The following circuit diagram shows the

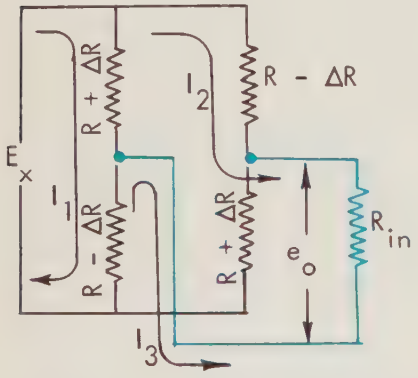

bridge with a load R_{in} across the output terminals. The load R_{in} represents the input impedance of the matching network. Write loop equations for currents I_1, I_2, and I_3 in terms of E_x, R, ΔR, and R_{in}. Substitute various multiples of R for R_{in} to obtain the relationship between the ratio of R_{in} to R and the ratio of output voltage with the load to open circuit output voltage. Plot the results on semi-log paper for values of R_{in}/R from 0.1 to 1,000 on the log scale. The values of

$$\frac{e_o \text{ (loaded)}}{e_o \text{ (open circuit)}}$$

will be between zero and one on the linear scale.

The same results may be obtained by use of the Thevenin equivalent circuit for the bridge, as shown in the following circuit diagram.

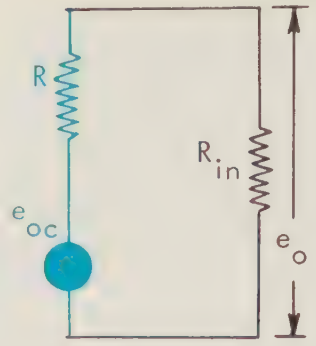

In this circuit diagram, e_{oc} and R are the Thevenin equivalent of the bridge shown in the previous diagram. Also,

e_{oc} = open circuit voltage for a given torque
R = output impedance of bridge
R_{in} = load resistance (usually the impedance of the matching network)
e_o = output voltage across the load.

Using the Thevenin equivalent circuit for the bridge will reduce the number of equations required to solve Part (d). The results will indicate that R_{in} should be at least 10 times as large as R for less than 10 per cent attenuation of output voltage.

Although output voltage may be reduced by loading, this is not the only criterion for determining the required impedance relationships. Current-sensitive devices operating at low power levels may be directly connected to the bridge if the output voltage swing is sufficiently low. The load current, in any case, should not be allowed to cause more than 25 milliamps of current in any gage. The peak gage current is comprised of the current at balance plus the load current due to unbalance.

Potentiometer May Be Used to Balance Strain Gage Bridge

An external adjustment may be required to bring the bridge into perfect balance at zero strain. If a commercial bridge balance or carrier-amplifier unit is used, the adjustment is built in and no external components are needed.

If an external adjustment is needed, however, several methods may be used. Only one will be described here. As shown in the following circuit diagram, a potentiometer may be connected across the excitation terminals of the bridge.

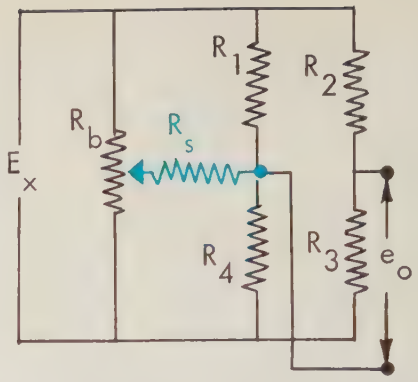

The wiper arm of the potentiometer is then connected to one of the bridge output terminals. The bridge will be balanced when the wiper arm is so adjusted as to indicate zero d-c voltage at the bridge output terminals.

To prevent excessive loading of the bridge, the resistance R_b must be large with respect to the gage resistance. A ratio of R_b to R equal to or greater than 10 is desirable. The actual value is not critical as long as a high ratio is used. Sometimes, the bridge may be adjusted very close to balance, but because of resolution limitations of the pot perfect balance cannot be obtained. If R_s, for this condition, is added between the pot arm and the bridge output terminal, the adjustment is broadened and the wiper arm position is not so critical. Also, with R_s in the circuit, the strain gages have some protection if R_b is adjusted to either extreme of its range. A good value for R_s is about one-tenth R_b.

Maximum Frequency Limit Arbitrarily Determined

The maximum signal frequency for which the measurement system must be designed depends on several considerations. The purpose of the test is one primary consideration. Many tests are made only to measure steady state operating characteristics. Although transients may be present, it is not necessary to provide the frequency response needed to measure them if they are not important to the test.

Steady state does not imply that all conditions of operation are constant, but rather that any variations must be repetitive or cyclic in nature. An example of this type of steady-state operation is the response of a servo system to a sinusoidal input of constant frequency and amplitude.

Several types of operation may, in a broad sense, be considered as transients.

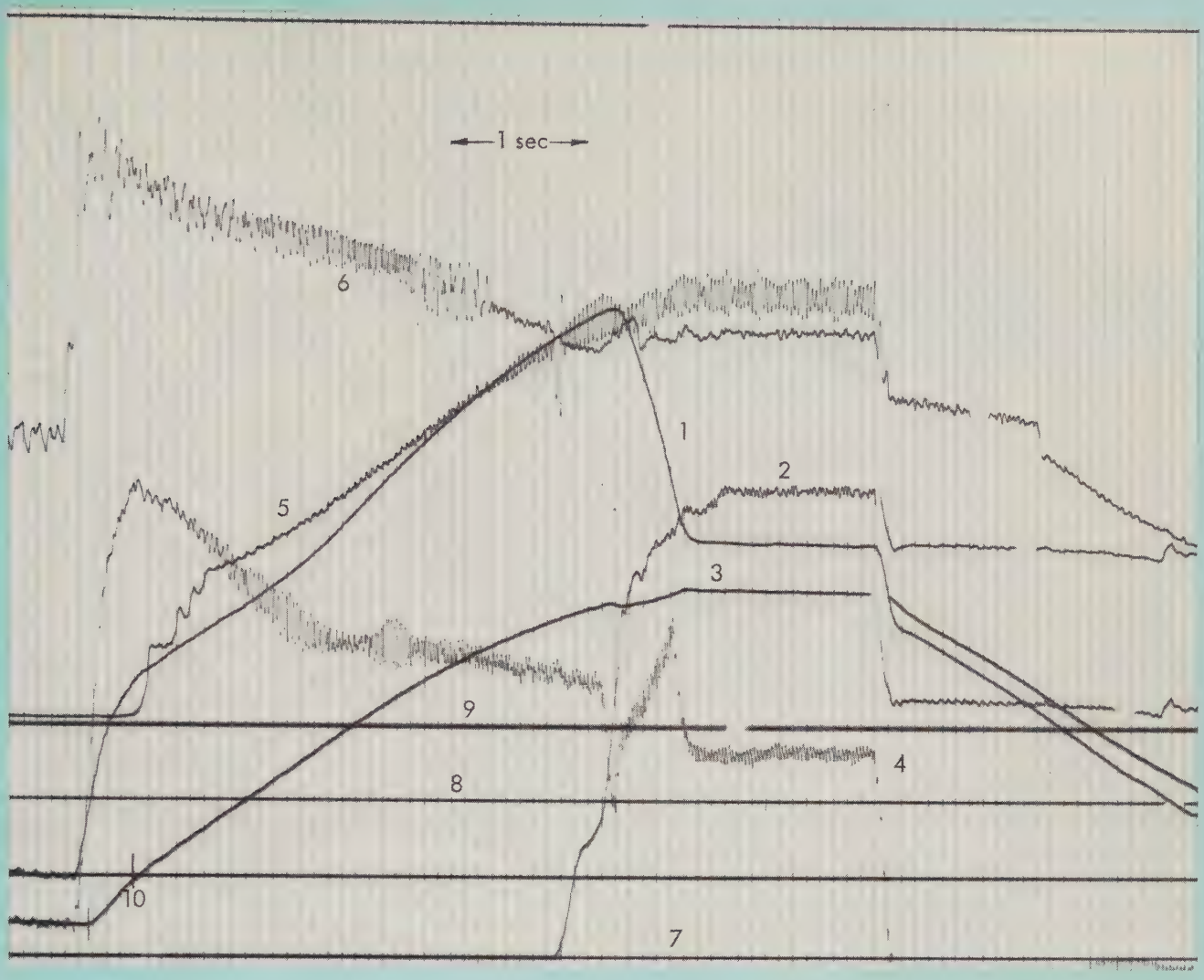

Fig. 1—Reproduced here is a typical light beam oscillograph record made by the Fuels and Lubricants Department of the General Motors Research Laboratories during an automobile transmission test. The traces shown on the record are as follows: engine speed *1*, clutch pressure *2*, dynamometer speed *3*, output torque *4*, governor pressure *5*, and main line pressure *6*. The paper speed for this record was 0.9 inches per second. This provided a time base of 1.111 seconds per inch. Each timing mark (vertical lines) represents a timing interval of 0.1 second. The test was calibrated for an engine speed of 1,000 rpm per in., a clutch pressure of 30 psi per in., a dynamometer speed of 1,000 rpm per in., an output torque of 200 lb per in., a governor pressure of 30 psi per in., and a main line pressure of 30 psi per in. Line *7* is the zero reference line for engine speed, clutch pressure, dynamometer speed, and output torque. Line *8* is the zero reference line for main line pressure and line *9* is the zero reference for governor pressure. Point *10* indicates the portion of the dynamometer speed curve which is used to determine the frequency response required for recording the transients.

For example, acceleration is a transient condition when measuring speed. In mechanical systems, speed and torque transients may be caused by gear back lash, belt elasticity or slip, linkage tolerances, or other factors which introduce non-linearities at some point in the test. The transients which are usually most important to measure are those resulting from a sudden or step-change in load.

The upper limit of frequency may be determined by measuring the system response to a step input in either direction or both directions. Any difference in step-input response in the two directions will indicate the presence of factors which are unilateral in character and will produce different transients depending on the direction of the step change.

Because the nature of the transients involved in a real system usually is not accurately known, actual practice requires some arbitrary selection of the maximum frequency limit. The limit to be used for Part (e) of the problem will be calculated from the maximum rise of the transmission output shaft speed. This rise in time, expressed in rpm per second, may be determined by preliminary recording of the transmission output speed with the dynamometer load. Examination of the test record would show the point of the greatest slope of the speed versus time curve at which the highest frequency component of the speed signal was present. The maximum frequency capability of the galvanometer should be at least 10 times greater than this high frequency component of the speed signal.

Part (e)—Determine Required Frequency Response and Select a Galvanometer

The test record used to determine the maximum required frequency response for recording the transients is a typical

GALVANOMETER NUMBER	FREQUENCY RANGE (CPS)	SENSITIVITY (IN. PER MICROAMPERE)	COIL RESISTANCE (OHMS)	EXTERNAL DAMPING RESISTANCE (OHMS)
1	0-30	0.217	30	350
2	0-180	0.0037	40	83
3	0-350	0.0022	22	25
4	0-600	0.0004	24	1,000
5	0-1,200	0.000109	24	200
6	0-3,000	0.000031	52	55

Table I—This is a listing of the important characteristics of six galvanometers from which one is to be selected to meet the required frequency response.

light beam oscillograph record of a transmission test made at the General Motors Research Laboratories (Fig. 1). The maximum slope of the dynamometer speed curve, which is the same as transmission output speed, can be found by inspecting the record. If the change in time Δt during which the maximum rate-of-change of the speed signal occurred is taken as one-half the period of the highest frequency, the highest frequency to be recorded may be calculated as:

$$f = \frac{1}{2(\Delta t)}.$$

The galvanometer is to be selected entirely on the basis of required maximum frequency response. Table I lists the most important characteristics of several galvanometers. Select the appropriate galvanometer to use for the torque measuring system from those listed. The galvanometer selected must respond to at least 10 times the frequency calculated from the maximum rise-time of the dynamometer speed record (Fig. 1).

Why a Light Beam Oscillograph Was Used as Recorder Component

After the maximum frequency response of the unit under test is determined, the next step is to select the recorder for the measuring system. As stated in Part (e), a light beam oscillograph was used to record the transients occurring during the transmission test. The discussion to follow explains why this type of recorder was selected.

Some of the factors which influence the type of recorder to use for a measuring system are based on the type of test being run, such as: the number of simultaneous measurements to be made; the type of presentation desired—for example, a permanent visual record as compared to stored information in electrical form if recorded on tape; and accuracy required. Other factors which influence the choice of recorder are determined by comparing the characteristics of each type of recorder. These would include: number of channels available, frequency response, sensitivity, accuracy limitations, and type of presentation.

Torque measurements usually are made in conjunction with several other variables such as speed, temperature, and pressure. For the torque measuring system discussed in this problem, therefore, a multi-channel type of recorder was desirable. This, then, narrowed the choice of recorder to a light beam oscillograph, a multi-channel pen motor recorder, or a multi-channel instrumentation type tape recorder.

In practice, from 8 to 16 channels are required to measure all parameters of interest in a test of an engine or a transmission. Also, it is usually required that a visible record be available rather than a stored electrical signal. The requirement of a visible record eliminated the tape recorder from consideration, except possibly as an intermediate step which would require playing the taped information into a visible record type of recorder. This left either the multi-channel pen motor type of recorder or the light beam oscillograph.

The pen motor type of recorder has one advantage over the light beam oscillograph—its record is immediately available without the development step required by the light oscillograph. For most applications, the superiority of the light beam oscillograph in sensitivity, frequency response, and accuracy outweigh the advantage of the immediate record availability of the pen motor recorder. For these reasons, therefore, the recordings for the torque measuring system were made by a light beam oscillograph.

Various Circuit Configurations Will Provide Galvanometer Damping

Damping is required in the galvanometer circuit to prevent excessive overshoot and phase shift during transients or high frequencies. Damping is accomplished in several ways, all of which produce a reaction proportional to the rate of change of the galvanometer deflection or current.

A galvanometer coil has the usual properties of an inductance to resist a change in the current. If a resistance path of the proper value is provided, the coil will produce a current to partially resist the sharp change due to the transient and thus provide electromagnetic damping. The required value of damping resistance is specified by the galvanometer manufacturer.

If a portion of the moving part of the galvanometer is suspended in a fluid, a resisting or damping force is produced by the fluid which is directly proportional to the velocity of the galvanometer deflection. Fluid-damped galvanometers are manufactured for the higher frequencies of galvanometer operation but some external damping resistance is still required. Because fluid viscosity is a function of temperature, the galvanometer operating temperature must be closely controlled for constant damping characteristics. The manufacturer accomplishes this by using a heated magnet block in which the galvanometers are installed.

The following circuit diagram shows a galvanometer circuit with resistors R_{se}, R_{sh}, and R_o, the output impedance of the matching network. These combine to provide the required value of damping resistance.

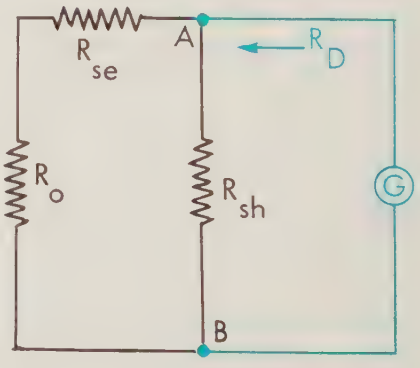

R_D = required damping resistance, specified by manufacturer

R_o = output impedance of matching network

R_{se} = series resistance in galvanometer circuit

R_{sh} = shunt resistance across galvanometer

R_D = resistance from A to B with galvanometer removed

The required damping resistance R_D may be determined as follows by writing the equation for the resistance of the circuit from A to B with the galvanometer removed:

$$R_D = \frac{R_{sh}(R_{se} + R_o)}{R_{sh} + R_{se} + R_o} \quad (1)$$

If R_{sh} is infinite (no shunt resistance used), equation (1) is reduced to:

$$R_D = R_{se} + R_o. \quad (2)$$

If $R_{se} + R_o$ is much greater than R_D—that is, $R_{se} + R_o = 100R_D$—equation (1) then becomes:

$$R_D = \frac{R_{sh}(100R_D)}{R_{sh} + 100R_D} \quad (3)$$

or,

$$R_D = 0.99\ R_{sh} \cong R_{sh}. \quad (4)$$

In practice, the simplest way to obtain the required damping resistance is to add series resistance between the matching network and the galvanometer to give

$$R_D = R_o + R_{se}.$$

If the matching network output impedance R_o is greater than the required damping resistance R_D, some shunt resistance R_{sh} must be used to give:

$$R_D = \frac{R_{sh}R_o}{R_{sh} + R_o} \quad (5)$$

Because galvanometers are generally quite sensitive, particularly for low frequencies, it may be desirable to add resistance in series to reduce overall sensitivity when large values are being measured. This may be done to establish the operating range of the galvanometer, but proper damping must then be provided by using shunt resistance to give:

$$R_D = \frac{R_{sh}(R_o + R_{se})}{R_{sh} + R_o + R_{se}}. \quad (6)$$

It is possible that, either through design or good fortune, the matching network output impedance R_o will be exactly equal to the required damping resistance R_D. For this unique condition, no series or shunt resistance is required for damping.

In summary, damping may be provided by any one of several circuit configurations. In determining the method to use, the following factors must be considered:

- Comparative value of R_o with respect to the required damping resistance. If $R_o > R_D$, shunt resistance must be used. If $R_o < R_D$, series resistance must be used
- Signal level. If attenuation is required, series attenuating resistance may be used in combination with shunt damping resistance.

Part (f)—Determine Damping Resistance in Galvanometer Circuit and Required Attenuation of Matching Network

Determine the required damping resistance R_D for the galvanometer circuit and the signal attenuation for the galvanometer selected in Part (e). Provide for four inches of galvanometer deflection at maximum torque. Sketch a circuit diagram of the completed measuring system and separate the elements into their three basic functions: transducer, matching network, and recorder.

Redesign Measuring System to Give a Higher Frequency Response

As mentioned, the maximum frequency limit is determined somewhat arbitrarily. Assume, therefore, that preliminary recordings made with the measuring system just designed indicate that a higher frequency response is required. Increase the maximum frequency response calculated in Part (e) by a factor of 10 and redesign the measuring system to meet the new frequency requirement as follows:

(1) Select a new galvanometer. (Refer to Table I)

(2) As before, provide for four inches of galvanometer deflection at maximum torque

(3) Compute the required galvanometer current. Compare this with the maximum signal available from the galvanometer to determine whether voltage amplification or attenuation is required and how much

(4) If voltage amplification is required, use the following characteristics of a typical d-c amplifier:
- Input impedance = 100,000 ohms
- Output impedance = 1 ohm
- Amplification = fixed steps of 20, 30, 50, 70, 100, 200, 300, 500, 700, and 1,000 selected by switch position. (Note that no continuous adjustment is available)
- Frequency response = 0 to 40,000 cycles per second

(5) Calculate damping resistance, or resistances, required

(6) Provide a continuous gain adjustment at the proper location on the system. Signal-to-noise ratio must be maintained as high as possible through the slip rings

(7) Sketch a circuit diagram of the redesigned measuring system and group the components in their proper basic category as transducer, matching network, and recorder.

It should be noted that a d-c amplifier is specified, if amplification is required. The explanation for this is that both static and dynamic components of torque should be recorded. A static component produces a d-c voltage at the output of the strain gage bridge. A d-c amplifier, therefore, is essential to obtain all of the information desired.

The solution to this problem will appear in the October-November-December 1960 issue of the General Motors Engineering Journal.

Bibliography

1. Harned, John L., "Recording Instruments Aid Research Involving Measurement of Dynamic Phenomena," *General Motors Engineering Journal*, Vol. 4, No. 1 (January-February-March 1957), pp. 18-23.

Other related literature in this area includes the following:

"Description, Operating Principles, and Specifications of Consolidated Series 7-300 Galvanometers," Bulletin Number 1528, Consolidated Electrodynamics Corporation, Pasadena, California.

Perry C. C., and Lissner, H. R., *The Strain Gage Primer* (New York: McGraw-Hill Book Co., Inc., 1955).

Contributors to July-Aug.-Sept. 1960 Issue of

GENERAL MOTORS ENGINEERING JOURNAL

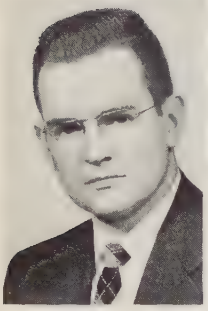

ROBERT W. CAMPBELL, contributor of the problem "Determine the Basic Design Parameters for a Strain Gage, Shaft-Type Torquemeter," and the solution appearing in this issue, is a research engineer with the Electronics and Instrumentation Department of the GM Research Laboratories.

Mr. Campbell joined the Research Laboratories in 1955 as an engineering co-op student while attending the University of Detroit. After receiving a bachelor of electrical engineering degree in 1957, he became a full-time member of the Electronics and Instrumentation Department and assumed his present position.

Some of Mr. Campbell's previous major projects have included the application of electronics and instrumentation measuring and control techniques to research projects dealing with such areas as vibration analysis, heat transfer, high-speed slip rings, and digital computers. His undergraduate thesis while at the University of Detroit dealt with an investigation into the use of high voltage pulses to excite resistance-type transducers. He is presently concerned with the application of electronics and related control circuitry to automotive vehicles.

The technical affiliations of Mr. Campbell include membership in the Instrument Society of America. Prior to joining GM, he had five years experience as an electronics technician.

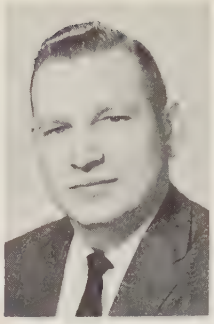

WILLARD D. CHEEK, co-contributor of "New Low Energy Photon Sources Applied to Industrial and Medical Needs," is a senior research physicist in the Physics Department of the GM Research Laboratories. His work has included the study of nuclear characteristics of samarium and gadolinium isotopes and the development of various uses of cadmium sulfide as a radiation detecting instrument.

Mr. Cheek attended Marquette University where he obtained the degrees of bachelor of naval science (1946), bachelor of electrical engineering (1948), and master of science (1949).

He joined the Research Laboratories in 1956 in his present position after having been employed as a physicist by the U. S. Navy at the Los Alamos Scientific Laboratory. Prior to this he was an assistant professor of physics and mathematics and assistant dean of men at Carroll College.

The technical affiliations of Mr. Cheek include membership in the American Physical Society, American Nuclear Society, and the Society for Non-Destructive Testing. He also is a member of Eta Kappa Nu, Sigma Pi Sigma, and Pi Mu Epsilon, honorary societies.

He was co-author of the paper, "Low Energy Photon Sources for Industry," published at the Second Industrial Conference on Peaceful Uses of Atomic Energy at Geneva, Switzerland, in 1958.

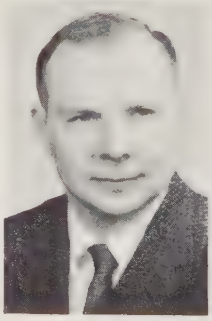

WILLIAM E. COUNTS, co-contributor of "Radioisotope Techniques Applied to Fundamental Corrosion Studies of Spark Plug Ceramics," is a research engineer with AC Spark Plug Division's Research Laboratory.

Mr. Counts was granted a B.S. in ceramic engineering degree from the Georgia Institute of Technology in 1943 and the M.S. degree in ceramics from Pennsylvania State University in 1949. While at Pennsylvania State, he was engaged in glass research and refractory research projects.

Mr. Counts joined AC Spark Plug in 1950 as a ceramic engineer. His previous projects have included work on glass seals and resistors for spark plugs, ceramic colors, and ferrite magnets. He is presently engaged in a study of refractory and semi-conducting ceramics and their fundamental properties.

The technical affiliations of Mr. Counts include membership in the Electronics Division of the American Ceramic Society. His work in the field of spark plug seals and resistors has resulted in the granting of two patents. He has had a previous paper on fluoride model structures published in the *Journal of the American Ceramic Society*.

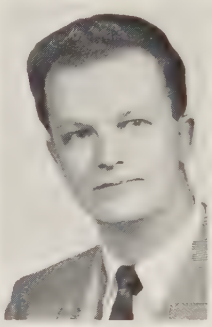

RICHARD C. DRUTOWSKI, contributor of "Rolling Friction of Balls on Plates," is supervisor of friction research in the Mechanical Development Department of the GM Research Laboratories. His current work concerns studies of rolling friction to discover the mechanism by which energy is lost during rolling and to increase the understanding of the behavior of materials under stress.

Mr. Drutowski joined the Research Laboratories in 1948 as a college graduate-in-training. In 1949 he was promoted to research physicist in the Mechanical Development Department and in 1956 to senior research physicist. He assumed his present position in 1957. Before joining GM, he was employed by the Naval Research Laboratories.

Mr. Drutowski attended the University of Michigan from which he was granted a B.E. degree in mathematics and electrical engineering in 1944 and a M.S. degree in physics in 1946. He is a member of Eta Kappa Nu, Tau Beta Pi, and Sigma Xi, honorary societies.

His paper appearing in this issue is based on a previous paper, "Energy Losses of Balls Rolling on Plates," published in *Transactions of the A.S.M.E.* He also was a co-author of the paper, "The Effect of Ball Bearing Steel Structure on Rolling Friction and Contact Plastic Deformation," published in *Transactions*.

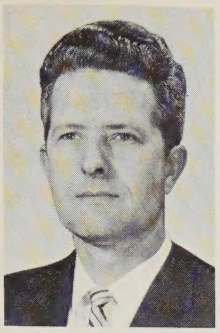

FARNO L. GREEN, co-contributor of "New Low Energy Photon Sources Applied to Industrial and Medical Needs," is a senior research physicist in the Physics Department of the GM Research Laboratories.

Mr. Green joined the Research Laboratories in 1956. In addition to research in radioisotopes, he has served as a consultant for several GM Divisions.

Mississippi College granted Mr. Green the B.A. degree with special distinction in mathematics and physics in 1941. He received the M.S. degree in physics from Louisiana State University in 1949, and has done advanced study towards a doctorate at the University of Tennessee.

Mr. Green's professional career has included educational work as head of the physics department at Wayland College, Plainview, Texas, and at Howard College, Birmingham, Alabama. Before joining General Motors, Mr. Green was a physicist at the Oak Ridge National Laboratory working on cyclotron design, theory, and utilization. He was in charge of the 44-inch cyclotron program and nuclear physics applications using the 86-inch cyclotron for radioisotope production.

Mr. Green is a member of the American Physical Society and a charter member of the American Nuclear society. He has had papers published in *Nuclear Science and Engineering* and *I.R.E. Transactions on Nuclear Science*. He was co-author of the paper, "Low Energy Photon Sources for Industry," published at the Second Industrial Conference on Peaceful Uses of Atomic Energy at Geneva, Switzerland, in 1958.

DR. WILLARD E. HAUTH, JR., co-contributor of "Radioisotope Techniques Applied to Fundamental Corrosion Studies of Spark Plug Ceramics," is a staff scientist with the Research Laboratory of AC Spark Plug Division. His present responsibilities include supervision over the research and development of ceramic insulator materials, ceramic semiconductors, ceramic and electronic components, and production control of ceramic processes and materials.

Dr. Hauth was granted a B.S. degree from Alfred University in 1946. Three years later he received his Sc.D. degree from Massachusetts Institute of Technology. He then joined the faculty of Iowa State College as an assistant professor of ceramic engineering. In 1951, Dr. Hauth left Iowa State College to join the International Resistance Company as manager of ceramic research. He was associated with this firm until January of 1959, when he left to join General Motors.

Dr. Hauth is a member of the American Ceramic Society, the National Institute of Ceramic Engineers, and Sigma Xi, honorary society. He has been a frequent contributor to the technical and scientific literature, having had 10 papers published in the field of ceramics and electronics.

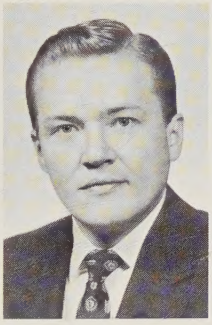

DONALD P. KOISTINEN, co-contributor of "A Study of Residual Stresses in Hardened Steel Induced by Phase Transformations," is a senior research physicist with the Physics Department of the GM Research Laboratories. His previous projects have included X-ray diffraction studies of phase composition and residual stresses in steel with applications to fundamental metallurgical problems. He is currently concerned with basic studies of the crystallography of solid-state transformations in metals with particular interest in steel.

Mr. Koistinen joined the Research Laboratories in 1952 as a physicist shortly after receiving the B.S. degree from the University of Michigan. Three years later he was promoted to research physicist. He assumed his present position in 1958. Mr. Koistinen continued his education after joining the Research Laboratories and received a M.S. degree in physics from Wayne State University in 1958.

He is a member of the American Physical Society and has been a frequent contributor to the scientific literature. He has authored and collaborated on papers which have been published in *Transactions of the American Society for Metals, Acta Metallurgica, Proceedings of the American Society for Testing Materials*, and *Transactions of the American Institute of Mining and Metallurgical Engineers.*

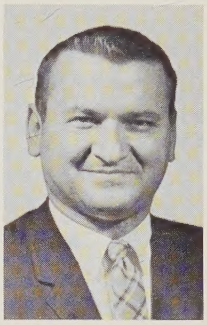

PETER P. KOZAK, contributor of "Patents and Basic Research" and coordinator of this issue's "Notes About Inventions and Inventors," is a patent attorney in the General Motors Patent Section, Detroit Office.

Mr. Kozak is primarily concerned with patent problems involving chemical and metallurgical subject matter. The major categories of his work include the preparation and prosecution of patent applications, patent infringement and validity investigations, and patent license negotiations.

Mr. Kozak attended the University of Wisconsin where he earned the degrees of B.S. in chemical engineering and LL.B. In 1952 he joined General Motors as a patent engineer in the Washington Office of the Patent Section. He transferred to the Dayton Office in 1954 and to the Detroit Office in 1957. He is a registered patent attorney and a member of the Wisconsin Bar.

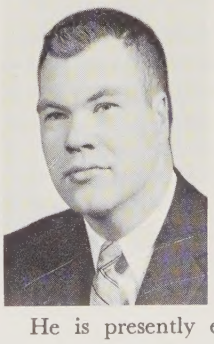

RICHARD E. MARBURGER, co-contributor of "A Study of Residual Stresses in Hardened Steel Induced by Phase Transformations," is a senior research physicist with the Physics Department of the GM Research Laboratories. He is presently engaged in studies of

phase transformations in solids with applications to alloys.

Mr. Marburger joined the Research Laboratories in 1952 as a junior physicist. The following year he was inducted into the Air Force and served as a lieutenant at the Physics Branch, Wright Air Development Center. He was separated from service in 1955 and returned to the Research Laboratories as a research physicist. He assumed his present position in 1958.

Mr. Marburger was granted a B.S. degree in 1950 and a M.S. degree in 1952 from Wayne State University. He is a member of the American Physical Society and Sigma Xi, honorary society. He has been a frequent contributor to the scientific literature, having had papers published in *Physical Review*, *Journal of Chemical Physics*, *Journal of Applied Physics*, *Acta Metallurgica*, and *Transactions of the American Society for Metals*.

JAMES D. MATCHETT,

co-contributor of "A Thermal Energy Storage System for Solar Powered Earth Satellite Power Plants," is a project engineer with the Engineering Research Department of Allison Division.

Mr. Matchett attended Purdue University where he obtained a B.S. in mechanical engineering degree in 1957. He continued his education at Purdue for another year, taking graduate studies. He then joined Allison in August, 1958. He is presently completing requirements for a M.S. degree from Purdue in an off-campus program jointly sponsored by Purdue and Allison.

Mr. Matchett's current work concerns the design and development of high temperature loops for circulating liquid metals, investigation of high performance heat exchangers, analysis of heat transfer problems of advanced propulsion systems and satellites, and analysis of thermal energy storage systems.

He is a member of the S.A.E. and A.S.M.E. He currently serves as local section representative of the A.S.M.E.'s junior committee for region VI. He also is a member of Sigma Xi, Pi Tau Sigma, and Tau Beta Pi.

DR. ROBERT F. MILLER,

contributor of "Diffusion—a Means of Semiconductor Device Fabrication," is group leader, Advanced Device Development, Semiconductors-Research and Engineering Department at Delco Radio Division. He is currently engaged in solid state diffusion research and improved diffusion techniques, and in the research and engineering development of semiconductor materials and devices.

Dr. Miller joined Delco Radio in 1957 as an engineer in the Semiconductors-Research and Engineering Department. He was promoted to his present position in 1959. Prior to joining General Motors he had experience in education and in industry, having served as electrical engineering instructor at University of Wisconsin, lecturer and acting department head (physical sciences) at Milwaukee School of Engineering, and engineer at J. I. Case Company.

The University of Wisconsin granted him the B.S. degree in electrical engineering in 1947, the M.S. degree in electrical engineering in 1954 and the Ph.D. degree in 1957.

Dr. Miller's technical affiliations include membership in the American Institute of Electrical Engineers, Institute of Radio Engineers (Professional Group of Electron Devices), and the American Society for Engineering Education. He also is a member of Tau Beta Pi, Phi Kappa Phi, Eta Kappa Nu, and Sigma Psi, honorary societies. Dr. Miller is a registered professional engineer in the State of Wisconsin.

FRED G. ROUNDS,

contributor of "The Effects of Lubricant Composition on Sliding Friction of Steel on Steel," is a senior research engineer with the Fuels and Lubricants Department of the GM Research Laboratories. One of his current projects is a study on the effects of lubricants and surface treatments on ball bearing fatigue. Some of his past projects have included studies on the effects of added gases on engine performance, the coking tendencies of lubricants, hydrocarbon composition ion engine exhaust gas, and Diesel exhaust odor.

Mr. Rounds joined the Research Laboratories as a college graduate-in-training in 1949 shortly after graduating from the State College of Washington with a B.S. in chemical engineering degree. Successive promotions to junior research engineer and research engineer led to his present position.

Mr. Rounds is a member of the American Chemical Society and several honorary societies including Tau Beta Pi and Phi Lambda Upsilon.

Two patents have been granted as a result of Mr. Rounds' work in the area of fuels and combustion, and he is the author of several technical papers on this subject. His paper appearing in this issue of the JOURNAL is a condensation of a paper published in *Chemical and Engineering Data*.

CURTIS L. WALKER,

co-contributor of "A Thermal Energy Storage System for Solar Powered Earth Satellite Power Plants," is section chief of the Fluid Dynamics and Heat Transfer Section, Engineering Research Department, Allison Division. He is presently responsible for the direction and supervision of fluid dynamics and heat transfer research projects, including problems associated with space power systems.

Mr. Walker joined Allison Division in 1957 as a senior research engineer. Prior to joining GM, he was associated with the National Advisory Committee for Aeronautics as an aeronautical research scientist and also was with the Turbomotor Division of Curtiss Wright.

Mr. Walker received a B.S.M.E. (Aero) degree from the University of Oklahoma in 1950, where he was elected to membership in Tau Omega, honorary society.

His technical affiliations include membership in the American Rocket Society and the Institute of the Aeronautical Sciences. He also is a member of the A.S.M.E. technical committee on astronautical heat transfer.

RESEARCH

ASSIGNMENT IN GM

The basic research program at the GM Research Laboratories includes investigations in the branch of science known as solid state physics—the study of the properties of solid materials.

Part of this study involves the growing of cadmium sulfide crystals—a type of crystal that does not exist in nature in a pure and perfect form. This crystal is a compound semiconductor with two kinds of atoms as contrasted with the elemental semiconductors containing one kind of atom, such as germanium and silicon.

In the photograph above, Edward F. Weller, left, assistant head, Physics Department, and Robert Bockemuehl, a senior research engineer in the Physics Department, discuss a new cadmium sulfide field-effect phototransistor recently developed by the GM Research Laboratories. Mr. Weller directed the overall program and Mr. Bockemuehl was in charge of the development work.

This experimental phototransistor, believed to be the first of its type, has been successfully used in various electronic circuits. The electrical properties of cadmium sulfide are greatly affected by light and other radiation, making it a unique circuit device in phototransistor applications. For example, its amplification can be controlled by changing the color or the intensity of light striking it.

The inset shows a unit mounted on a special printed circuit board and also in a standard transistor header with a transparent cover. The field-effect model has the small size, high efficiency, and ruggedness common to other semiconductor components.

Mr. Weller joined the Research Laboratories in 1946 as a junior engineer. He was promoted to research engineer in 1947 and to senior engineer in 1950. He assumed his present position in 1952. Mr. Weller graduated from the University of Cincinnati in 1943 with a degree in electrical engineering.

Mr. Bockemuehl joined the Research Laboratories in 1952 as a college graduate in training following graduation from the University of Michigan with a B.S.E. degree in electrical engineering. He was promoted to junior engineer the same year and in 1954 was made a research engineer. Mr. Bockemuehl assumed his present position in 1956.

GENERAL MOTORS

ENGINEERING JOURNAL

PRINTED
IN
U.S.A.